Chicken Embryo Chorioallantoic Membrane Assay for Pre-Clinical Evaluation of Efficacy and Safety of Anti-angiogenic and Hypoxic Cell Starving Tumor Interventions.

Dissertation*

zur

Erlangung der naturwissenschaftlichen Doktorwürde
(Dr. sc. nat.)

vorgelegt der

Mathematisch-naturwissenschaftlichen Fakultät

der

Universität Zürich

von

Dheeraj Shinde

aus

Indien

Promotionskomitee

Prof. Dr. med. vet. Max Gassmann (Vorsitz)
Dr. rer. nat. Thomas A. Gorr (Leitung der Dissertation)
Prof. Dr. med. Johannes Vogel (Leitung der Dissertation)
Prof. Dr. Carsten Lundby
Prof. Dr. Ian Frew

Zurich 2014

Contents

Summary

Angiogenesis inhibitors (AIs) diminish or block the de novo formation of capillaries from pre-existing blood vessels and have been considered a breakthrough concept in cancer therapy for many years. To date, however, pre-clinical data on AIs did not translate very productively into the clinic. AI monotherapy can apparently raise the tumor´s aggressiveness and has been associated with an increasing likelihood for metastases to occur. Perhaps, this AI-mediated increase in tumor virulence stems from the drugs propensity to escalate both extent and severity of tissue hypoxia. In contrast, treatments that normalize the usually chaotic tumor vasculature with its erratic blood flow back to a functional network are indeed able to elevate in vivo oxygen tensions within the malignant mass in correlation with a reduced occurrence of cancer spread.

Despite the frequent use of AIs to combat cancer growth and malignant progression, the impact of manipulations on fundamental physiological parameters such as vascular normalization, blood flow and local tissue oxygenation within the tumor are insufficiently understood. This is mostly due to the lack of good pre-clinical models to evaluate tumor angiogenesis and its responses to different anti-angiogenic compounds. Prof. T. Cerny, president of the Swiss Cancer League, therefore stressed in an interview with the Neue Zürcher Zeitung the urgent need for additional research to identify most effective anti-angiogenic treatment strategies at minimal negative impact for the patient (NZZ, No. 58, March 11, 2009).

An effective anti-cancer therapy needs to target not only the oxygenated/aerobe compartment of the tumor adjacent to its vascular structures through blood-borne cytotoxins but also the vessel-remote areas enriched with severely hypoxic/glycolytic cells. Owing to the selection in favor of surviving hypoxic cells, a selective kill of oxygenated cells only furthers malignant progression since the tumor might develop widespread resistance to treatment and adopt a much more virulent phenotype. Therefore this project tests the established AI Avastin® (vascular endothelial growth factor (VEGF) antibody) alone and in combination with the Monocarboxylate Transporter 1 (MCT1) Inhibitor α-Cyanohydroxycinnamate (CHC).

The combined AI/anti-MCT1 strategies can target simultaneously both oxygenated and hypoxic tumor compartments. MCT1 inhibitors lead in hypoxic cells to glucose starvation by rerouting glucose from hypoxic to oxygenated cells and thus might indirectly eradicate hypoxic/glycolytic tumor cells and render hard-to-treat malignancies more susceptible to therapy. The combination of MCT1 inhibition (to target hypoxic cells) with AI agents (to starve oxygenated regions from nutrients) is conceptually a very promising and novel approach. The efficacy of these combination therapy protocols was examined by the animal saving ex ovo Chorio-allantoic membrane (CAM)/tumor explant assay. Using the CAM assay, so far we were able to induce solid tumors with human hepatoma (Hep3B), mammary carcinoma (MCF7), and glioblastoma (U87), cell lines on chicken embryos. For U87 tumors, explants showed clear decreased blood perfusion (FLUX arbitrary unit) with combinotorial treatment of AI (Avastin®) and MCT1 inhibitors as compared to Avastin® alone and controls. Tumor sizes were determined by analysis of tumor images, using computer-aided image analysis, which reproduced comparable results showing additive effect of Avastin® & MCT1 inhibitors. Tumor oxygenation was inferred by pimonidazole staining which echoed the similar findings. To study tumor cell spreading on CAM under said treatments a more virulent cell line MDA-MB 231 was used which showed an overall increase in spread (motility) of MDA-MB231 cells with AVA treatment as compared to controls while reduction in motility was observed with combinatorial treatment. To check the efficacy of CAM/migration assay, as a side project tumor cell spreading was also studied in Ewing sarcoma tumor with IL-6 treatment which showed dose dependent increase in cell migration.

In conclusion, we demonstrate the applicability of CAM/explant methodology as a cheap, easy-to-implement pre-clinical drug screen allowing 1) high-throughput screening of drugs and 2) an animal saving alternative to rodent models. By combining angiogenic inhibitors with agents able to selectively target hypoxic microenvironments in the tumor, the intervention protocol might be able to shrink primary masses and minimize the risk of malignant progression and tumor spread at the same time. Of course, these strategies need further analyses of suitable cell models and drug combinations in CAM and murine models followed by clinical studies.

Zusammenfassung

Angiogenesehemmer (AHs) unterdrücken oder blockieren die de novo Bildung von Kapillaren aus schon vorhandenen Blutgefässen und wurden deswegen für viele Jahre als Durchbruch in der Krebstherapie angesehen. Heute zeigt sich jedoch, dass die viel versprechenden Daten aus vorklinischen Studien sich nicht sehr produktiv in der Klinik umsetzen liessen. AH Monotherapie kann offenbar die Aggressivität eines Tumors steigern und wurde mit einer erhöhten Wahrscheinlichkeit für Metastasenbildung assoziiert. Möglicherweise rührt die AH-induzierte Steigerung der Tumorvirulenz von der dem Wirkmechanismus immanenten Neigung der AHs sowohl die Ausdehnung als auch die Intensität des Sauerstoffmangels zu verstärken. Im Gegensatz dazu erreichen Therapien, die die üblicherweise chaotische Gefässversorgung mit fehlerhafter Durchblutung normalisieren, eine Verbesserung der Sauerstoffversorgung in der Tumormasse, was mit einer geringeren Metastasierungstendenz einhergeht.

Trotz des verbreiteten Einsatzes von AHs zur Bekämpfung des Wachstums solider Tumore und des Fortschreitens einer Krebserkrankung sind die Effekte der Manipulation fundamentaler physiologischer Parameter wie Gefässnormalisierung, Durchblutung und lokaler Sauerstoffversorgung in Tumoren nur unzureichend verstanden. Das liegt grösstenteils an einem Mangel an guten vorklinischen Modellen, mit denen Tumorangiogenese und deren Antwort auf verschiedene anti-angiogenetisch wirksame Substanzen untersucht werden könnten. Deshalb forderte Prof. T. Cerny, Präsident der Schweizer Krebsliga vor einiger Zeit in einem Zeitungsinterview mit der Neuen Züricher Zeitung zusätzliche Forschungsanstrengungen, um neue, effektivere anti-angiogenetische Therapiestrategien mit minimalem negativen Effekten auf den Patitenten zu finden (NZZ, No. 58, March 11, 2009).

Eine effektive Krebstherapie muss nicht nur die sauerstoffreichen, aeroben Bereiche des Tumors, die neben den Blutgefässen liegen, mittels über das Blut herantransportierten Zytostatika treffen, sondern auch die gefässfernen, stark hypoxischen Tumorzellen. Wegen der positiven Selektion von hypoxischen Tumorzellen, verstärkt eine ausschliessliche Vernichtung oxigenierter Tumorzellen nur die maligne Progression der Krebserkrankung

und könnte zur Entstehung einer Therapieresistenz und der Entwicklung eines bösartigeren Phänotyps der Krebszellen führen. Daher wurde in dem vorliegenden Projekt ein etablierter AH, Avastin® (vascular endothelial growth factor (VEGF) Antikörper), allein und in Kombination mit dem Monocarboxylate-Transporter 1 (MCT1) Inhibitor α-Cyanohydroxycinnamate (CHC) getestet.

Die kombinierte AH/ant-MCT1 Strategie kann gleichzeitig die oxigenierten und hypoischen Tumorareale treffen. MCT1-Inhibitoren schneiden die hypoxischen Tumorzellen von der Glukose- und damit Energieversorgung ab, indem sie die Glukose den oxygenierten Tumorzellen zuführen. So können indirekt die hypoxischen Tumorzellen ausgemerzt und schwer therapierbare Krebsleiden besser behandelbar werden. Diese Kombination von MCT1-Inhibitoren (um hypoxische Tumorzellen zu treffen) mit AHs (um sauerstoffreiceh Tumorareale von der Nährstoffversorgung abzuschneiden) ist ein konzeptionell neuer, viel versprechender Ansatz. Die Effektivität dieser Kombinationstherapie wurde mit dem versuchstiersparenden ex ovo Chorio-allantoic-membrane (CAM) Assay nach Explantation von Tumorzellen durchgeführt. Mit dieser Methode konnten wir bis jetzt humane Hepatom- (Hep3B), Mammakarzinom- (MCF7) und Glioblastom- (U87) Zellen zu solidenn Tumoren auf dem CAM des Hühnerembryos anzüchten. U87-Tumorexplantate zeigten eine klare Durchblutungsverminderung nach Kombinationstherapie mit AH, Avastin® und MCT1-Inhibitor im Vergleich zu Avastin® Monotherapie und unbehandelten Kontrolltumoren. Das Tumorwachstum wurde mit Hilfe computergestützter Bildanalyse gemessen und zeigte einen vergleichbaren additiven Effekt der Avastin® und MCT1-Inhibitor Behandlung. Die lokale Tumorhypoxie wurde mit Hilfe einer Pmonidazolfärbung untersucht und bestätigte diese Befunde. Um die spontane Zellausbreitung der Tumore unter den genannten Therapien zu untersuchen wurde eine virulentere Zelllinie, MDA-MB 231, benutzt, mit der sich zeigte, dass eine Avastin® Monotherapie die Zellausbreitung (Zellbeweglichkeit) in das normale CAM-Gewebe im Vergleich zu unbehandelten Kontrollen erhöhte, während die Avastin® / MCT1-Inhibitor Konbinationsbehandlung die Zellausbreitung unterdrückte.

Schlussfolgernd konnten wir mit dieser Studie demonstrieren, dass die CAM/Tumorzellexplantationsmethode als einfache, kostengünstige vorklinische

Medikamentenscreeningmethode geeignet ist und 1) einen hohen Durchsatz für Medikamententeste erlaubt und 2) eine versuchstiersparende Alternative zu den sonst üblichen Nagermodellen ist. Durch die Kombination von Angiogenesehemmern mit Substanzen, die spezifisch hypoxische Tumorareale treffen, wird es möglich sein, den Primärtumor zu schrumpfen und dabei gleichzeitig das Risiko einer malignen Progression und Metastasierung zu minimieren. Natürlich bedarf diese Strategie noch weiterer Untersuchungen an geeigneten Zellmodellen und anderen Medikamentenkombinationen in CAM- und Mausmodellen, gefolgt von klinischen Studien.

Abbreviations:

AIs: Angiogenesis inhibitors

Ang: Angiopoietin

ARNT: Aryl hydrocarbon receptor nuclear translocator

ATP: Adenosintriphosphat

AVA: Avastin®

B16-F10: Murine Melanoma

bFGF: Basic fibroblast growth factor

BMDCs: Bone marrow derived cells

CAFs: Carcinoma-associated fibroblasts

CAM: Chorioallantoic membrane

CHC: α-cyanohydroxycinnamate

CML: Chronic myeloid leukemia

CXCR4: C-X-C chemokine receptor type 4

ECM: Extracellular matrix

EDF1: Endothelial differentiation-related factor 1

EGF: Epidermal growth factor

eNOS: endothelial nitric oxide synthases

EphB4: Ephrin type-B receptor 4

FDA: Food and Drug Administration

FGFR: Fibroblast growth factors receptor

FGFs: Fibroblast growth factors

Hep3B: Human hepatoma

HIF1: Hypoxia inducible factor 1

HIF2: Hypoxia inducible factor 2

HIFa: Hypoxia inducible factor alpha

IL-6: Interleukin 6

IL-10: Interleukin 10

iNOS: inducible Nitric oxide synthases

LDG: Lactate dehydrogenase

MCT1: Monocarboxylate transporter 1

MCT4: Monocarboxylate transporter 4

MMP: Matrix metalloproteases

MSCs: Mesenchymal stem cells

NF-kB: Nuclear factor kappa-light-chain-enhancer of activated B cells

nNOS: neuronal Nitric oxide synthases

NO: Nitric oxide

NOS: Nitric oxide synthases

PDGF: Platelet-derived growth factor

PDGFR: Platelet-derived growth factor receptor

PIGF: Placenta-derived growth factor

RCC4: Renal clear cell carcinoma

ROS: Reactive oxygen species

SDF1: Stromal cell–derived factor 1

TAMs: Tumor Associated macrophages

TGF-β: Transforming growth factor beta

Tie1: Tyrosine kinase with immunoglobulin-like and EGF-like domains 1

TMs: Transmembrane helices

TSP1: Thrombospondin1

U-87: Glioblastoma

VEGF: Vascular endothelial growth factors

VEGFR: Vascular endothelial growth factors receptor

WHO: World Health Organization

Project A

(Chick embryo chorioallantoic membrane assay for pre-clinical evaluation of efficacy and safety of anti-angiogenic and hypoxic cell-starving tumor interventions)

1. Introduction:

1.1 Overview to cancer biology

Although cancer a heterogeneous disease, originates from a single cell (first proposed by Theodor Boveri in 1902 [1]) harboring a mutant DNA sequence that manipulates the crucial regulatory pathways involved in cell survival, proliferation and apoptosis.

Based on statistics from World Health Organization (WHO): Cancer is one of the major cause of death worldwide, accounting for 8.2 million deaths in 2012 [2] and is projected to rise continuously, to an estimated 13 million deaths within the next two decades. In 2012 itself cancer burden was increased to 14 million new cases, a figure expected to rise to 22 million in next two decades [2]. Looking at this statistics, clearly a better understanding of the molecular mechanisms underlying the various forms of cancer remains of utmost importance to improve therapies and eventually develop cancer cure.

In 1873 Theodore Billroth was the first to successfully perform a surgical procedure to treat cancer of the larynx [3]. The next century saw rapid progress and is often referred to as "the century of the surgeon". To date surgery is one of the most effective methods in the treatment of localized primary tumor and associated regional lymphatic nodes. Use of Radiation therapy was first reported in 1896 by Emil Grubbé to treat breast cancer [4], [5] and has been widely used since 1920s. The 1940s saw the advent of chemotherapy with Nitrogen mustard (mechlorethamine) introduced in 1949 to become the first chemical agent approved by the Food and Drug Administration (FDA) for the treatment of leukemias and lymphomas [6]. This development was followed by rapid progress made in immune therapy (e.g. Herceptin) and hormone therapy (e.g. Tamoxifen). Until the late 1980's the majority of the medications used in cancer treatments were DNA-damaging agents designed to kill or inhibit rapidly

dividing cells (e.g. Cisplatin), which, however, also had substantial adverse effects on proliferating normal cells.

During the last decades, numerous advances in the field of cancer therapy (anti-angiogenic protocols, chemotherapy, gene therapy etc.) have helped physicians, while researchers increasingly focused on the outcome of combining surgery with medications and/or radiation. But despite the latest advantages, the known genetic instability and cellular heterogeneity particularly solid neoplasms still carry high risk of a therapy-driven selection of cell clones resistant to chemo- and/or radiation treatment. As an alternative: combination therapies should be designed to simultaneously target multiple cancer cell-specific pathways in order to prevent the emergence and spread of resistant clones.

Tumorigenesis is a multistep process, initiated by so-called driver mutations, allelic deletions or chromosomal translocations. The occurrence of secondary events (e.g. passenger mutations) will eventually drive the advanced transformation of normal human cells into highly malignant derivatives with growth/survival advantage over wild type progenitors. Most tumor transformative processes are not inherited but triggered by somatic mutations invoked by etiological agents like carcinogenic chemicals, smoking, infections (e.g. Papilloma virus, Hepatitis B/C), excessive sun exposure, radiations, stress, tobacco, diet and obesity etc (WHO statistics suggest about 30% of cancer deaths are due to behavioral and dietary risks [2]). These DNA defects cause regulatory circuits that govern normal cell proliferation and homeostasis to derail, thereby producing malignant phenotypes. There are more than 100 distinct types of cancer, and subtypes of tumors that can be found within almost all organs. Since neoplasms carry numerous mutations, this genetic heterogeneity also confers a growth advantage to the malignant mass itself and is responsible for development of drug resistance during treatment. In 2000 Hanahan and Weinberg [7] suggested that this complexity illustrated by a huge catalog of cancer cell genotypes, basically indicates six essential alterations in cell physiology that are essential for malignant growth and progression of tumors, commonly referred as hallmarks of cancer (figure 1a, 1b). Throughout the past decade, further evidence suggested two additional

(newly emerging) hallmarks and two enabling characteristics of cancer (figure 1b) to influence the pathogenesis of some or perhaps all cancers.

a)

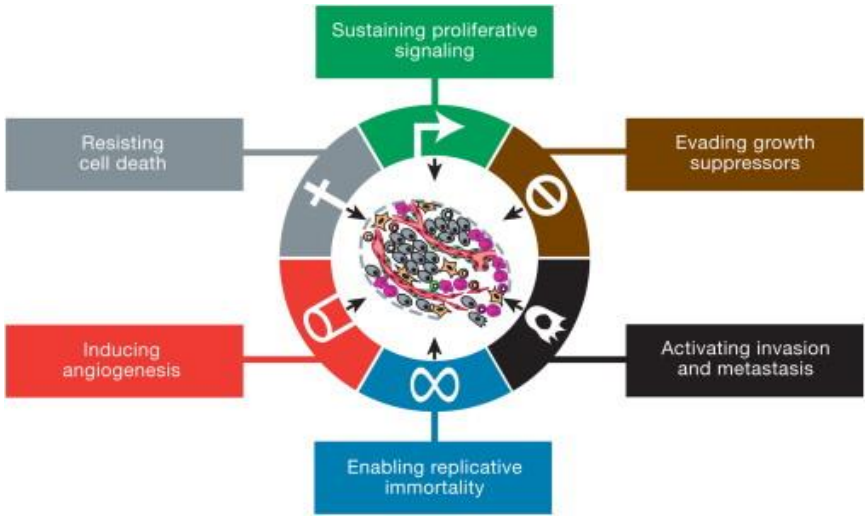

b)

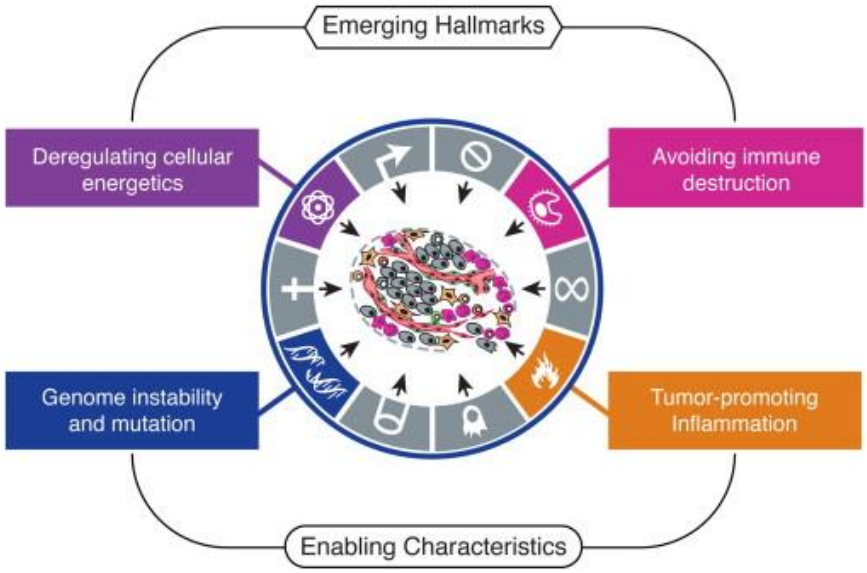

Figure 1. The hallmarks of cancer. (a) Six hallmarks of cancer first suggested in 2000 by Hanahan and Weinberg [7]. (b) With the past decade of extensive research, added evidence suggested the role of two emerging core hallmarks and two enabling characteristics in the pathogenesis of some or perhaps all cancers (figure acquired from Hanahan and Weinberg [8]).

As an outcome of genetic alterations, microenvironmental heterogeneity etc. many solid cancers are characterized by phenotypic and functional diversity among the population of malignantly transformed cell progeny, some of which able to endorse a growth and survival benefit to the entire mass [9], [10]. A landmark publication by Fidler and Hart demonstrated for the first time in 1982 the existence of biological diversity in metastatic neoplasms [11].

Tumor cell proliferation is often fueled by stimulated glycolysis, even under aerobic conditions (Warburg effect), and an ever-increasing demand of glucose and oxygen. As the size of the neoplasm increases more and more cells come to lie outside the region that can be supplied with substrates from the capillary network of the tumor. Since the tumor vasculature is categorically a poor provider of a continuous supply of substrates to the tumor cells (for details, see section: 1.3.2: *Tumor metabolism*), the neoplastic mass of cells is often characterized by an enormous microenvironmental heterogeneity and steep inward diffusion gradients for O_2 and glucose (i.e. maximal concentrations at vessel proximity to minimal concentrations at vessel-remote areas of malignancy) plus outward-operating gradients of lactate and other metabolic end products.

This tumor heterogeneity leads to the expression of diverse factors [e.g. endothelial differentiation-related factor 1 (EDF1), vascular endothelial growth factors (VEGF), interleukin 10 (IL-10) and TGF-β], which may induce a complex immunosuppressive response, both locally and regionally [12], [13], but which also may vary depending on the type of lesion [14].

A number of recent studies utilizing next generation sequencing has confirmed tumor heterogeneity [15] and its role in acquired drug resistance [16]. This hypothesis is well supported by the clinical observations. E.g. chronic myeloid leukemia (CML) characterized by genetic abnormality (translocation) shows better response to therapy as compared to extremely heterogeneous tumor types (e.g. ovarian cancer, breast cancer) [17]–[19].

1.2 Angiogenesis in physiology

Angiogenesis, i.e. the process of growing new blood vessels from pre-existing ones requires the coordination of multiple signaling pathways, cell–cell and cell–matrix interactions [20]. While angiogenesis is typically dormant in adults, except for its temporary activation during menstrual cycle-specific processes (e.g. ovulation, endometrial growth, implantation, placentation, etc.) or wound healing, it is often stimulated in numerous pathologies (diabetic retinopathy, rheumatoid arthritis, cardiac ischemia, psoriasis, tumor growth). Angiogenesis can broadly be classified into intussusceptive angiogenesis and sprouting angiogenesis, which both occur during embryogenesis as well as in adults [21], [22]. Intussusceptive angiogenesis, which occurs by internal splitting of the preexisting capillaries, plays a particularly critical role in embryogenesis with its rapid growth [23], [24]. This particular mode of vascular expansion is driven through the rearrangement, but not the proliferation, of endothelial cells. Intussusceptive angiogenesis occurs via four subsequent steps, including (i) protrusion of opposing endothelial cells into the capillary lumen, (ii) formation of a tube-shaped tissue bridge extending across the lumen enveloped by endothelial cells, (iii) formation of a core structure at the contact points between pericytes and myofibroblasts (i.e. these cells are responsible to synthesize collagen fibers for the growth of wider vessels), (iv) serial transformation of the point of contact to enlarge in the pillar diameter [24], [25]. While intussusceptive angiogenesis was first discovered by Caduff *et.al*. in postnatal lungs of rats [26], [27], it is now known to occur in the choroid of the eye, vascular baskets around glands, intestinal mucosa, kidney, ovary, and uterus [28], [29]. Rate limiting steps in intussusceptive angiogenesis are far less understood then in sprouting angiogenesis.

Sprouting angiogenesis, the predominant form of angiogenesis in embryonic development, wound healing, reproduction [30], [31], and tumors [8], [32] is primarily initiated in regions insufficiently supplied with oxygen in the attempt to maintain or stabilize the delivery of O_2 and blood-born substrates. That way parenchymal cells (myocytes, hepatocytes, neurons, astrocytes, etc.) aim to stay aerobic by secreting pro-angiogenic growth factors to foster sprouting angiogenesis [33], [34]. The entire process starts through the nitric oxide ($NO^{\bullet}$) dependent vasodilation in conjunction with a local breakdown of the endothelial integrity of

the parental vessel. It then proceeds via the (i) degradation of the basement membrane by proteolytic enzymes, (ii) proliferation and migration of endothelial cells, starting with a tip cell that moves along a gradient of pro-angiogenic factors, (iii) formation of tube like structures through increase in numbers of endothelial cells, (iv) synthesis of new basement membrane and (v) recruitment plus stabilization of vascular smooth muscle cell [33].

Although vascular endothelial growth factors (VEGF) are considered the most critical drivers of angiogenesis [35] (table 1), the process of neovascularization requires a plethora of growth and other modulating factors, including fibroblast growth factors (FGFs) [36], transforming growth factor-β (TGF-β), angiopoietins [35], platelet-derived growth factor (PDGF) [37], and the ephrin family of cytokines [38]. VEGFs and FGFs are two classes of heparin-binding glycoproteins that promote both physiological (productive) and pathological (non-productive) angiogenesis in response to hypoxia. VEGFs include placenta-derived growth factor (PlGF), viral VEGF homologs and a family of the structurally related dimeric glycoproteins VEGF-A, VEGF-B, VEGF-C and VEGF-D. All VEGF family members share a highly preserved VEGF homology domain, encoded by exons 1 to 5. These growth factors act via endothelial-specific receptor tyrosine kinases, VEGFR1 (vascular endothelial growth factors receptor 1) (Flt1), VEGFR2 (KDR/Flk1), and VEGFR3 (Flt4) [39], [40] to govern both proliferation and differentiation of the endothelial lineage from the earliest stages of development.

VEGF Family	**Functions**	**VEGF Receptors**
VEGF-A	Angiogenesis vascular maintenance	VEGFR1, VEGFR2, neuropilin-1
VEGF-B	Not known	VEGFR1
VEGF-C	Lymphagiogenesis	VEGFR2, VEGFR3
VEGF-D	Lymphagiogenesis	VEGFR2, VEGFR3
VEGF-E (viral factor)	Angiogenesis	VEGFR2
PIGF	Angiogenesis Inflammation	VEGFR1, neuropilin-1

Table 1: List of VEGF family members

FGFs also prompt neovascularization and have been implicated in the growth of new blood vessels during wound healing and embryogenesis. In *Drosophila*, the homologous signaling between FGF ligand (BRANCHLESS, BNL), emanating from hypoxic target tissues, and FGF receptor (BREATHLESS, BTL) located on the surface of sprouting tracheal branches, is coordinated with exquisite sensitivity by the hypoxia inducible factor alpha subunit (HIFα, Sima) cascade [41], [42]. In this model it is clear that HIFα/Sima is instrumental for sensitizing (i.e. driving BTL induction), progressively ramifying and guiding the gas-exchanging surfaces of tracheal sprouts towards incoming BNL cues from O_2-deprived tissues, much like productive sprouting angiogenesis operates during wound healing or embryogenesis of mammals (figure 2). In vertebrates 22 members (molecular mass ranging from 17 to 34 kDa) of the FGF family are differentially expressed in many tissues. Essential angiogenic isoforms include the acidic FGF1 and the basic FGF2. FGF1 and FGF2 promote the proliferation of endothelial cells and the physical organization of endothelial cells into tube-like structures. The FGF-Receptor family is comprised of four members, FGFR1-FGFR4 [43]–[45].

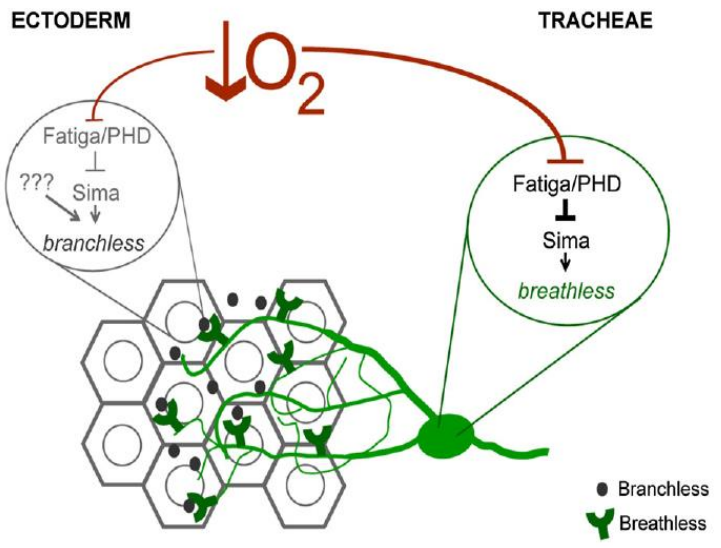

Figure 2: Sprouting tracheal branches in *Drosophila*, is coordinated with exquisite sensitivity by the hypoxia inducible factor alpha subunit (HIFα, Sima) cascade, (figure acquired from Centanin *et al*. [41])

Angiopoietins, important partners of VEGF signaling, are involved in the formation of mature blood vessels. Four angiopoietins Ang1, Ang2 and Ang3 (mouse)/Ang-4 (human) act by binding to Tie1 (Tyrosine kinase with immunoglobulin-like and EGF-like domains 1) and Tie2 tyrosine kinases receptor [46]. It has been observed that angiopoietins primarily bind to Tie2 receptor tyrosine kinases, while the role of Tie1 is still controversial. These receptors are selectively expressed within the vascular endothelium (despite expression in some other cells, such as in the haemopoietic lineage) [47]. Especially Ang1 and ephrin-B2 are subsequently required for further remodeling and maturation of the initially immature vasculature during development as well as adulthood [47], [48].

Although Ephrins were first/initially characterized in the nervous system [49], [50], later knockout studies suggested their key role in vascular development. Ephrins are membrane bound proteins that serve as ligand for Ephrin receptors (largest known subfamily of receptor protein-tyrosine kinases). Mainly Ephrin-B2 and EphB4 (Ephrin type-B receptor 4) receptors are involved in establishing arterial versus venous identity, perhaps in fusing arterial and venous vessels at their junctions [49], [51].

1.2.1 Pathological angiogenesis with particular focus on tumors

Typically angiogenesis is quiescent during adulthood, with only 0.01% of endothelial cells undergoing division [52]. However endothelial cells can retain their ability of rapid cell division (during angiogenesis) in response to an external stimulus. Such stimuli mainly include metabolic stress (e.g. low pO_2, low pH or hypoglycemia), immune/inflammatory response, genetic mutations and mechanical stress [34]. However, any shift in the delicate balance between stimulators and inhibitors can lead to a number of angiogenesis-related disorders where new blood vessels either grow excessively or insufficiently [52], [53]. Such an imbalanced production of pro- versus anti-angiogenic factors is, presumably, why the process of pathological angiogenesis, in contrast to the physiological situation during embryogenesis or menstruation, often yields aberrant and poorly functional vascular

networks. Pathological angiogenesis is suspected to underlie more than 70 disorders to date. As point in case, excessive neovascularization is known to occur in conditions like diabetic retinopathy, age-related macular degeneration, rheumatoid arthritis and psoriasis. Conversely, in disorders such as coronary artery disease, preeclampsia, chronic wounds etc. angiogenesis is generally insufficient, causing EC dysfunction/vessel malformation delayed wound healing, regeneration and revascularization [34], [52], [53].

The presence of a capillary network in tumors and its generation from the host vascular bed was first demonstrated by Virchow and Thiersch as early as 1863. In 1908 Goldmann established the requirement of a vascular system for a solid tumor to grow [54]–[56]. To date it is clear that occurrence of angiogenesis and malignant progression of tumors is intimately coupled by one of the most prevalent and cell-behavior/metabolism-altering characteristics of the tumor microenvironment: severe tissue hypoxia.

Tissue hypoxia can be defined as the condition where the progressing imbalance between O_2 consumption (=high, due to wildly proliferating cancer cells) and supply (=low/unsteady, due to poorly functional tumor vascular networks) has finally reached a point where O_2 partial pressure (pO_2) is equal to, or falls below, a tissue (cell)-specific critical value [57]. For a healthy subcutaneous tissue, the median pO_2 usually lies between 40 and 60 mmHg where a regulated (more or less constant) O_2 consumption rate is matched by high oxidative (mitochondrial) adenosine triphosphate (ATP) production rates, which allow aerobic metabolism. In growing tumors [58], the widening supply/demand imbalance yields median pO_2 of, approximately, 10 mmHg [59], thus indicating severe local hypoxic microenvironment across the neoplasm, accompanied by switch to anaerobe metabolism [57].

Tumor hypoxia triggers transactivation of numerous genes (below) and generally associates with the malignant progression of the disease along with heightened resistance to chemo/radiation therapy. Hypoxia-assisted genomic instability and mutations are known to exert a strong selection pressure on malignant cells [60], [61], which drives these cells

towards a more virulent phenotype and an increased tendency to develop distant metastases. Different subcategories of tumor hypoxia are diffusion-, perfusion-, or anemia-related [60]–[62]. Diffusion-related hypoxia is caused by inadequate O_2 /nutrient supply to distant cells (>70 μm) from nearest blood vessel mainly due to increase in diffusion distance as an aftermath of tumor expansion. Perfusion-related hypoxia is mainly caused by inadequate blood flow to tissue, while anemia-related hypoxia describes a reduced O_2 carrying capacity of the blood, mainly because of tumor- and/or therapy-induced anemia [60]–[62].

Regardless of subtype, pathological angiogenesis sparked by growing malignancies is notorious for yielding tortuous and leaky vessels along with a highly erratic blood flow. Most solid malignancies, particularly highly aggressive ones such as glioblastomas, colon carcinomas and renal cell carcinomas, are actively engaged in *de novo* vascularization. In this regard, tumor angiogenesis has opened a critical therapeutic opportunity as many entities strictly depend upon growing new vessels to achieve a size beyond 1-2 mm^3 and to disseminate to distant organs [63] (see section: 1.3: *Tumor Microenvironment and Angiogenesis*). As outlined above, tumor hypoxia is critical and responsible to initiate angiogenesis in the attempt to counter increasing diffusion insufficiencies of nutrients and oxygen [64], [65], which, for solid malignancies, is considered to be rate limiting for further development and spreading [63]. The main angiogenic cytokine, VEGF [66], [67], and its endothelial-specific receptors VEGFR1 (Flt1) and VEGFR2 (KDR/Flk1) [68], [69], are known to be co-induced by cancer cells during low oxygen partial pressures (pO_2) in part via the hypoxia inducible factors 1 and 2 (HIF-1/-2) to generate new capillary sprouts which are believed to aid, as the tracheal ramification in *Drosophila* does, in maintaining the oxygen carrying capacity of the vasculature during hypoxia. Particularly neoplasias with high local vascular permeability often show VEGF/ PlGF overexpression [70]. Other factors frequently seen to be involved in tumor angiogenesis include PDGF, FGFs, Ang2, epidermal growth factor (EGF), transforming growth factor beta-1 (TGF-β1), interleukin 1-beta, tumor necrosis factor alpha, and matrix metalloproteinases [71]–[73]. Because many tumors are able to induce production of VEGF in their surrounding stromal tissue [73], and since the basal lamina, exposed during this vascular leak, is prone to recruit and trigger platelets to

release permeability and angiogenic factors in the local environment, both types of paracrine signaling will further intensify the local angiogenic response (figure 3) [74].

It, thus, emerges that both growth and spread of solid malignancies critically depend on angiogenic signaling pathways, whose balance, however, has frequently been tipped in favor of neovascularization (figure 3). Importantly, and counter to common perception, tissue (tumor) oxygenation generally shows little, if any, signs of improvement despite ongoing angiogenesis. Tumor angiogenesis does little to prevent or mitigate the development of tissue hypoxia during growth. As point in case, recent spectral imaging studies by Hardee *et al.* on microvessel hemoglobin saturation clearly demonstrated that, even in areas of very active angiogenesis in tumors, a significant portion of the neoplastic tissue contained deoxygenated blood from trapped and hemorrhaged red blood cells [75], [76]. Collectively, erratic perfusion, endothelial leakiness, edema and continually impaired tissue oxygenation all contribute to the non-productive form of angiogenesis typically seen in tumors [76], [77].

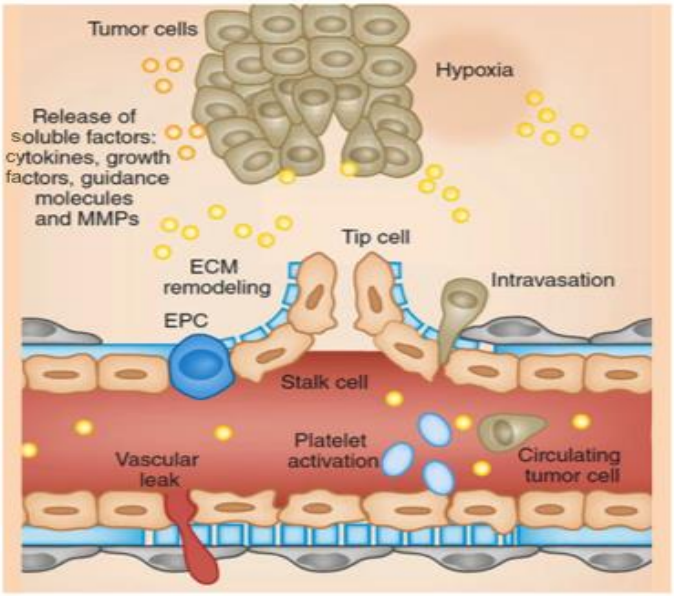

Figure 3: Angiogenic signaling pathways are induced and exploited by the malignant tumors with angiogenic switch tipped in favor of neovascularization. Major driver in this process is the oxygen tension within the tumors microenvironments (figure acquired from [78])

1.3 Tumor Microenvironment and Angiogenesis

Cancer cells are generally influenced by their surrounding microenvironment and are in constant adaptation to spatial and temporal changes of this milieu. The stromal component of this microenvironment is mainly composed of fibroblasts, myoepithelial cells, endothelial cells, macrophages, leucocytes and extracellular matrix (ECM). Early evidence about the effects of the environment on the tumor were reported in the 70s by Solt and Farber [79]. It has also been shown that pre-existing genetic mutation in the stromal tissue itself can mediate tumor formation in target epithelial cells [80], [81]. Monifer *et al.* showed that there are concurrent and independent genetic alterations in the stromal and epithelial cells of mammary carcinoma [80]. Upon transformation into a malignant cell, a number of signaling pathways are derailing.

Yet, the tumor microenvironment also has a crucial role in regulating the angiogenetic capacity of the mass via signaling between epithelial tumor cells and stromal fibroblasts [82]. Nearby tumor associated stroma is known to provide nutrients and oxygen to growing tumors through its vasculature [63]. To gain direct excess to blood vessels tumors have to first invade the surrounding stroma and transmit paracrine signals to induce angiogenesis. Solid evidence suggests the role of stromal cells in tumor progression, invasion and metastasis [83]–[85]. Regarding the cellular component, tumor microenvironments can be broadly classified into two categories, i.e. i) Cells already present in the tissue (e.g. fibroblasts, endothelial cells etc.) and ii) recruited cells (e.g. inflammatory cells, immune cells). In this section I discuss different tumor microenvironment associated cells and their critical role in tumor angiogenesis.

Fibroblasts regulate epithelial cell differentiation, inflammatory response to tissue insults and are also involved in synthesis and deposition of extracellular matrix (ECM) [86], [87]. Carcinoma-associated fibroblasts (CAFs) [88] present in the tumor microenvironment are thought to be involved in tumor progression [89]. As majority of ECM proteins (e.g. collagens, fibronectin) are produced by CAFs. CAFs play a foremost role to profoundly alter the ECM structure [90]. ECM accumulation around tumors leads to increased interstitial

fluid pressure thus obstructing the diffusion of nutrient and oxygen supply to tumors [91], [92]. Hence, CAF activity can induce tissue hypoxia/ischemia, which might lead to the stabilization of HIF-1α and, eventually, stimulated angiogenesis through VEGF induction. CAFs are also involved in tumor progression, as suggested in a recent mouse xenograft study by Orimo *et al*. [93]. According to this work, mixing human breast carcinoma cells with CAFs promoted tumor growth and angiogenesis through secretion of stromal cell–derived factor 1 (SDF1) from CAFs and the binding of the factor to the CXCR4 (C-X-C chemokine receptor type 4) receptor on tumor cells [93]. Furthermore, CAFs have been implicated in invasion [94] and metastases [95], [96]. In short CAFs have a significant role in promoting tumor growth and angiogenesis.

Basic fibroblast growth factor (bFGF) is a heparin binding growth factor (see FGF family description in section "Angiogenesis in Physiology") that motivates tumor cell proliferation through FGFR signaling by both paracrine and autocrine modes [97]–[99].

Thrombospondin 1 (TSP1), a glycoprotein that facilitates cell-cell and cell-matrix interactions, acts as a strong angiogenic inhibitor [100]. TSP1 binding to CD36 on the endothelial cell surface renders these cells insensitive to VEGF [101], [102]. Moreover, TSP1 expressed in stroma shows an initial strong inhibitory effect on tumors [103]. However, several publications also show the down-regulation of TSP1 expression in numerous breast cancer cell lines [103], [104].

The cytokine TGF-β controls important cell functions like cell proliferation or cellular differentiation in most cells [105]. An interesting paradox exists with regard to the angiogenic effect of TGF-β [82]. While under in-vivo conditions a potent pro angiogenic effect was demonstrated [106] in-vitro data illustrated growth inhibition of endothelial cells by TGF-β [107], [108]. In addition, TGF-β1 is known to either stimulate expression of Tsp1 [109], [110] or of VEGF [111], [112]. In short, depending on the microenvironment, TGF-β can lead to pro-angiogenic changes via VEGF or anti-angiogenic changes via TSP1.

Platelet-Derived Growth Factors (PDGFs) are regulatory proteins that control cell growth and cell division. PDGF is a potent stimulator for FGFs expression [113] and eventually VEGF in tumor associated stroma [114]. Further, Brogi *et al*. showed inhibition of PDGF activity by administering PDGFR, which in turn inhibited tumor angiogenesis [111]. These data evidence PDGF to act as strong inducer of stromal VEGF expression. However the activity of PDGF still needs to be studied in details as it has also been shown to stimulate TSP1 (angiogenic inhibitor) expression [115].

The expression of hormones like estrogen and androgen also affects the tumor microenvironment. Both these steroids are thought to inhibit the expression of TSP1 [116], [117] but through different mechanisms. In a recent publication, Gupta *et al*. demonstrated estrogen to have a proangiogenic effect on estrogen receptor-negative breast cancers [118]. Lipid synthesis in stromal fibroblast is known to activate neovascularization of tumors. One component in this signaling is the production of sphingosine 1 phosphate, which is able to suppress Tsp1 expression and, that way, support tumor angiogenesis [119].

For tumor cells to show invasion and metastasis they have to be able to degrade the extra cellular matrix (ECM). Matrix metalloproteases (MMP) play a crucial role in matrix degradation and remodeling [120] and, eventually, in supporting tumor angiogenesis. By using MMP inhibitors (batimastat), Noel and colleagues succeeded in eliminating the tumor-promoting effect of fibroblasts in mice bearing MCF7 induced tumors [121]. In addition to this, MMPs are also involved in converting latent TGF-β to active forms, thus stimulating mammary tumors growth [122].

Bone marrow derived cells (BMDCs) are specialized cells that migrate to tumors often due to the secretion of chemokines by tumor cells or as consequence of a tumor-associated inflammatory response. BMDCs, nestled within the tumors microenvironment, are known to contribute to the malignant progression of various entities [123]–[125]. The most common cell types among BMDCs include mesenchymal stem cells, neutrophils, macrophages, mast cells, and T cells [126].

Mesenchymal stem cells (MSCs) have a unique differentiation plasticity along osteogenic, chondrogenic and adipogenic lineages [127]–[129]. The cells are abundantly recruited to inflammatory or wounded sites as well as locations of growing neoplasms. Within the tumor microenvironment, malignant cells secret a large variety of cytokines (CCL2, CCL7, and CXCL12 (SDF-1)) and growth factors (VEGF, bFGF, IL-8, EGF, HGF, and PDGF), all of which are potent cues for the recruitment of MSCs [130]–[134]. The precise mechanism of the role of MSCs involvement in tumor growth and progression is yet to be determined, but it is thought that MSCs promote tumor growth through secretion of pro angiogenic growth factors [135], [136].

Hypoxia and high lactate levels are responsible to recruit Tumor Associated Macrophages (TAMs) to both tumors and wounds [137]. TAMs, in turn, fuel the expression of pro-angiogenic growth factors (e.g. bFGF, VEGF, TNFα etc.) in the majority of solid malignancies [137]. Mast cells also confer proangiogenic effects in tumors as recently demonstrated by Soucek *et al*. In this work, Myc-induced pancreatic islet tumors were superior over control islets in recruiting mast cells for tumor expansion. In contrast, mast cell inhibitors rapidly elicited hypoxia and death of tumor cells [138].

1.3.1 HIF and Tumor Angiogenesis

Changes of gene activity at transcriptomic level are critical for cells to successfully adapt and survive periods of O_2- and nutrient-deprivation. The transcription factors HIF-1 (Hypoxia-inducible factor-1) and HIF-2, i.e. master regulators of the hypoxic cell response, are highly conserved heterodimeric protein containing O_2-regulated HIF-1α or HIF-2α subunits and a constitutively expressed HIF-1β subunit, also known as ARNT (aryl hydrocarbon receptor nuclear translocator). The α and β subunits of HIF are members of the basic-helix-loop-helix PER-ARNT-SIM domain (bHLH-PAS) family of transcription factors. Under normoxic conditions, HIF-1α/-2α are rapidly inactivated and degraded in an O_2-dependent manner whereas hypoxia results in stabilization, accumulation and finally

transcriptional competence of active alpha subunits. Stabilized HIF-1α/-2α subunits translocate into the nucleus of hypoxic cells where they form 1α:1β or 2α:1β heterodimers and, in this form, possibly control several hundreds of hypoxia-responsive genes [139], many of which are involved in angiogenesis (e.g., VEGF), anaerobic metabolism (e.g., glucose transporters and glycolytic enzymes; see next section for details), O_2 transport (e.g., erythropoietin), and other activities crucial for cell survival and metastasis [44], [45].

Contribution of HIF-1α in tumor growth is well documented. Studies in mouse models demonstrated a significant role for HIF-1 in tumor angiogenesis and growth [140], [141], despite the fact that signaling cascades other than HIF-1 also impinge on VEGF mRNA steady state levels in hypoxic cells. As outlined above, hypoxic conditions and activated HIF-1 will directly activate VEGF and VEGFR1 transcription [140], [142]. Higher expression of HIF-1α and VEGF correlates in human patients with more aggressive and malignant lesions [143], [144]. Carmeliet *et al.* demonstrated that loss of function of HIF-1α in mouse embryonic stem (ES) cells reduces hypoxia-induced expression of VEGF and prevents formation of large vessels in ES-derived tumors resulting in hypoxic microenvironments within the tumor mass [145]. A recent study on HIF-1α demonstrated autocrine signaling between VEGF and its receptors to regulate endothelial cell and tumor cell metabolism [146]. Deletion of HIF-1α in endothelial cells interrupts this loop necessary for hypoxic induction of VEGFR-2 by VEGF signaling through VEGFR-1 [145], [146]. These examples illustrate the predominant role of the hypoxic stimulus in the regulation of tumor angiogenesis.

Nitric oxide (NO), a free radical and important signaling molecule in the regulation of vascular tone is produced by nitric oxide synthases (NOS) via l-arginine-nitric oxide pathway [147]. Three distinct isoforms of NOS, neuronal NOS (nNOS; NOS1) [148], inducible NOS (iNOS; NOS2) [149], and endothelial NOS (eNOS; NOS3) [150] exhibit unique tissue/cell type distributions and regulatory mechanisms [151]. nNOS and eNOS are constitutively expressed with functions largely limited to neurons and endothelial cells [152]. NO and eNOS functions merge with the oxygen sensing machinery to define vascular

function and angiogenesis [153]. The third member iNOS is profoundly induced by hypoxia, particularly when co-occurring with inflammatory cytokines. Notably, endothelial iNOS is required for hypoxia mediated VEGF expression but does not affect expression of other HIF-1α responsive genes [154]. As a consequence, HIF-1α stimulated NO production would result in cooperation with VEGF to promote vascular permeability [155]–[158].

In addition to HIF, the induction of neovascularization in response to hypoxia can also be mediated by NF-κB (nuclear factor kappa-light-chain-enhancer of activated B cells) [159]. Schmidt *et al*. showed that junB, a hypoxia-responsive transcription factor activated by NF-κB, induces VEGF expression independent of HIF activity [160]. Given the multiplicity of mechanisms and target genes involved in angiogenesis, hypoxic microenvironments in tumors evidently promote angiogenesis, and hence tumor growth, via HIF-dependent and independent mechanisms.

1.3.2 Tumor metabolism (glycolysis)

In normal and transformed cells, presence of oxygen stimulates the complete oxidization of acquired glucose to pyruvate, and inside mitochondria further to CO_2 and H_2O, thus keeping the glycolytic conversion of glucose to the lactate end product at minimum. As long as O_2 is not limiting, oxidative phosphorylation of carbohydrate substrates yields up to 38 molecules of adenosintriphosphat (ATP) per glucose molecule whereas anaerobic glycolysis produces only 2 ATPs per glucose. Yet, once supply of oxygen starts to dwindle, glucose flux through glycolysis is markedly elevated to somewhat compensate for the far lesser energetic efficacy by higher substrate throughput (i.e. Pasteur effect [161]). In addition, cancer cells [162]–[164], but not only those (see below), are able to sustain their high mitotic activities on the basis of aerobic glycolysis. This so-called Warburg effect is characterized by a significantly increased rate of glycolytic sugar consumption and lactate build-up under aerobic oxygen tensions. When Otto Warburg first described prominent aerobic fermentation as unique dedifferentiation-feature of tumor cells some 80 years ago, he saw in it the tumor's compensatory reprogramming effort to the initial *and* cancer-causing insult: an irreversible

injury of respiration ("Die aerobe Glykolyse der Tumorzelle rührt in jedem Falle von einer Störung der Atmung her"; translation: "Aerobe glycolysis in tumor cells is *in every case* due to an impaired respiration"; O. Warburg, 1929) [165], [166]. Warburg had, in essence, associated the mutually antagonistic relationship between respiration (= impaired) and glycolysis (= activated), as formulated by the Pasteur effect, to the genesis of cancer. His discovery has had a very strong impact on the oncological community and, to this day, aerobic up-regulation of glycolysis [163] or a predominantly glycolytic metabolism in general [167] are regarded as near-universal property of primary and metastatic cancers, i.e. remain associated with tumorigenesis. However, during the post-Warburg era it became evident that a strong basal glycolytic capacity is neither the cause nor a universal characteristic of malignancies ([162], [168] for critical review on Warburg effect and its interpretation). Instead, cancer cells are able to carry out the oxidative phosphorylation of glucose by mitochondria in the presence of oxygen just as effectively as normal cells do. Aerobe cancer cells utilize, in absolutely comparable fashion to non-transformed cells, only minor (~20-25%) contributions of their ATP production from the anaerobic glucose-to-lactate conversion (e.g. McA-RH7777 Hepatoma [169], MCF7 breast carcinoma [170],) while fueling a ~75-80% fraction of their energy budget by the complete oxidation glucose-to-CO_2 oxidation [171], [172]. Moreover, a tight coupling between proliferative and glycolytic rates exists even in non-cancer cells (i.e. primary thymocytes), as was revealed by Brand and Hermfisse [173], [174]. According to these authors, resting thymocytes meet 88% of their ATP demands via oxidative glucose breakdown, whereas proliferating thymocytes switch almost entirely to glycolysis and gain 86% of their ATP from glucose-to-lactate catabolism. As hypothesized by Brand and Hermfisse, this switch to glycolysis in fast growing cells and tissues could, through the production of potent scavengers for reactive oxygen species (ROS) (i.e. pyruvate), be part of an antioxidant strategy to minimize oxidative stress during sensitive phases of the cell cycle (i.e. S phase, above) [173], [174]. Thus, a Warburg effect-type glycolysis is neither restricted to cancerous backgrounds nor does it derive from dysfunctional oxidative processes or is, in any way, causally linked with the development of tumorigenesis.

1.3.3 Production and uptake of lactate in cancer cells

Through anaerobic glycolysis a significant proportion of pyruvate is reduced into lactate by lactate dehydrogenase (LDH). Physiological concentrations of lactate in normal tissues fluctuate around 1.8 - 2.0 mM. In contrast, 4 - 40 mM lactate may occur in human tumors such as cervical cancer [175], [176]. Deoxygenated tumor cells export lactate together with protons through the monocarboxylate transporter 4 (MCT4), a member of the lactate-proton symporter family, and that way avoid intracellular acidification [177]. Yet, in stark contrast to cultured cancer cells, in tumors the exported lactate is not lost as extracellular waste but "recycled" by oxygenated cells via monocarboxylate transporter 1 (MCT1) where it fuels the oxidative metabolism (TCA cycle). It becomes clear that glycolytic and oxidative tumor cells mutually regulate their access to energy metabolites and that monocarboxylate transporter (MCT) proteins are at the heart of this interdependence.

The MCT family in humans consists of 14 members (MCT1-MCT14), encoded by the SLC16 gene family [178]. The stereotypical MCT protein has intracellular N- and C-termini, 12 transmembrane helices (TMs), and a large cytosolic loop between TMs 6 and 7 [179]. While MCT1-4 are all known to facilitate the proton-linked transport of metabolic monocarboxylic acids such as lactic acid, MCT1 functions primarily in the uptake/import of monocarboxylates through the plasma membrane. Besides being a high affinity importer for L-lactate, MCT1 can also shuttle acetate, pyruvate, D-β-hydroxybutyrate, acetoacetate and propionate across the membrane [178]. Compared to other family members, MCT1 evidently transports a rather wide range of carboxylates. MCT2 has, relative to MCT1, a higher affinity for L-lactate, pyruvate, acetoacetate and D-β-hydroxybutyrate. Since MCT1 and MCT2 are situated on different cells when expressed in same tissue they may occupy different roles as metabolic shuttles [180], [181]. MCT3 was first identified in chicken and is only expressed in specific tissue (choroid plexus and retinal pigment epithelium) [182], [183]. MCT4 is mainly associated with the export of lactate from cells with high glycolytic fluxes (i.e. Pasteur effect) during hypoxia [177]. Hence, MCTs make important contributions to the carcinogenesis, malignant progression and spreading of cancer cells by playing a dual role:

by exporting lactate from hypoxic and importing it into aerobic regions, they are vital to the interactive symbiosis between differently oxygenated tumor areas. By exerting pH control functions (lactate/H^+-symporter), they are key to the emergence of the acid-resistant phenotype.

1.4 Anti-angiogenic cancer therapy: Yin and Yang

Angiogenesis inhibitors (AIs), i.e. compounds that specifically block the sprouting of capillaries from pre-existing blood vessels (= angiogenesis), have been considered a breakthrough in cancer therapy for many years. Currently (2013) numerous different anti angiogenic drugs (bevacizumab, aflibercept, sunitinib, sorafenib, pazopanib, everolimus and axitinib) have been approved by the FDA for the treatment of 10 different types of cancer [184][185]. However, clinical experience with AIs showed that while these compounds work well in slowing the growth of primary tumors they can trigger cancer recurrence and increasing incidence of metastasis. Also the effect of anti-angiogenic therapy is short-lived, as withdrawal from such treatment induces rapid re-growth of tumor vessels and relapse [186], [187]. In addition, two major papers by Pàez-Ribes *et al*. and Ebos *et al*. in *Cell* demonstrated the role of antiangiogenic therapy as a driving force in tumor progression to stages of greater malignancy, echoed by increased invasion into surrounding tissue and in some cases boosted lymphatic and distant metastasis [188], [189]. AI therapy presumably raises the tumor´s aggressiveness by increasing both extent and severity of tissue hypoxia within the targeted mass (figure 4). In contrast, treatments that normalize the usually chaotic tumor vasculature with its erratic blood flow were indeed able to elevate *in vivo* oxygen tensions within the malignant mass in correlation with a reduced occurrence of cancer spread. Thus, normalized tumor blood supply is associated with a therapeutic gain.

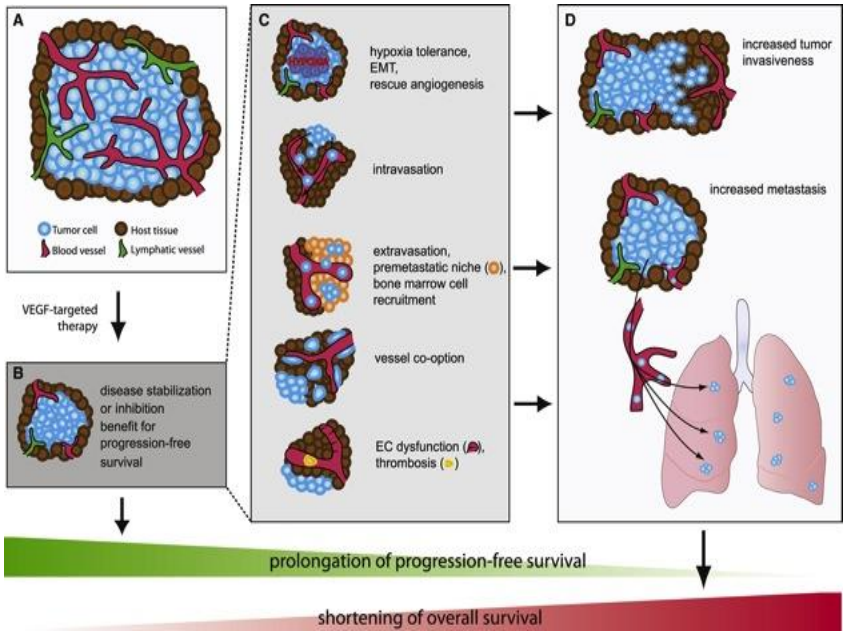

Figure 4: Mechanistic model how antiangiogenic therapy induces increased tumor invasiveness and metastasis reducing overall patient survival. a) Growing tumor inducing angiogenesis, b) Anti-VEGF therapy leads to slowing the growth of primary tumors, c) Anti-VEGF therapy presumably raises the tumor´s aggressiveness by increasing both extent and severity of tissue hypoxia within the targeted mass, d) thus triggering cancer recurrence and increasing incidence of metastasis (figure acquired from [192]).

In addition to the sobering clinical outcome of AI therapy, the impact of AI compounds on fundamental physiological parameters such as vascular normalization, blood flow and local tissue oxygenation within the tumor are insufficiently understood, despite the frequent use of these drugs to combat cancer growth and malignant progression. This enormous gap between goal and reality is mostly due to the lack of good pre-clinical models to evaluate tumor angiogenesis and its responses to different anti-angiogenic compounds.

To target tumor angiogenesis and, that way, tumor size and virulence, a panoply of drugs has been tested and several advanced into clinical use (cf. above). Along with the heightened risk of cancer recurrence, the clinical application of AI drugs showed a number of severe side effects such as hypertension, kidney damage or arterial thromboembolic events. Given that tumor angiogenesis can result from several parallel hypoxia signals, any single-agent approach seems insufficient to induce adequate tumor responses and subsequent

improvement of the disease-free and overall survival [76], [190]. Not surprisingly then, mono-therapeutic angiogenesis inhibition protocols have yet to deliver convincing evidence for tumor remission [190]. Even excessive vascular regression in the tumor with high doses of anti-VEGF/anti-VEGFR protocols may be counterproductive because it basically leaves (much of) the tumor inaccessible for blood-born cytotoxins. Thus, there is growing awareness that tumor angiogenesis mechanisms are rather heterogeneous and that they may or may not depend on VEGF-signaling. In addition, very recently published work suggests that the principle heterogeneity of the tumor regarding its energy metabolism favors the selection of the most aggressive and hypoxia tolerant tumor cell clones as an unwanted side effect of any anti-angiogenic therapy (figure 4).

A major consequence of the insufficient, yet over-stimulated, tumor vasculature is the fact that most solid tumors, regardless of type and despite continuing angiogenesis, nonetheless develop severe regional hypoxia as they grow, due to a progressive mismatch between the high O_2 demands of proliferating cells and the erratic or inadequate O_2 supply by the tumor's vasculature (see sections: 1.2.1: *Pathological angiogenesis with particular focus on tumors* for background). As hypoxic tumor cells are forced to primarily use glucose for glycolytic energy production and will release lactic acid as end product, this footprint of anaerobe glycolysis activity by the hypoxic patches is known to create a lactate gradient in inverse orientation to the oxygen gradient across the malignancy. However, *in vivo* this lactate is not lost but re-used by well oxygenated cancer cells [191]. Not only are tumors a metabolic patchwork of aerobic and hypoxic cells, but the ratio of both populations might change upon medical treatment. Anti-angiogenic monotherapy, for example, was unexpectedly found to select for more hypoxia tolerant tumor cells that can withstand hypo-perfusion better but are also more prone to produce metastases [76], [77], [192]. Therefore it is mandatory to address hypoxia resistant tumor cells specifically and in parallel with an anti-angiogenic cancer therapy. For all these reasons, a "back-to-the-board" reevaluation of anti-angiogenic therapies by proper pre-clinical models is urgently needed [77], [192], [193].

1.5 New therapeutic anti-cancer strategy

In answer to this need my thesis project intended to analyze and target certain metabolic pathways and angiogenesis of glioblastoma, breast carcinoma and melanoma cells, explanted on the surface of the chorioallantoic membrane (CAM) of the chick embryo. As noted above O_2 profiles across solid tumors are quite heterogeneous. Effective anti-cancer therapies, therefore, need to target not only the oxygenated/aerobe compartment of the tumor but also the severely hypoxic/glycolytic cells. This overarching goal should be considered because a selective kill of oxygenated cells might leave too many surviving hypoxia tolerant cell clones. Ensuing selection among these clones might only further malignant progression in the residual mass, and, that way, greatly assist in the emergence of a phenotype prone to develop therapeutic resistance and a highly metastatic behavior (figure 4, 5).

Thus, to reduce the incidence of tumor recurrence and spread a strategy needs to be worked out, which aims to kill cells in vessel-remote, deeply hypoxic areas of the tumor in parallel with anti-angiogenic therapies to prevent or minimize this selection toward more aggressive tumor cell clones. Such an aerobe-/hypoxic-area hitting strategy could combine AIs such as Avastin® (VEGF antibody), with the Monocarboxylate Transporter 1 (MCT1) CHC that blocks lactate uptake. The groups of Mark Dewhirst (Duke Univ. Med. Center) and Pierre Sonveaux (Univ. Louvain Med. School) were previously able to show that the CHC blockade of the MCT1-mediated uptake of lactate is able to drive oxygenated tumor cells to commit to aerobic glycolysis through the acquisition and use of glucose instead of lactate as prime energy providing substrate. Through CHC treatment, oxygenated cells start to increasingly compete with hypoxic areas for glucose, which can eventually result in a highly efficient kill particularly of hypoxic cells. According to this concept, inhibition of MCT1 should trigger a re-routing of glucose from hypoxic to oxygenated cells, thereby dooming the hypoxic cells due to glucose starvation (figure 5). A more efficient treatment of hypoxia tolerant cells residing in deoxygenated tumor regions and, in consequence, a more efficient means in opposing an emerging therapeutic resistance of the cancer, can fruitfully exploit the reliance of these cells on glucose-fueled anaerobic glycolysis together with the above mentioned concept of the tumor as a metabolic symbiont [191].

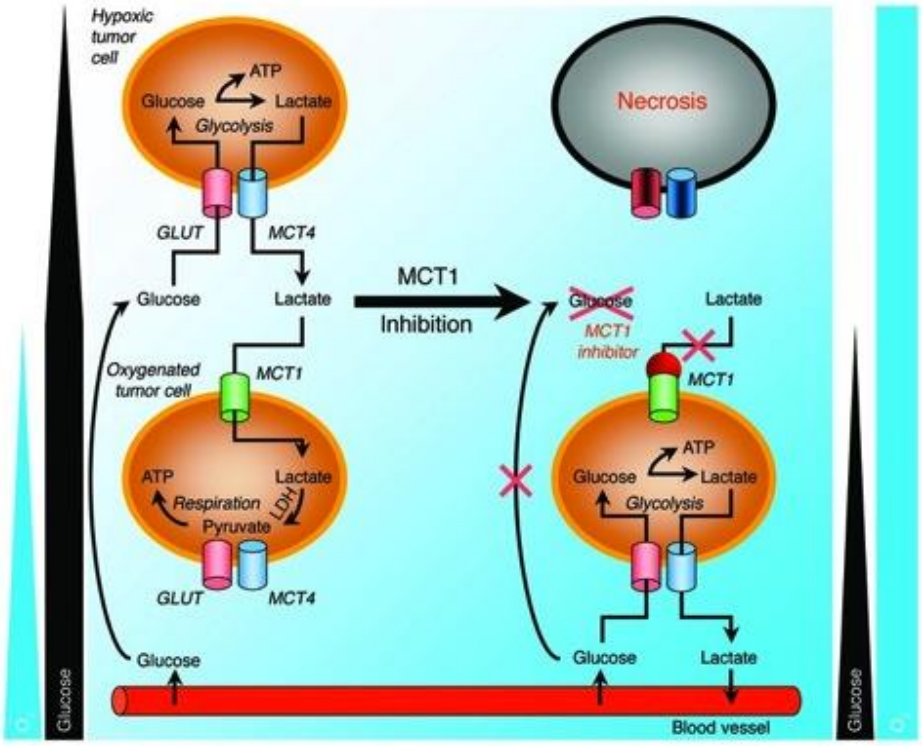

Figure 5: Lactate released from hypoxic cells is recycled by well-oxygenated cells of the tumor where it fuels high rates of oxidative substrate turnover and respiration. This oxidative signature spares glucose from consumption by oxygenated cells and allows the sugar to diffuse into the hypoxic areas of the neoplasm where it sustains anaerobic metabolism. Blocking lactate uptake by inhibition of MCT1 triggers a re-routing of glucose from hypoxic to oxygenated cells, thereby dooming the hypoxic cells due to glucose starvation (figure acquired from [191]).

Coinciding with the lactate-import function by aerobe cells, MCT1 protein in xenografted tumors was mainly expressed within well-vascularized (positive CD31 staining) and oxygenated (negative HIF-1α and pimonidazole staining's) tumor margins. In contrast, hypoxic (positive HIF-1α and pimonidazole staining) and poorly vascularized regions of the tumor were completely devoid of MCT1 signal [177], [191]. Importantly, upon selective inhibition of MCT1, either by CHC treatment or as shRNA-driven knockdown, oxidative tumor cells switched from lactate oxidation to aerobic glycolysis (i.e. acquisition of Warburg phenotype). This prevented adequate glucose delivery to glycolytic hypoxic cells, which consequentially, died from glucose starvation even at a high distance to the drug-supplying blood vessels [191]. This glycolytic switch was associated with a decrease in oxygen

consumption of surviving tumor cells and, consequentially, an increasing tumor pO_2 [191]. Thus, MCT1 inhibition is a potent anti-cancer strategy that indirectly eradicates hypoxic/glycolytic tumor cells and thus might render hard-to-treat malignancies more susceptible to therapy. The combination of MCT1 inhibition (to target hypoxic cells) with vessel normalizing agents (to render oxygenated cells more accessible for blood born drugs) is conceptually a very promising and completely novel approach.

1.6 Chorioallantoic membrane (CAM) assay

One century ago a US biologist J.B. Murphy showed that inoculation of Jensen rat sarcoma in developing chick embryos gives a fast growing tumor and could be maintained by continuous passage from egg to egg [194]. Fertilized chicken eggs (embryos) during their early stage of development are considered a border line model that bridges *in vitro* and *in vivo* systems and provides a highly vascularized membrane scaffold to study angiogenic processes in the context of tumorigenesis. Moreover, the CAM assay during the early stages of chick development is not considered an animal experiment (see below for rationale). Thus, CAM-based screens of AI protocols will help to reduce the number of animals needed in pre-clinical tests of anti-tumor compounds.

CAM assays involve the xeno-grafting of tumor cell explants on top of the developing CAM. The developing chick embryo possesses four extra-embryonic membranes, including the a) yolk sac, b) allantois, c) amnion, d) serosa (chorion) membrane. On day 3.5 (d3.5) of embryo development the allantois appears from the ventral wall of endodermal hindgut. The allantoic vesicle expands very rapidly from d4 to d10. During this period the fusion of the mesodermal layer of allantois with the mesodermal layer of the chorion generates the CAM. The CAM develops an extremely rich vascular network that is connected via allantoic arteries and veins to the embryonic circulation. By d8 immature blood vessels and smooth muscle cells dispersed into the mesoderm, grow quickly to give rise to the capillary plexus. Rapid capillary proliferation is seen until d11 after which it starts to decline. By d14, the capillary plexus is well located at the surface of the ectoderm and by d18 the vascular system has

reached its final topography [195]. Eventually, by day 14, the mean surface area of the CAM measures approximately 65cm^2 [196], while the thickness of the fully expanded CAM ranges between 20-100 µm [197], [198]. In addition to the respiratory exchange of oxygen and carbon dioxide as "embryonic lung", the CAM also serves as reservoir for waste products (urea in early development; uric acid in later development). It is also involved in calcium mobilization from the shell, during bone growth [199].

The CAM assay represents a valuable methodological alternative to the most commonly used model of experimental tumors: xenografted cancer cells in immunodeficient mice. This inoculation of tumor cell lines into mice has several disadvantages. First, such models are limited with respect to the number of tumors that can be observed within one animal. Second, the accessibility of the tumors is generally hampered by at least the skin of the animals. In the *ex-ovo* mode of a CAM assay (figure 6) the membrane can be inoculated with several different tumors in parallel and is not covered at all by host tissue [200]–[202].

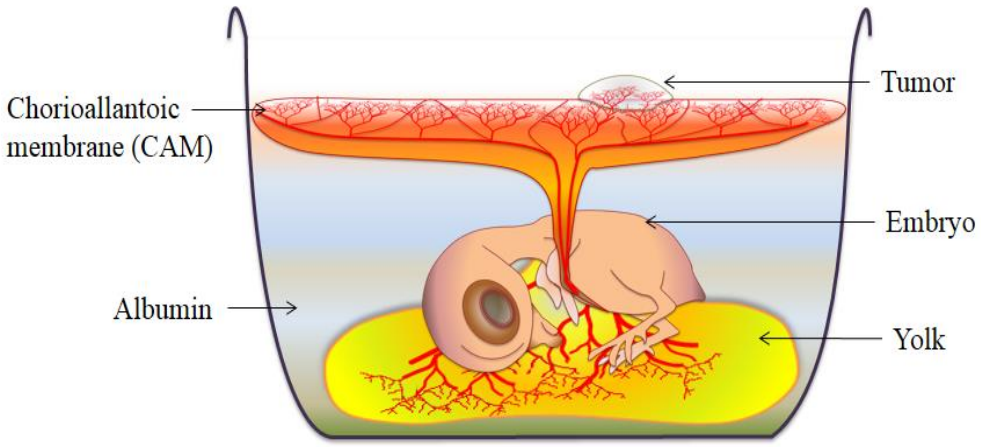

Figure 6: E*x-ovo* assay enhances the accessibility of the CAM and chick embryo, allowing easy *in vivo* documentation of effects and facilitating experimental manipulation of the embryo.

Hence, tumor grafts are directly accessible, a huge gain for controlled manipulations (e.g. drug application) or optical readout methods. Third, the use of tumor models in animals is always an ethical problem due to potential suffering of the animals. In contrast, the CAM contains no nerves during early embryo development; thus tumor growth cannot induce pain

in the embryo. Consequently, by Swiss law the CAM assay is not considered an animal experiment up to embryonic day 14.5 of development [203], [204]. Fourth, owing to the lack of a mature lymphoid system, early stage chick embryos are naturally immunodeficient and, thus, cannot reject xenogenic tumor cells [200]–[202]. Fifth, the CAM assay greatly facilitates a high throughput of tumors treated with different therapeutic strategies. It also serves as repository for cells that escaped from the primary site and intravasated into the host vasculature or organs, thus, making the CAM an excellent tool to study kinetics and single step processes of tumor cell metastasis under quasi *in vivo* conditions [200]–[202]. There are number of modifications for the original chick embryo assay. Commonly used are *in-ovo* and *ex-ovo* assays. In *in-ovo* assays a small window is made into the eggshell and experiments are carried out on top of the CAM within the egg. This approach has significant limitations, in assessing CAM and photo documentation of experiments. Yet, *ex-ovo* assays (figure 6) enhance the accessibility of the CAM and chick embryo, allow easy *in vivo* documentation of effects and facilitate experimental manipulation or observation of the embryo. For example, with laser perfusion-imaging technique [205] applied on *ex-ovo* assay real-time monitoring of tumor blood flow can be done.

2. Specific Aims

i) To establish a pre-clinical angiogenesis model of different tumor types in form of the *ex ovo* chicken chorio-allantoic membrane (CAM)/tumor cell explant assay as a fast, cheap, easy-to-implement and animal-saving methodology for pre-clinical drug screenings. By using this bioassay we will assess the following parameters *for explanted tumor cells:* a) tumor growth, b) vascular functional performance (real-time blood flow using Laser-Doppler imaging; permeability of Evans blue), c) tissue oxygenation (pimonidazole staining), d) *in vivo* cell migration (ddPCR), e) Metastasis detection (MRI).

ii) anti-angiogenic Avastin® (VEGF antibody), monotherapeutic treatment;

iii) The same pro-/anti-angiogenic protocols as under (ii) but now in combination with an anti- monocarboxylate transporter 1 (MCT-1 inhibitor: CHC) strategy.

Regarding aim iii, angiogenesis inhibition is commonly regarded not only to starve the tumor by reducing the rate of vessel growth per time unit but also to spark normalization of both structure and function of the tumor vasculature in the attempt to raise the efficacy in the specific targeting of the tumors' oxygenated compartments close to blood vessels. In contrast, the anti-MCT1 protocol has recently been put forward as novel and effective means to selectively kill profoundly hypoxic tumor cells that are for example less radiosensitive. Thus, under (iii), both oxygenated and hypoxic compartments should be targeted, which is expected to shift the ratio between hypoxia tolerant and hypoxia sensitive cells in the tumor towards the ladder, which in turn, should sensitize the malignancy.

3. Materials & Methods

3.1 Reagents:

All cell culture media and media supplements were purchased from GIBCO Switzerland. The anti-VEGF antibody Bevacizumab (trade name: Avastin®, hereafter abbreviated AVA) was purchased from Roche (Genentech) Switzerland. α-Cyano-4-hydroxycinnamic acid (C-2020) (abbreviated as CHC) and Razoxane (ICRF 159; (±)1,2-di(3,5-dioxopiperazin-1-yl) propane) were bought from Sigma-Aldrich (R8657) (Switzerland) and Sunitinib (*N*-[2-(Diethylamino)ethyl]-5-[(*Z*)-(5-fluoro-1,2-dihydro-2-oxo-3*H*-indol-3-ylidene)methyl]-2,4-dimethyl-1*H*-pyrrole-3-carboxamide) (SUTENT) from Pfizer (Switzerland).

3.2 Cell Lines

Glioblastoma: U-87 MG (HTB-14TM) and murine melanoma: B16-F10 (CRL-6475TM) cell lines used in this study were purchased at ATCC® (American Type Culture Collection). Several lines were generously handed to us, i.e. MDA-MB231 cells from Prof. E. Dahl, (University Hospital of the Rheinisch-Westfälische Technische Hochschule Aachen, Aachen, Germany), Ewing Sarcoma cells (A4573 line) from Prof. Kontny (University Medical Center Freiburg, Freiburg, Germany) and renal clear cell carcinoma cells with (i.e. RCC4) and without (i.e. VHL reverted cell line: RCC4/VHL) loss-of-function (LoF) mutation in the VHL tumor suppressor gene from Prof. M. Wiesener (University of Erlangen-Nuremberg, Erlangen, Germany). Human hepatoma (Hep3B) and melanoma (501) cells [206] and breast carcinoma (MCF7, MDA-MB468) cells [207] were used in earlier publications of the laboratory and were available in the lab as stocks.

3.3 Cell Culture

Cell lines Hep3B, U87, RCC4 with VHL LoF (=RCC4) plus RCC4 with reconstituted wildtype VHL allele (=RCC4/VHL), MCF7, MDA-MB468 were all cultured in Dulbecco's Modified Eagle's Medium (DMEM). Eagle's minimum essential medium (EMEM) was used

for B16F10 cells, while 501 melanoma and Ewing Sarcoma cells were cultured in RPMI medium (RPMI Media 1640). Each medium contained high glucose levels (4.5g/l) was supplemented with 10% Fetal Bovine Serum (GIBCO 10270-106) and 1% penicillin/streptomycin. To maintain the selection pressure in RCC4 and RCC4/VHL cell lines the G418 (0.5mg/ml) aminoglycoside antibiotic was added to the medium at all times. All cell lines were maintained at 37°C in water–saturated room air with 5% CO_2 and an oxygen-partial pressure (pO_2) of 141.6 mmHg ([O_2] = 18.6% O_2).

3.4 Fertilized chicken eggs

Fresh fertilized eggs were purchased from a local hatchery (Animalco AG; Staufen, Switzerland; http://www.animalco.ch). In the laboratory eggs were stored at 10°C for up to one week before commencing incubation and embryo development. For egg incubation, a HEKA cabinet incubator with fully automatic egg-turning capacity (HEKA-Format) was used. The eggs were continually rotated throughout the incubation period at 37.5°C and a humidity of 60-62% for 72 hours before starting the CAM assay. To maintain aseptic conditions when preparing the embryos *ex ovo,* all used tools where wiped with 70% ethanol (ETOH) while other reagents maintained under sterile conditions. Prior to incubation all eggs were thoroughly wiped with paper towels soaked with 70% ETOH to remove any feathers, dirt and excrement [208].

3.4.1 Ex ovo CAM assay

After 72 hours of incubation the eggs were wiped again with 70% ETOH and marked on the topside to indicate the side of the embryo and keep it in an upright position. On days 3 of chick development eggs were cracked horizontally with the marking facing up, through gentle blows on a metal edge lying perpendicular to the long axis of the egg. Sufficient cracking led to leaking of egg white, which indicated the beginning perforation of the egg membrane. Trough gentle pressure along the egg`s equator the egg finally opened and it's in contents were gently poured into small, sterile plastic bowls with intact yolk sack containing embryo and yolk vessels on top. These *ex-ovo* chicken cultures were then covered

with petri dish leads and placed into incubators (Forma Scientific, Model-3336), were they were kept at 37°C and 60% humidity for the entire duration of the experiment. As all experiments were terminated before embryonic day 14.5 the CAM assays of this study were not considered an animal experiment according to Swiss legislation.

3.5 Cell Preparation and Tumor Explants

Prior to explanting cancer cells onto the CAM, or i.v. injecting them into the circulation of the membrane, cells were processed by trypsin/EDTA detachment and re-collected by centrifugation at 1000 rpm for 4 min, supernatant removal and a repeat spinning step for 2 mins to remove all remaining supernatant. Cell pellets were then re-suspended in medium at a final concentration of 4 million cells per 15 μl. On day 9 (d9) of chicken embryo development, 4 million cells (15μl) were explanted onto the CAM to trigger tumor formation. CAM survival was recorded for chicken embryos having single tumor explants, multiple (two) tumor explants and no explants at all. Similarly i.v. injections of tumor cells were also accessed to check chicken embryo survival.

3.6 CAM-cell line assessment

The suitability of the CAM models for development and malignant progression of tumor explants was assessed using nine different cell lines, including human Hep3B hepatoma, 501 melanoma, U87 glioblastoma, RCC4 and RCC4/VHL renal cancer, MDA-MB-468 andMCF7 breast carcinoma, A4573 Ewing sarcoma lines, as well as the murine B16F10 melanoma line. Initially, $2x10^6$ cells were loaded at off-center locations of the CAM that did not directly superimpose with the embryo (see figure 6) on d9 of chick embryo development. The media volumes of cells to be explanted ranged from 10-50 μl. Direct pipetting of the cell suspensions onto the CAM surface was found to yield superior rates of growing tumors compared to various cell retaining scaffolds (e.g. Teflon rings, 1% methylcellulose solution, miniature cotton balls, filter paper disks etc.).

Successful tumor establishment of the above cell lines was analyzed by scoring growth, solid mass formation (3D structure) and angiogenesis on d14 of embryo development. Positive scores were given, if growth (i.e. increase in surface area of tumors) was observed and negative scores for dried cell mass (dead cells) with no growth. Similarly, explants were observed for solid mass formation. Positive scores indicated tumor explants forming spherical structures on the CAM, whereas negative scores indicated cells diffusing away from the application site. Regarding angiogenesis, positive scores resulted when major vessels turned towards cues from the tumor explant and/or smaller vessels (capillaries) were being formed in the periphery of the neoplastic mass. Negative scoring was applied when no such vascular changes were visible. Scoring was carried out for each parameter to select a suitable cell line. Based on these three criteria, U87 cell line was finally selected as the line of interest for further experiments.

3.7 In vitro and chicken embryo-toxicity assay

Use of drugs at non-toxic concentrations was ascertained by applying a) increasing concentrations of the reagents mentioned above to cultured cells (*in vitro* toxicity), and b) doses of the respective compound, corresponding to validated safe-usage applications with human patients (see below), onto the CAM on d10 of embryo development (i.e. *in vivo* toxicity).

Regarding (a), cytotoxic effects of different anti-angiogenic drugs to U87 cells were assessed for concentration ranges shown in Table 2 with cultures kept at an average confluency of 80%. Stocks were prepared as follows: Sunitinib 40mg/ml in DMSO, Razoxane 40mg/ml in DMSO, CHC 1mol/l in DMSO and AVA 25mg/ml. 24 hours after drug application, cell viability was assessed via Trypan blue dye exclusion assays by staining a 1:1 dilution of the cell suspension with a 0.4% Trypan Blue solution. Cell counts were then determined using a Neubauer Counting chamber. (BLAUBRAND® counting chambers, Cat. No. 718605).

Table 2: Drug treatment on U87 cells.

Avastin®	0 mg/ml (PBS)	0.01 mg/ml	0.05 mg/ml	0.1 mg/ml	0.5 mg/ml	1 mg/ml	5 mg/ml
Sunitnib	0µM (DMSO)	0.01 µM	0.1 µM	1 µM	10 µM	100 µM	
Raxozane	0 µM (DMSO)	5 µM	10 µM	50 µM	100 µM	200 µM	
CHC	0 mM (DMSO)	5 mM	10 mM	15 mM	25 mM		

Regarding (b), calculated mg/kg embryo concentrations of the respective drugs used embryo weights taken from published chick embryo development charts [201], [209] along with non-toxic, yet effective, doses from human applications. Normally on d10 of development, the chick embryo weighs on average 2.26 gm. Thus, 0.0226mg of AVA (derived from 10mg/kg for human application of AVA IgG; [210]), 0.00226mg of Sunitnib ≅ 1mg/kg (derived from 50 mg orally once daily [211]), and CHC (60mg/kg) were applied onto the CAM. The 60mg/kg dose of CHC was used based on *in vitro* cell toxicity data and the fact that 100mg/kg CHC and 80mg/kg showed complete inhibition of tumors [212]. Thus to study the effect of AVA in combination as well, CHC concentration was reduced to 60mg/kg.

In addition, the outcome after i.v. injection of the same amount of AVA into CAM vesssels was examined. As control, an equal volume of PBS was loaded onto another CAM. Embryos were observed until day 14.5 for any occurring fatalities.

3.8 Drug treatments

On d10 of embryonic development, one day after tumor cell explants the chicken embryos were treated with anti-angiogenic drug treatment AVA (10mg/kg), with MCT1 inhibitor CHC (60mg/kg) alone and with the combination of both compounds. Body weight of living embryo on day 10 was taken into consideration while loading drugs [201], [202].

3.9 Impact of drug treatment on tumor growth

Growth kinetics of U87 tumors was monitored by taking digital images of tumors on developmental days 10, 12 and 14. These images where analyzed with MCID^{TM} software by marking the tumor borders and assuming a spherical volume of the explanted mass (i.e. volume v=4/3πr3, with r=1/2√ (D1xD2)). The treated tumors were compared to controls, whose volume was set to 100% [213]. Starting with an initial volume set to 100% on day 2 (embryo development d10) post-explantation, the relative volume increase on day 4 (embryo d12) and 6 (embryo d14) of AVA, CHC and AVA+CHC treated tumors was compared to PBS-treated control explants.

3.10 Assessment of perfusion

Blood flow around the tumor periphery was measured by employing real-time Laser Doppler perfusion imaging (moorFLPI, Moor Instruments) [205] that measures blood flow in microcirculation without physical contact with the tissue or the use of dyes or tracer elements. The techniques works, in principle, by irradiating low power monochromatic light onto the tissue and collecting returning photons, whose frequency spectra show considerable broadening due to their multiple scatterings by moving blood cells. This Doppler shift-based change of the laser frequency is then analyzed. The result is a computer-generated color-coded image of the spatial distribution of micro vascular blood flow. Red colors indicate maximal, and blue tones least, amount of motion (figures 12b, e). Next, relative fluxes can be calculated in the region of interest using the software provided with the laser Doppler imaging system. Routine applications grafted 4 million tumor cells onto the CAM and allowed tumors to grow for 6 days. Laser Doppler measurements on d14 of embryo development (6 days after tumor explantation) were performed by focusing the imager specifically on the tumor (as major area) and the surrounding CAM tissue. To block background interference due to the yolk sack perfusion, different contrast solutions such as Evans blue, Trypan blue in glycerol/PBS in varying concentrations, were injected beneath the CAM. While these dyes reduced the motion artifacts to some extent, results were still inconclusive, presumably due to the protocols poor compatibility with the chicken embryo.

Injecting the contrast agents directly underneath the chorioallantoic membrane into the egg white often resulted in the premature death or stunted growth of the embryo. Eventually, however, a small cut into a poorly vascularized region of the CAM allowing the insertion and placement of a spoon-shaped strip of polystyrene plastic directly underneath the tumor explant prior to readout, was found to be superior in blocking background noise from tumor-associated perfusion signals (figure 12).

Next, relative fluxes were calculated in the region of interest using software provided with the laser Doppler imaging system (MOOR Instruments, UK). For every explant-carrying CAM 12 different regions (each with 4200 pixel area) were measured around the tumors treated with anti-angiogenic protocols versus PBS-treated control tumors at high resolution/low speed settings (10sec/frame). To gather information on the CAM-internal variance of flow, 4 out of 12 regions measured blood flow on remote CAM sites, while 8 regions documented blood perfusion around the periphery of the tumors.

3.11 Pimonidazole Staining

To visualize extent and severity of tissue hypoxia in U87 grafts tumor-bearing embryos were injected i.v. on d14 with the hypoxia specific probe pimonidazole (aka Hypoxyprobe™-1, NPI, Inc.; dose used: 60mg/kg) 20 mins prior to tumor harvest. Dissected tumors were fixed in 4%PFA for 48 hours and then cryo-protected by 30% sucrose solution (48 h). Tissue was then snap frozen in ice-cold isopentane (kept at -20°C) and tissue sections of 12µm thickness prepared with cryotome. Sections were washed in PBS 3-times for 5-mins and blocked for one hour with 1% goat serum in PBS (to avoid non-specific antibody reaction). Next, sections were incubated overnight at 4°C with pAb2627 anti-pimonidazole rabbit antiserum (NPI, Inc; diluted 1/800 in PBS), followed by Cy-3 conjugated secondary goat antirabbit antiserum (Jackson ImmunoResearch 111.165.003) diluted 1/700 in PBS. The slides were then cover-slipped with an anti-bleaching reagent and images were acquired using identical settings of the camera/light intensity. Pimonidazole signals were quantified using MCID software according to a) intensity, and b) area. To calculate normalized pimonidazole staining intensities as proxy for the severity of tissue hypoxia the average signal measured

in the stained region was divided by the average background signal of the tissue. Percent pimonidazole positive area as proxy for the extent of tumor hypoxia was calculated as ratio of the stained ("pimo-positive") area divided by the total tumor area in a given section. These ratios after treatment are expressed relative to control sections, set to 100%.

3.12 Vessel Staining with Evans blue

Evans blue staining was done, to visualize the effect of drug treatment on U87 tumor vessels. Tumor-bearing embryos were injected i.v (150µl). On d14, 20 mins prior to tumor harvest, with 4% Evans blue dye dissolved in PBS. Dissected tumors were snap frozen and tissue sections prepared with cryotome. The slides were then cover-slipped with an anti-bleaching reagent and images were acquired.

3.13 Generating fluorescing stable tumor cell clones.

U87 glioblastoma and MCF7 breast carcinoma cells were transfected with a GFP expression plasmid (gift from Prof. Kontny as University Medical Center Freiburg, Freiburg, Germany; basis of from BD biosciences Clontech Inc: 6084-1) or an IRFP expression plasmid (gift from Prof. Ian Frew Univ. of Zurich, Switzerland, basis of Addgene Inc: 31856) was used for another MCF7 transfection. For transfection respective plasmids (0.8ug) and 2 µl Lipofectamine™ 2000 (Invitrogen Inc.) were diluted separately in Opti-MEM® I Reduced Serum Medium (Invitrogen Inc. 31985-062) and incubated for 5 minutes. The diluted plasmid and Lipofectamine™ 2000 were mixed and incubated at room temperature for 20 min to generate the transfection mixture. Cells were washed with serum-free opti-MEM medium, the transfection mixture was added to the twenty-four-well plates and incubated for 6 hr. Transfected cells were maintained at 37°C in an environment of 5% CO_2. After 24 hrs the cells were split into 12 well plates containing increasing concentrations of G418 (0 mg/ml, 0.05 mg/ml, 0.1 mg/ml, 0.2 mg/ml, 0.4 mg/ml, 0.8 mg/ml, and 1 mg/ml). Cells were fed with selection medium every 2nd day to maintain the selection pressure and inspected daily for toxicity. Depending upon the microscopic examination an optimal concentration of

G418 (0.1mg/ml) was selected. Using standard medium and optimal G418 concentration, cells were plated in a 96-well plate with 10 cells per well in a final volume of 100 µl. Cells were kept under selection pressure for 3 weeks and routinely analyzed for positive clones with fluorescence microscopy and only those wells were selected for further propagation that had more than 90% GFP positive cells. During the whole G418 selection process samples of un-transfected cells were used as negative control.

3.14 *In Vivo* cell migration Assay

To study cellular invasiveness and metastasis, *ex-ovo* Cam assay was arranged as described above. Highly tumorigenic MDA-MB231 breast carcinoma cells, with ascertained *in vivo* metastatic behavior [214], [215] were used for this assay since U87/GFP clones did not yield any spread of cells away from the initial explant (e.g. in liver) during the short time window of inoculation (6 days). The more aggressive MDA-MB231 cells were incubated in cell culture with 20µM fluorescent CellTracker™ Green CMFDA (5-chloromethyl fluorescein diacetate) dye (Invitrogen, Cat No: C2925) in serum free medium for 30mins followed by removing the culture medium from plates and rinsing cells with PBS, and trypsin treatment for detachment. The detached cells were collected in culture medium and centrifuged at 1000 rpm for 4 min, supernatant removal and a repeat spinning step for 2 mins to remove all remaining supernatant. Cell pellets were then re-suspended in medium at a final concentration of 4 million cells per 15ul and explanted on CAM. The embryos were returned to the incubators (Forma Scientific, Model-3336), were they were kept at 37°C and 60% humidity for the entire duration of the experiment. On d14.5, tumor-carrying CAM was dissected and frozen for cutting into 4 zones (2mm x 15mm each) for DNA extraction (figure 17c).

3.15 DNA Extraction

For each sample 300µl of Lysis buffer (100mM NaCl, 50mM Tris pH8.0, 10mM EDTA pH 8.0, 0.1%SDS) was used followed by addition of 18µl of proteinase K (20mg/ml) (Macherey-Nagel, Ref-740506). Samples were incubated for 3hrs at 55°C. After incubation,

the samples were heated to 95°C for 20 min to inactivate proteinase K and immediately transferred onto ice, followed by the addition of 30 µl of 3M sodium acetate and 750 µl of ice cold ethanol (100%). This was followed by an overnight incubation of the samples at -20°C. On the next day, the samples were spun at full speed for 30 min at 4°C, and the pellet of precipitated nuclei acid was washed again with 300 µl of ice-cold ethanol (70%). Following another full speed centrifugation step (20 min at 4°C) the supernatant was removed and the pellet re-suspended in 100 µl of distilled water.

3.16 ddPCR

To find "traces" of human DNA as proxy for the presence of cancer cells within CAM tissue we used the droplet digital PCR (ddPCR) technique and primers suited to selectively amplify regions of the hypervariable D-Loop sequence of human (cancer cell measure) versus chicken (normalization product with constant expression across CAM zones) mitochondrial DNA (mtDNA) in the samples (figure 7). The ddPCR was performed as described in [216]. Briefly, genomic DNA was extracted from the MDA-MB231 explant itself (zone 0 in figure 17b) as well as from zones 1, 2 and 3 (each representing a 2mm x 15mm wide strip of tissue: figure 17b) to determine the quantity of human D-loop amplicon, normalized to the chicken D-loop amplicon, as a function of distance from the initial explant. The approach reveals species specific amplification of the D-loop product with regard to positive controls (genomic DNA from a) humanMDA-MB231 cells, b) chicken liver) and the expected decreasing quantity of the human amplicon with regard to zones 0-3 (increasing distance form graft) (figure 17b). For the quantitative ddPCR we employed the same specific primers in conjunction with an internal fluor-probes labelled with FAM: (Fluorescein), and Yakima yellow i.e.: a) human specific ddPCR: Fwd primer: 5´CTAAATAGCCCACACGTTCC 3´, Rev primer: 5´ TAGGATGAGGCAGGAATCAA 3´, probe: 5´ FAM-TCACGATGGATCACAGGTC-BHQ1 3´) and b) chicken specific PCR Fwd primer: 5´ TACTTCATGACCAGTCTCAGG 3´, Rev primer: 5´ AGTTCAGGAGTTATGCATGG 3´, probe: 5´ Yakima Yellow ACCGTACCTCTGGTTCCTC BHQ1 3´). The primer probe pairs were used in a single reaction together with 1ng/ul of zone 0-3 extracted DNA and 10ul of

2x supermix (ddPCR™ Supermix for Probes #186-3010: Bio-Rad), in a 20ul reaction. PCR was carried out at 95 °C × 10 min (1 cycle), 94 °C × 30 s and 60.5 °C × 30 s (40 cycles), 98 °C × 10 min (1 cycle), and 12 °C hold.

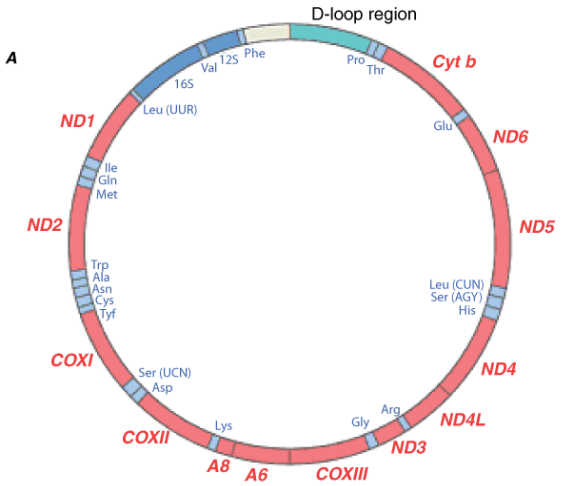

Figure 7: Human mitochondrial DNA with a D-loop region at upper right position. (figure adapted from Harrison's Principles of Internal Medicine, 17th edition [292]).

3.17 MRI Metastases detection.

To detect metastases in liver, 4 million U87 and MCF7 cells were labeled with iron particles prior MRI imaging in order to increase the MRI contrast of the postulated metastasis in the subsequent measurement. For that purpose, cells treated with Ferucarbotran (Resovist: Bayer) at 100 µg Fe/ml (BAYER Resovist®) were inoculated onto the CAM on d9. Again, explants were treated with AVA, and CHC alone and in combination. The experiment was stopped on d14.5 through i.v. injection of 100mM KCL solution. Next, embryos were transferred into 15 screw cap tubes and stored at 4°C for further MRI imaging. All measurements were performed in a Bruker 4.7 T BioSpec 47/40 (Bruker BioSpin MRI GmbH, Ettlingen, Germany) with a gradient strength of 375 mT/m and a slew rate of 3375 T/m/s equipped with a linear polarized 1H mouse whole body transmit-receive RF coil.

After a gradient-echo (GRE) localizer in 3 spatial directions, the imaging protocol included an axial T2-weighted Turbo Rapid Acquisition with Relaxation Enhancement (Turbo-RARE) sequence with following parameters: echo time TE 11ms; effective echo time TE 33 ms and repetition time TR 4440 ms; matrix 256 x 256; FoV 25 x 25 mm, rare factor 8,

number of averages = 6, slice thickness = 1 mm, acquisition time 10 min 39 sec). For water diffusion assessment a diffusion-weighted spin-echo echo-planar imaging (EPI) was applied (effective TE = 29 ms, TR = 5000 ms, number of averages = 10, fat saturation; slice thickness = 1 mm, two b-values with 0 s/mm2 and 717 s/mm2, acquisition time 6 min 40 sec). All MRI experiments where performed in collaboration with Dr. Andreas Boss and Dr. Christian Eberhardt (Institut für Diagnostische und Interventionelle Radiologie Universitätsspital Zürich). We thank them for their immense support and guidance.

4. Results

(Manuscript is submitted to carcinogenesis journal, which includes data, as marked in this section)

4.1 Assessing CAM/tumor explant

The chorio-allantoic membrane (CAM) model as pre-clinical and animal saving methodology for assessing both, development and malignancy of cancers, was performed with tumor cells explanted on the surface of the CAM in *ex ovo* assays. Nine different cell lines were examined as candidate explants and included human hepatoma (HEP3B), murine (B16F10) and human (501) melanoma, human glioblastoma (U87), human renal clear cell carcinoma with innate loss-of-function (LoF) mutation in the VHL tumor suppressor gene to generate constitutively active HIF signaling (i.e VHL LoF; cell line: RCC4) versus a VHL-reconstituted, HIF-inducible clone (cell line: RCC4/VHL) and three breast carcinoma cell lines of lesser (MCF7) and more virulent tumorigenic behavior(MDA-MB-468 and MDA-MB 231).

CAM compatibility of all above cell lines was analyzed through scoring cell growth, solid mass formation (3D structure) and induction of angiogenesis of a given tumor cell explant on the CAM on day 14 (d14) of chick embryo development. 80% of chicken embryos bearing explants survived.

From the nine cell lines tested only HEP3B, U87 and MCF7 (figure 8) formed vascularized solid masses (Table 3). Grafts of all other cell lines were either smaller, not vascularized or did not develop at all (dried cell mass). HEP3B, U87 and MCF7 tumors, however, yielded reproducible post-explant growth patterns. Subsequent microscopic observations showed that tumor grafts (i.e. HEP3B, U87) on the CAM remained dormant at first but started to develop a vascular network around the tumor periphery as a result of angiogenesis by day 4 of inoculation. In addition, larger vessels running more distant to the graft where attracted by the tumor. Increased perfusion could be seen as direct evidence for the functionality of the tumor capillaries under higher Doppler magnification (figure 12e and 14a-c).

Neovascularization and tumor growth steadily progressed until d6 after cell explanation.

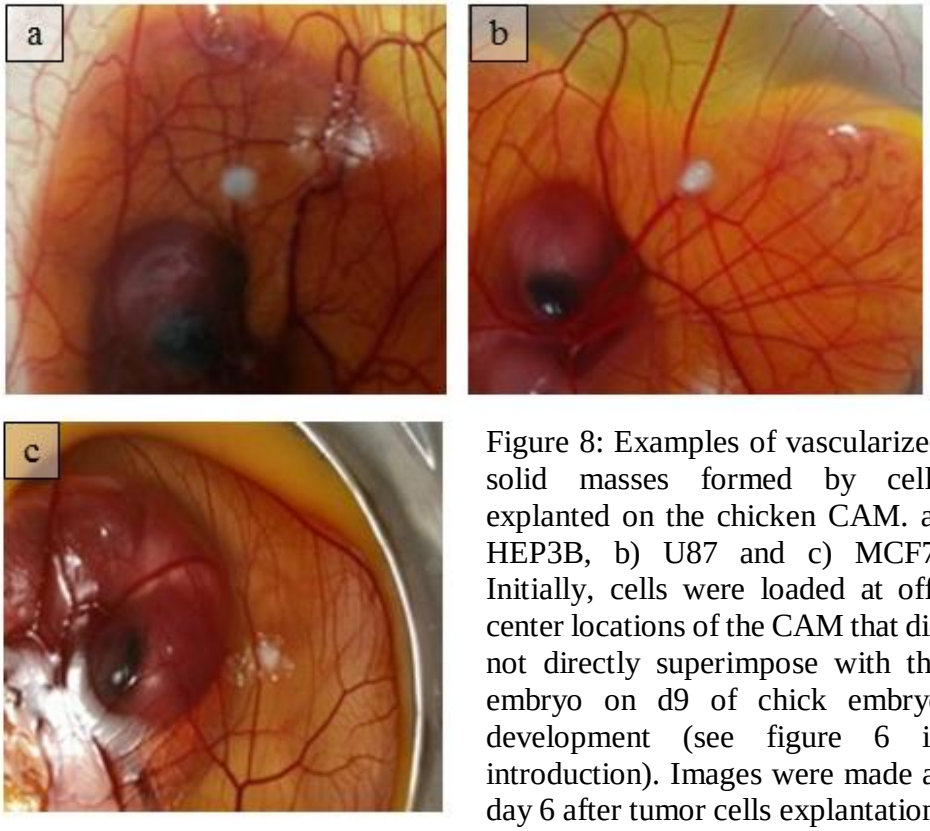

Figure 8: Examples of vascularized solid masses formed by cells explanted on the chicken CAM. a) HEP3B, b) U87 and c) MCF7. Initially, cells were loaded at off-center locations of the CAM that did not directly superimpose with the embryo on d9 of chick embryo development (see figure 6 in introduction). Images were made at day 6 after tumor cells explantation.

As described in table 3 top scores of CAM suitability were found for HEP3B and U87 cells, which let us to select U87 cells as line of interest since it represent a highly proliferative glioblastoma neoplasm, which *in vivo*, however, rarely metastasizes [217], [218]. In contrast, malignant breast cancer (MDA-MB 231) is a well described entity with high risk of spreading to many different organs, particularly bone, brain, liver and lung [214], [215]. For these reason we selected the U87 line as our main CAM model for primary tumor characteristics. In parallel, MDA-MB 231 cell lines where used in examining metastatic behavior in CAM assays (Data from table 3 included in manuscript).

Table 3: Scoring chart detailing the growth patterns of different cell lines on CAM.

Type	Cell Lines	Cell Growth	Solid Mass Formation	Angiogenesis	Cell lines of Interest
Renal carcinoma	RCC4	-	-	-	-
Renal carcinoma	RCC4/VHL	-	-	-	-
Murine melanoma	B16F10	+	-	+	++
Human hepatoma	HEP3B	+	+	+	+++
Human melanoma	501 Mel	+	-	-	+
Glioblastoma	U87	+	+	+	+++
Breast carcinoma	MCF7	+	+	+	+++
Breast carcinoma	MDA-MB468	+	-	+	++
Breast carcinoma	MDA-MB231	+	-	-	+

4.2 H&E staining:

Hematoxylin and eosin (H&E) staining was used to evaluate histological details in U87 tumor sections (figure 9). Tumor cells, recognized by their much larger cells and hyper-chromatic nuclei, were detected in intimate contact with the membrane surface (figure 9, left) and while invading the chorioallantoic mesenchyme (figure 9, right). Development of tumor vascularization can be seen at CAM/tumor interphase (Figure 9 included in manuscript).

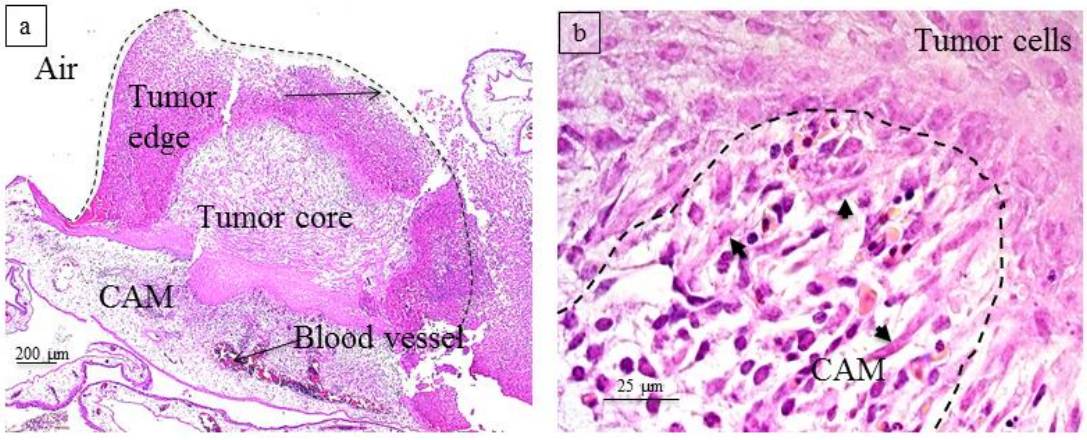

Figure 9: H&E stained paraffin section of a U87 tumor 6 days after cell explantation. Left: overview of explant/CAM interface. Right: detailed view of tumor cells (large nuclei)

invading CAM mesenchyme. Hematoxylin and eosin (H&E) staining showed histological details in U87 tumor sections. Tumor cells can be recognized by their much larger cells and hyperchromatic nuclei, while invading the chorioallantoic mesenchyme (figure 9, right).

4.3 Drug Toxicity Assay for U87 cell line

To study the *in vitro* cytotoxic effects of different anti angiogenic drugs and the MCT1 inhibitor (CHC) on U87 cells 80% confluent cell cultures were used. 24 hours after drug application (for concentrations see Materials & Methods), cell viability was assessed using Trypan blue dye exclusion assays. Figure 10 shows the percent of viable cells for increasing concentrations of a) AVA, b) Sunitnib, c) Raxozane and d) CHC. As compared to non-treated controls (100% viable cells) 0.01, 0.05, 0.1, 0.5, 1, and 5mg/ml treatments of AVA hardly resulted in any toxicity. Even at maximal 5mg/ml AVA 93% (±2%) of cells retained viability. Similar results of marginal toxicity were seen with Sunitnib (0.01, 0.1, 1 and 10 μM concentrations; 94% (±0.75%) viability at 10 μM) and Raxozane treatments (5, 10, 50, 100, and 200 μM concentrations; 96% (±0.92%) viability 200 μM). In contrast, CHC application induced significant cell death in a dose-dependent manner. While 1mM CHC was hardly toxic on cells (viability of 96 ±2.06%) ~30%, 70% and 95% cell death were noted at 10, 15 and 25 mM, respectively (figure 10). Data from figure 10b & 10c is not included in manuscript.

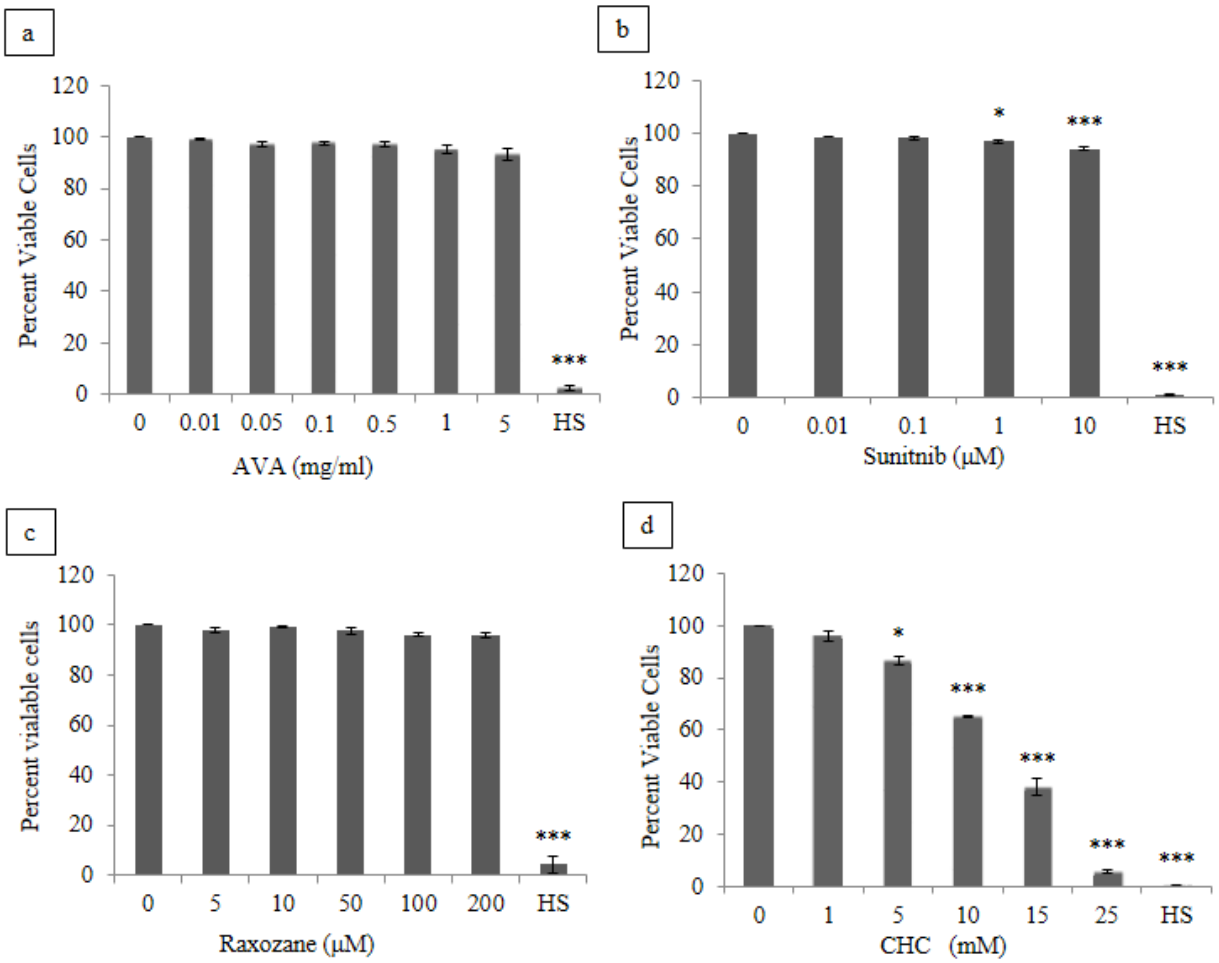

Figure 10: Viability of U87-MG glioblastoma cells (80% confluent cell cultures) in response to increasing concentrations of the indicated compounds a) AVA; b) Sunitnib; c) Raxozane; d) CHC. Cell death was induced by 0.1M NaCl solution (i.e. HS=high salt solution) and all treatments compared to non-treated controls. No significant cytotoxicity could be seen with AVA treatments whereas CHC imparted significant cell death in U87-MG glioma cells at concentrations of 5 mmol and above. Data are means ±SEM, n=3. Statistical differences among the mean coverage against controls were tested with one-way ANOVA, and significance was accepted at $p<0.05$. Asterisk indicates a statistically significant difference (* = $p<0.05$, ***=$P<0.001$).

4.4 Testing drug toxicity on the CAM

Regarding the *in vivo* toxic effects CHC, Raxozane and Sunitnib were applied onto the CAM and AVA i.v injected. On day 9 of chick embryo development (n=3 assays/compound) 0.0154mg of AVA (10mg/kg), 0.00154mg of Sunitinib (1mg/kg), 0.0154mg Raxozane (10mg/kg) and 0.0924mg of CHC (60mg/kg) in PBS/DMSO were applied (see below for dose rationale). As control, an equal volume of PBS for AVA and DMSO for other drugs

was loaded onto other CAMs. Embryos were observed for the next 4 days. Microscopic observations revealed no major incidences of hemorrhage, hyperemia or coagulation at the application site of the CAM and all embryos survived till the end of experiment (day 14). As no fatalities were observed by any of these drug doses, we decided to use these concentrations in the subsequent experiments with tumor explants.

To compare the above drug dilutions with in-vitro toxicity data (figure 10a, d), the mg/kg doses had been converted to molar concentrations considering 1kg to be equivalent to 1liter (1kg≈1liter). Thus 60mg/liter CHC corresponds to 0.3171mM CHC applied onto the CAM. Similarly, concentrations calculated for AVA, Sunitinib and Raxozane corresponded to 0.01mg/ml, 2.5 μM and 37.3 μM respectively. These concentrations were all well within the non-toxic range for cells, (figure 10a, d).

4.5 Chicken embryo mortality

Moreover the effect of different drug and tumor cells application methods (i.v. vs. topical) on chicken embryo mortality were assessed by treating the CAMs on day 9 (d9) of chicken embryo development and observing for any embryo deaths until day 14 (d14). Overall i.v. injections had a higher mortality rate as compared to topical applications. Topical application of drugs onto the CAM had a survival rate of 90% (27 survived out of 30) whereas i.v. infusion survived 53.34% embryos (16 survived out of 30) (figure 11a). While embryo death was rare under untreated conditions with 93.34% survival rate (28 survived out of 30) (figure 11a) for tumor cell explant vs. i.v. infusion similar effect as for the drug application was seen. Chicken embryo survival rate was lower with i.v. cell infusion into CAM vessels (46.65%) as compared to topical tumor cell explantation (83.34%) onto the CAM (figure 11b).

This higher mortality rate with i.v. infusion is best explained by the delicate CAM vasculature and that placement of a needle into CAM vessels requires practice and skills. The major problems with i.v. infusion were a) sustained bleeding during and after i.v.

infusion, eventually leading to blood pressure drop as a cause for embryonic death and b) difficulty in introducing the needle into the vessel lumen due to small vessel diameter and low or no mechanical immobilization of the vessel at injecting site, as CAM membrane is a free floating structure on egg white.

Next the effect of multiple tumor cell explants on chicken embryo survival was investigated as well by explanting, on day 9 (d9) of chicken embryo development, 4 million cells (15ul) onto the CAM and quantifying the embryo deaths until day 14 (d14). Chicken embryo survival rate was lower (65%), when two explants (4 million each) where done on single CAM (13 survived out of 20) as compared to single 4 million cell explant (83.34%) on a CAM (25 survived out of 30) (figure 11c). Data from figure 11 not included in manuscript.

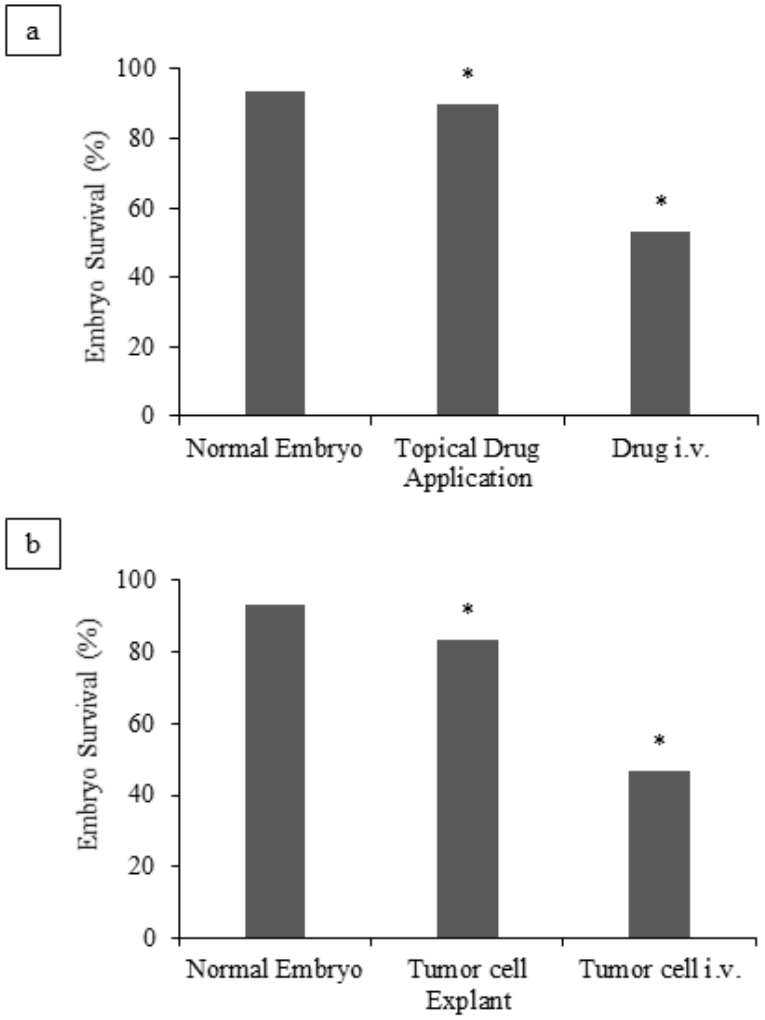

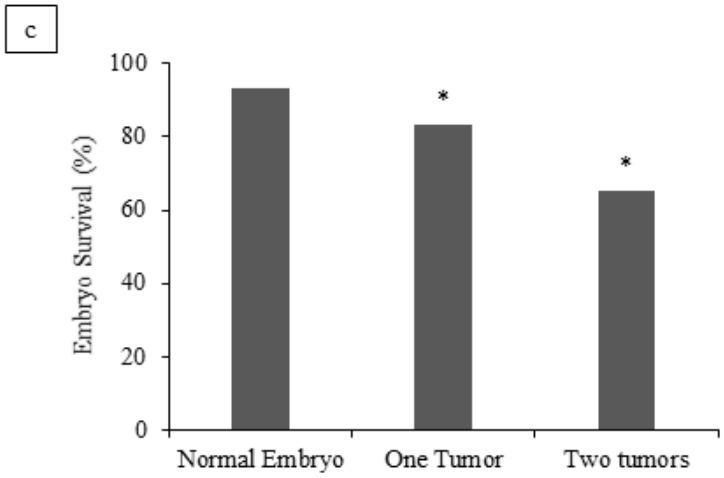

Figure 11: Chicken embryo mortality after drug application or tumor cell explantation, a) Topical application of Drugs on CAM had higher survival rate of 90% as compared to i.v infusion with 53.34% surviving embryos. b) For tumor cell (explantation vs. i.v. infusion) a similar effect was seen. Chicken embryo survival rate was lower with 46.65%, after i.v. cell infusion into CAM vessels as compared to tumor cell explantation (83.34%) onto the CAM. c) Multiple tumor cell explants on the CAM reduced chicken embryo survival rate to 65% when two explants where done on single CAM as compared to a single explant (83.34%). For 9a, 9b &9c Mantel–Cox test gave a significant difference between the groups (* = $p<0.05$ compared to normal embryo).

4.6 Technique for monitoring tumor blood flow

To measure the blood flow within the tumor and its periphery, a real-time blood perfusion imaging technique was utilized. This non-invasive approach measures blood flow in microcirculation without physical contact with the tissue. Thus, interfering influence on the measurement can be kept to a minimum. The result is a computer-generated color-coded image with red colors indicating maximal and blue tones least perfusion (figure 12b). Yet, initial CAM/Tumor explant assays yielded unsatisfactory results due to a considerable background interference (motion artifacts) observed in the image during flux measurements (figure 12a, b). These artifacts were mainly caused by overlay of the yolk sack blood perfusion in the vascular network of the embryo with the perfusion in the CAM, thus, creating erroneous color codes (e.g. figure 12b) (Figure 12 not included in manuscript).

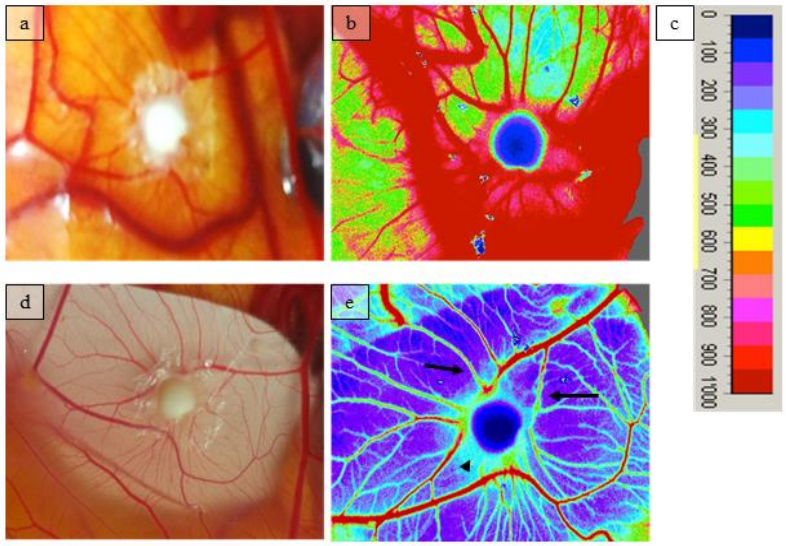

Figure 12: Technique for optimizing laser Doppler perfusion imaging a) Image of a tumor on the native CAM, b) color-coded perfusion image of the CAM shown in a) with red colors indicating maximal, and blue tones least, amount of motion (cf. color scale shown in c)). d) Tumor image with a plastic strip beneath for blocking the background perfusion signal arising from the yolk sack, e) color-coded perfusion image of the CAM shown in d) with red colors indicating maximal, and blue tones least, and amount of motion (cf. color scale shown in c)). Note the effective blocking of the perfusion signal arising from the yolk sack by placing the plastic strip directly underneath the explant bearing site (figure 12d, e) and, thus, producing less noisy, reproducible and conclusive flow images.

This problem was successfully solved by blocking tumor flow signals from background interference by inserting a solid polystyrene plastic strip through a small cut into a poorly vascularized region of the CAM and placing it directly underneath the explant bearing site (figure 12d). Now, blood flow measurements were less noisy, reproducible and conclusive. Figure 12e presents an exemplary color-coded image of blood flow measurements for the U87 explant shown in figure 12d. Arrows highlight blood vessels that were attracted by the tumor. Change in color intensity, indicating higher blood flow due to active angiogenesis, can be seen at the tumor periphery as a greenish “halo” around tumor (indicated by arrow head). In contrast, note the relative low perfusion in the core region of the tumor (cf. color coding scale for flux values, figure 12c). This approach was further used for flux measurements after drug treatment.

4.7 Drug treatment and growth kinetics of U87 Tumors

After successfully establishing U87 explants as model tumors in CAM assays this setup was subsequently used to measure tumor growth kinetics under anti-angiogenic drug (AVA, 10mg/kg) and MCT1 inhibitor (CHC, 60mg/kg) treatment, alone and in combination. Figure 13a-d clearly demonstrates, on exemplary U87 grafts, the decreasing tumor size as function of drug treatment. Particularly the AVA+CHC combination therapy evidenced its additive effect in inhibiting mass accumulation of the primary growth (figure 13d).

Image analysis allowed quantifying the tumor growth over time (see Material & Methods). By day 4 and 6 of the CAM assay, control tumor grafts (PBS treated) had increased their approximated volume by 1.1 and 2.6 fold respectively. On day 6 of the assay, the different treatments (figure 13e) indicated striking anti-tumor effects. While the angiogenesis-inhibiting effect of AVA monotherapy was able to slow growth of the primary mass (i.e. relative tumor volume, d6 of assay: 269.24 (better 270) % ± 16.48% (control) → 139± 11.89% with AVA), CHC alone (122.04% ± 22.28%) and AVA plus CHC (50.65% ± 41.13%) combinatorial treatment resulted, relative to control masses, in a marked retardation of tumor growth (shrinkage) Data from figure 13 is included in manuscript.

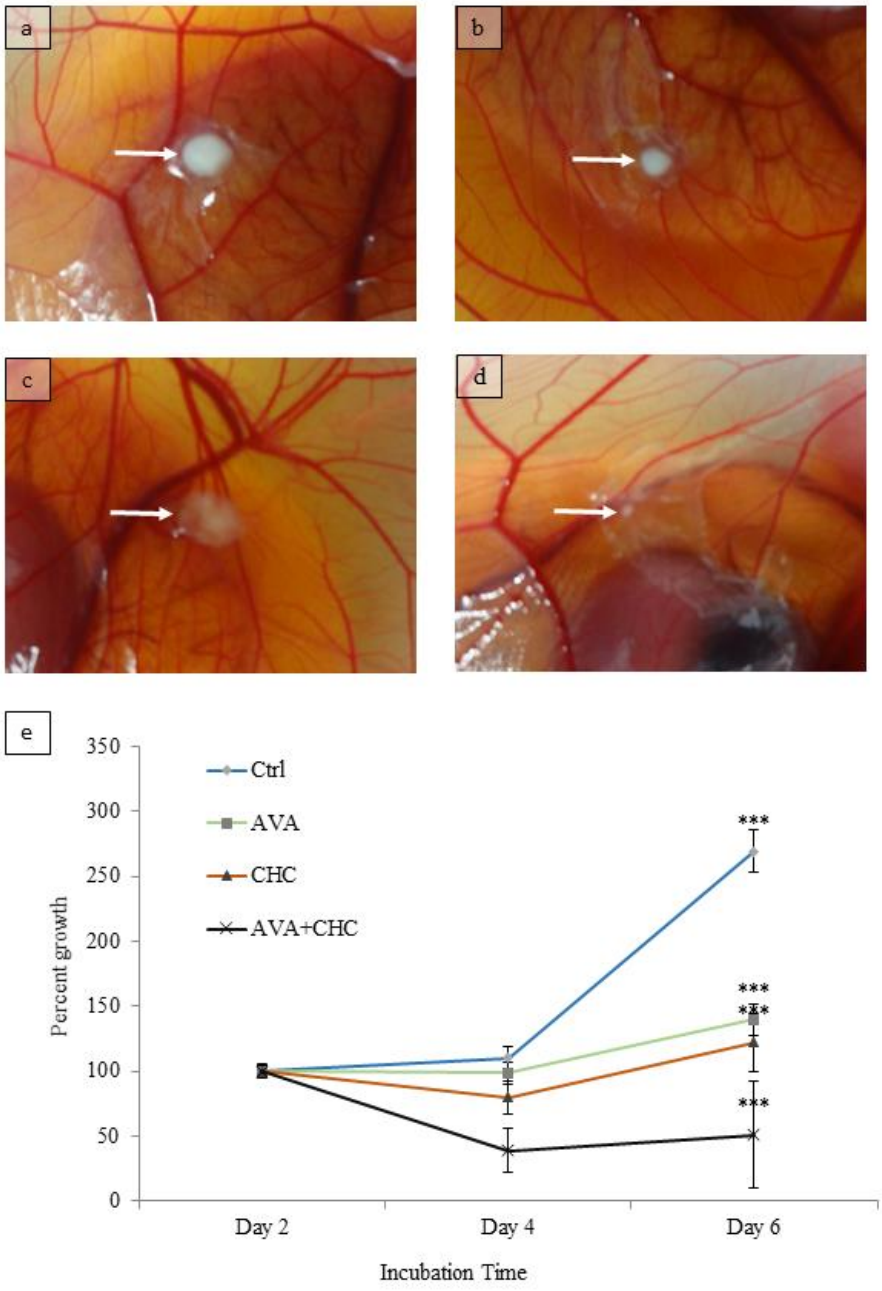

Figure 13: Tumor growth kinetics as function of treatment between day 2 and 6 of U87 cells after explanation onto the CAM (day 0 = explant day). Representative images of tumor explants subjected to: a) Control (PBS, 10µl topically applied around the explant); b) AVA (i.v. injected: 10mg/kg); c) CHC, (60mg/kg) topically applied around the explant; d) AVA+CHC (10mg/kg+60mg/kg). White arrows point to the respective primary mass. e) Quantification of tumor growth kinetics by image analysis (see Material & Methods for details). Starting with a tumor volume set to 100% at day 2 control, AVA, CHC and AVA+CHC treated tumors changed their size to 269.24 ± 16.48 %, 139.81 ± 11.89 %,

122.04 ± 22.28 % and 50.65 ± 41.13 %, respectively, within 4 days. Data are means ±SEM, n=6. Statistical differences among the mean coverages against controls were tested with two-way ANOVA, and significance was accepted at $p<0.05$. Asterisk indicates a statistically significant difference (***=$P<0.001$).

4.8 Angiogenesis and blood flow measurements in U87 tumors with AVA or CHC mono-therapy and combination of both

As routine protocol for subsequent assessment of tumor formation and angiogenic response due to drug treatment AVA 10mg/kg and CHC 60mg/kg alone and in combination was used. Figure 14 shows color-coded image of the spatial distribution of micro vascular blood flow in and around the tumor periphery. As can be seen, for control (PBS treated) and, surprisingly, AVA-treated grafts a greenish angiogenesis "halo" around the tumor is clearly visible (figure 14b). In contrast, CHC application visibly reduced the halo (figure 14c). From the tumor subjected to combinatorial treatment, only cell loading site can be seen, as compared with vehicle and AVA, CHC treated tumors (figure 14d).

Figure 14 illustrates the continuous reduction in blood flow when comparing control treatment (397.22 ± 31.96 flux units, 100%) with AVA (342.01 ± 40.18; 86%) or CHC (288.05 ± 43.43; 72.51%) monotherapies. Yet, blood flow dwindled to maximal extent in response to the AVA+CHC combinatorial treatment (198.61 ± 37.72; 48.99%), thus, highlighting the most potent anti-tumorigenic efficacy of this particular intervention. It is reassuring to note that flux at internal and tumor-remote CAM control sites was far less affected by these treatments, dropping only from 244.99 ± 25.81 units (100%, ctrl) to 204.48 ± 14.95 (83.46%) in the AVA+CHC group (figure 14f) (Data from figure 14 included in manuscript).

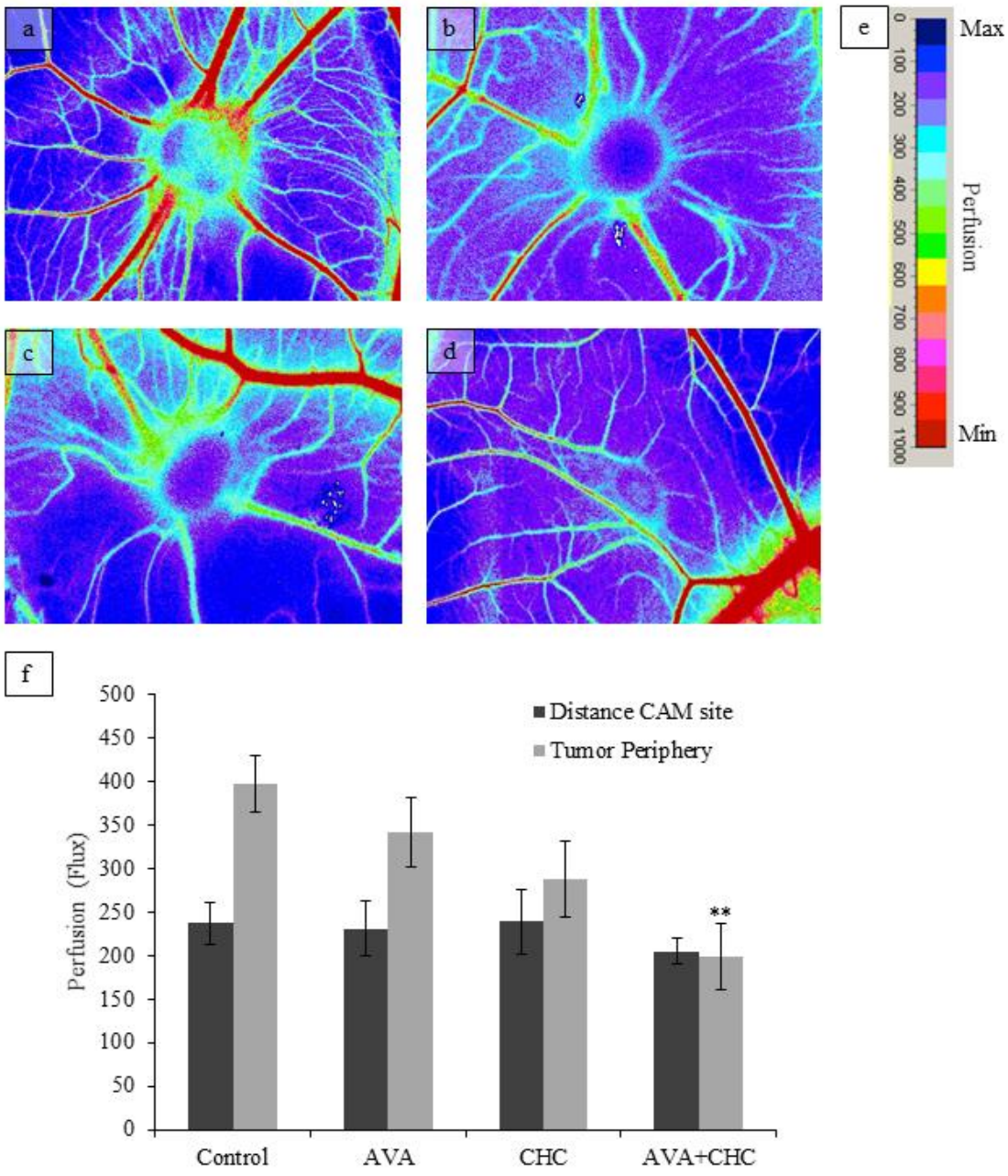

Figure 14: Laser Doppler blood perfusion imaging of U87 tumor explants. Panels a-e show representative blood flow recordings from tumors treated with (a-d) PBS (control), AVA, CHC and AVA+CHC (application mode and concentration used as in figure 13). e) Color scale for perfusion. i) Quantified blood flow (flux) measurements in U87 tumors in response to the indicated treatments. Note the significant reduction of peripheral tumor blood flow to almost CAM levels in response to AVA+CHC combinational treatment. Data are means

±SEM, n=6. Statistical differences among the mean coverage against control were tested with two-way ANOVA, and significance was accepted at $p<0.05$. Asterisk indicates a statistically significant difference (**=$P<0.01$).

4.9 Pimonidazole staining

To document the effects on tumor hypoxia by AVA-only (10mg/kg body weight), CHC-only (60mg/kg) and AVA+CHC treatments tumors were subjected to pimonidazole staining. Figure 15 shows exemplary sections in stereotypical orientation, i.e. on top the tumor surface exposed to air (tumor edge, hatched line), then tumor core (mid-section), followed by CAM interface (bottom). Pimonidazole signals were quantified using MCID software according to a) intensity (figure 15f), and b) pimo-positive area (figure 15g), set to 100% for respective control grafts. As expected, pimonidazole binding was absent in tumor regions close to the air-exposed surface while it mainly occurred in the core region of tumors and within the interface with the CAM. As can be seen in figure 15, AVA monotherapy augmented both intensity (figure 15 c, f) and area (figure 15 c, g) of pimonidazole staining in U87 tumors, which not only agrees well with the clinical observation of increasing therapy-resistance and tumor spread in AI-treated malignancies, but also provides evidence for an AI-therapy-dependent increase in tumor hypoxia. In contrast, CHC-only and AVA+CHC combinatorial applications reduced pimonidazole intensities in primary U87 masses to 90% (CHC-only) and 60% (AVA+CHC) of control tumors (figure 15f) whereas the pimonidazole-positive hypoxic areas (ratio) were reduced slightly to 90% of control explants (figure 15g). These data, therefore, strongly support the efficacy of CHC-based protocols in targeting and eradicating hypoxic cells in solid malignant tumors (Data from figure 15 included in manuscript).

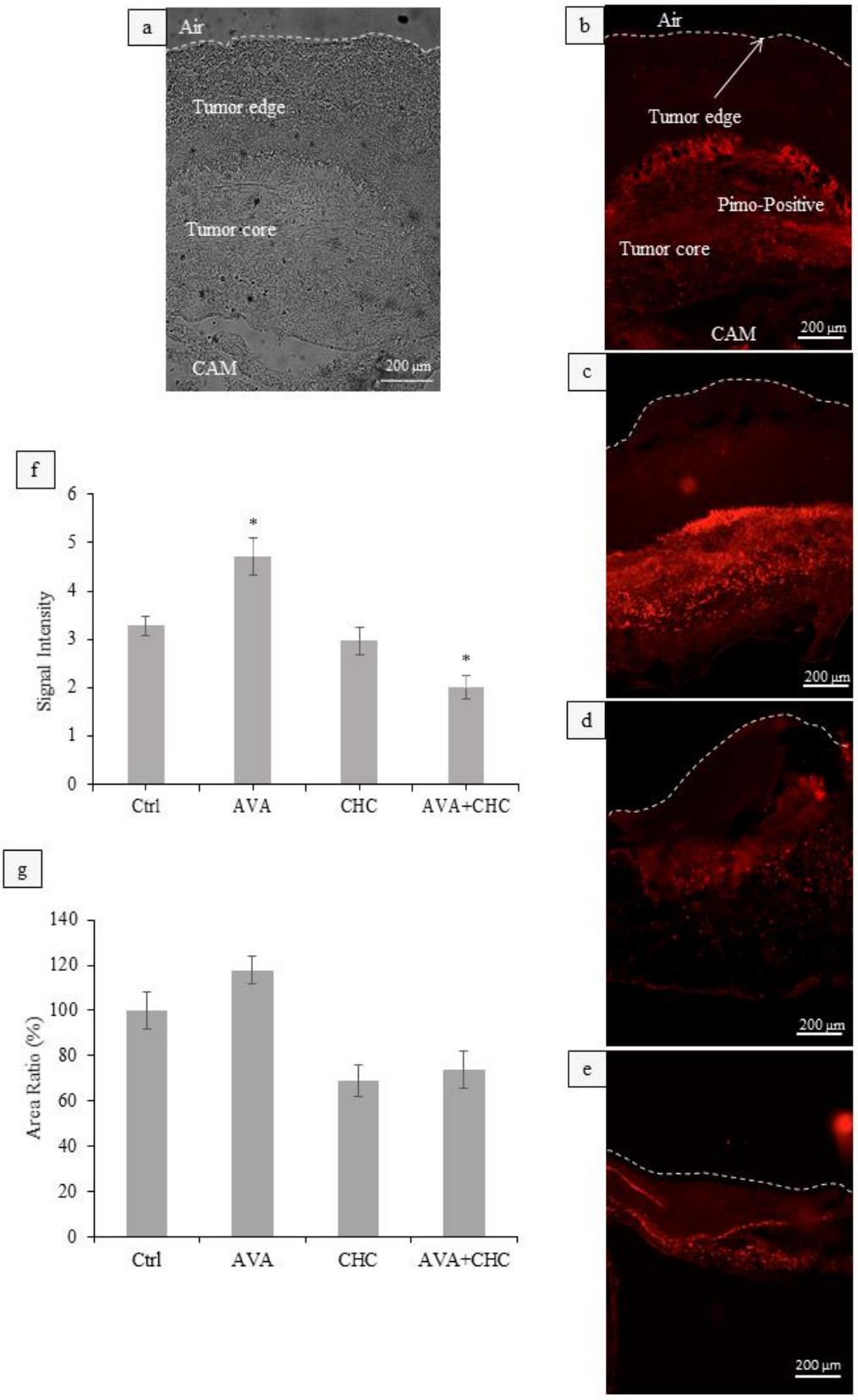
a
Air
Tumor edge
Tumor core
CAM
200 μm
b
Air
Tumor edge
Pimo-Positive
Tumor core
CAM
200 μm
c
200 μm
d
200 μm
e
200 μm
f
Signal Intensity
0
1
2
3
4
5
6
*
*
Ctrl
AVA
CHC
AVA+CHC
g
Area Ratio (%)
0
20
40
60
80
100
120
140
Ctrl
AVA
CHC
AVA+CHC

Figure 15: Assessment of local tumor hypoxia. a) Representative brightfield image to indicate different regions on the tumor section. b-e: Representative images of pimonidazole (Pimo) stained (red) cross sections of U87 tumors after (right top to bottom) control (PBS), AVA, CHC and AVA+CHC treatments (application mode and concentration used as in figure 13). Both the severity of tissue hypoxia, inidcated by the intensity of pimonidazole signals (Pimo signal/tissue background (f)) in the left-top graph and the extent of tissue hypoxia, defined as percent pimonidazole-positive areas (pimo-positive area/total tumor area (g)) in the left-bottom graph, were quantified as function of treatment (see Materials & Mehtods for details). While monotherapeutic AVA application elevated the intensity and area of tumor hypoxia, particulalry the intensity readout was drastically reduced upon CHC treatment and, even further significant reduction, with AVA+CHC treatment. Data are means ±SEM, n=4. Statistical differences among the mean coverage against control were tested with one-way ANOVA, and significance was accepted at $p<0.05$. Asterisk indicates a statistically significant difference (* = $p<0.05$).

4.10 Accessing the vascular morphology with i.v. injected Evans blue

To confirm the data obtained with Pimonidazole staining Evan blue was injected i.v. to look for the effect of drug treatment (AVA-only, CHC-only and AVA+CHC applications) on U87 tumor vasculature. Evans blue is a non-toxic dye widely used in the study of the morphology of the vasculature and its permeability. It binds to serum albumin forming a conjugate that can be identified by its red fluorescence in tissue sections using fluorescence microscopes. As expected, Evans blue was absent in tumor regions close to the air-exposed surface while dense stained vasculature could be seen at the interface with the CAM (figure 16). AVA monotherapy showed lower vascular density compared to controls in line with the clinical observation and the hypothesis that anti-angiogenic therapy could lead to tumor hypoxia. Combinatorial treatment showed the least vessel density at the interface thus strongly supporting the efficacy of CHC-based protocols in targeting and eradicating hypoxic cells in solid malignant tumors. Due to time and money constrains the experiments could not be repeated. But more detailed investigation is required in this regard to confirm the above findings from the staining (Data from figure 16 not included in manuscript).

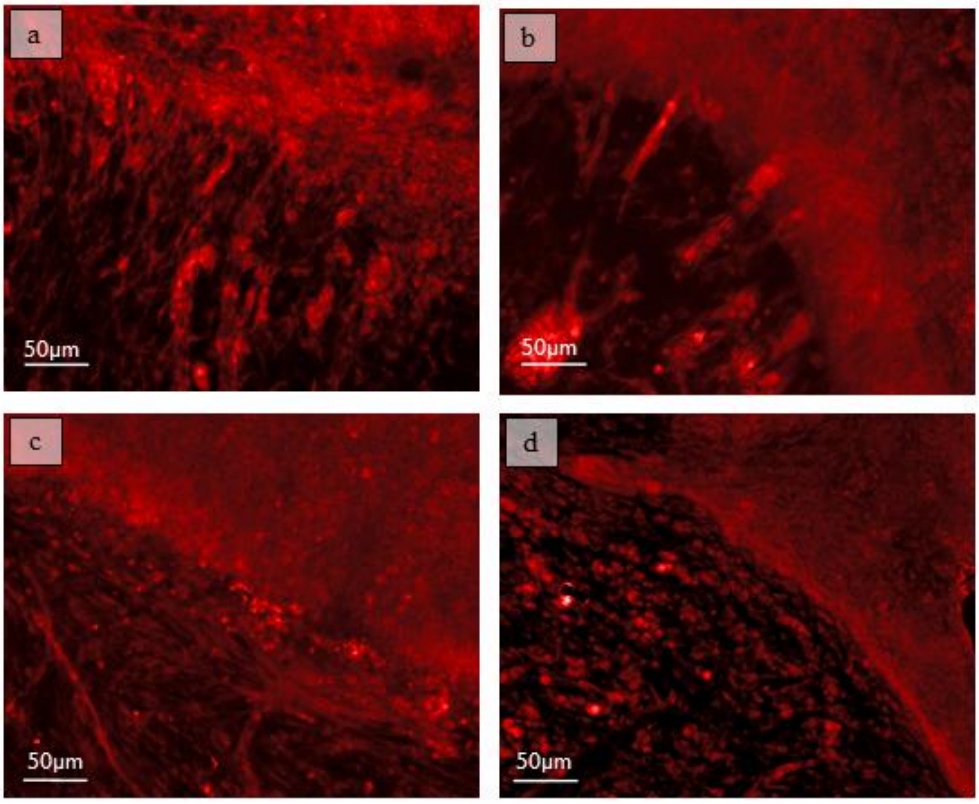

Figure 16: Assessment of vascular morphology. Evan blue staining was done to look for the effect of drug treatment (AVA-only, CHC-only and AVA+CHC applications) on U87 tumor vasculature. As expected, Evans blue binding was absent in tumor regions close to the air-exposed surface while dense stained vasculature could be seen at the interface with the CAM. AVA monotherapy (b) showed lesser dense vasculature compared to controls (a). While combinatorial treatment (d) showed minimal vessels at the interface thus strongly supporting the efficacy of CHC-based protocols in targeting and eradicating hypoxic cells in solid malignant tumors.

4.11 *In Vivo* cell mobility assay with aggressive MDA-MB231 cell lines.

To study tumor cell spreading, MDA-MB 231 cells, known to have a high risk of spreading, were used on the Ex-ovo Cam assay as a measure for metastasis and its response to the different therapy regimes investigated in the present study. First, CellTracker™ Green CMFDA dye labelled MDA-MB231 breast carcinoma cells where used to generate tumor explants that were then treated with AVA (i.v. injected: 10mg/kg) and (CHC, 60mg/kg) alone and in combination. Six days after tumor cell explantation representative images where made with a fluorescent microscope to track the cells on the CAM (figure 17a).

Unfortunately this method did not allow exact quantification of cell spreading. Therefore, genomic DNA was extracted from Tumor explanted CAM as well as nearby CAM tissue, divided into 4 zones (Zone 0, 1, 2, and 3) as detailed in materials and methods (figure 17b). PCR amplification showed the primers where species specific (figure 17 c). The presence of human DNA within the different zones of the CAM tissues was determined using ddPCR by amplifying human and chicken specific D-Loop sequences in the samples. The amount of human DNA was then normalizes to the amount of chicken DNA. Starting with zone 0 (tumor on CAM) was set to 100% for detected signals with Control (±7.6%), AVA (±4.7%), CHC (±4.1%) and AVA+CHC (±5.0%) treatments. Significant change in cell spreading was observed in zone 1 of control (30.68±3.2%), AVA (56.35±15.49%), CHC (22.49±1.1%) and AVA+CHC (14.97±1.9%) treatments with AVA showing highest cell motility. A similar although non-significant effect was seen in zone 2 as well with a motility of 1.8±0.4%, 6.0±0.1%, 1.5±0.7% and 0.5±0.4% for the respective treatments. Only negligible signals where detected in zone 3. These findings demonstrate the overall increase in spread (motility) of MDA-MB231 cells with AVA treatment as compared to controls and other treatments while reduction in motility was observed with CHC treatment and even further reduction with AVA+CHC treatment (figure 17d). Of note, these experiments again demonstrate the suitability of CAM/Tumor explant approach in study of cancer biology including cell motility (Data from figure 17 included in manuscript).

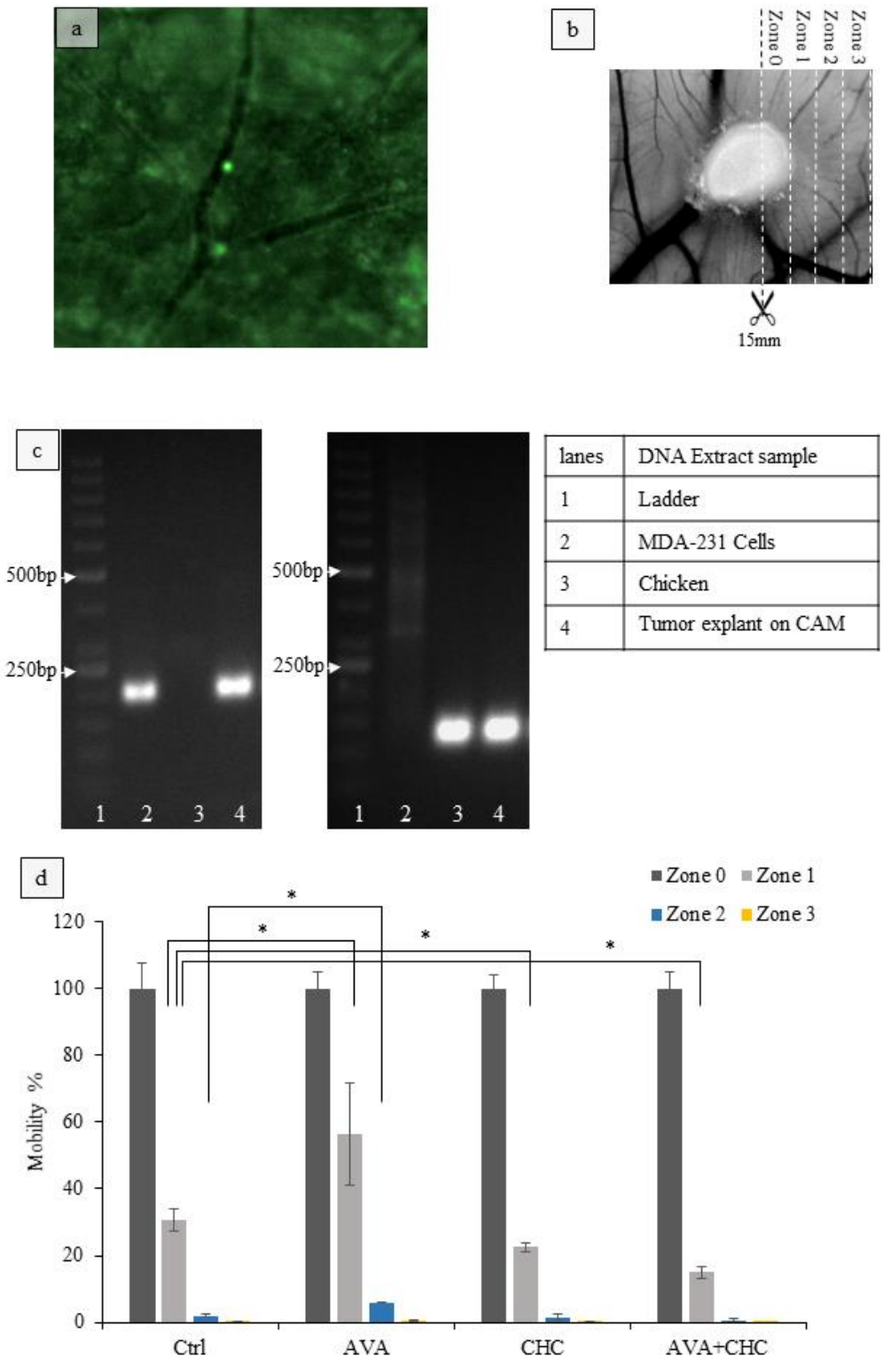

Figure 17: Spreading behavior of MDA-MB231 cells on the CAM in response to AVA and CHC (application mode and concentration used as in figure 13) treatments alone and in

combination. Six days after tumor explantation representative images where made from CAMs bearing tumors of CellTracker™ Green CMFDA dye labelled MDA-MB231 cells (figure 17a). For exact quantification of cell spreading genomic DNA was extracted from tumor explanted CAM as well as nearby CAM tissue, divided into 4 zones (Zone 0, 1, 2, and 3) as detailed in materials and methods and sketched in figure 17b. PCR amplification revealed species specific amplification of the D-loop product with regard to positive control genomic DNA from a) humanMDA-MB231 cells [figure 17c, lane 2], b) chicken liver) [figure 17c, lane 3] and DNA extract from tumor explant from CAM [figure 17c, lane 4]. The content of human DNA within CAM tissues was determined using ddPCR by amplifying human and chicken specific D-Loop sequences in each sample. Starting with zone 0 (tumor explanted CAM) that was set to 100% for detected signals with control (±7.6%), AVA (±4.7%), CHC (±4.1%) and AVA+CHC (±5.0%) treatments. Differences in cell spreading were observed in zone 1 of control (30.68±3.2%), AVA (56.35±15.49%), CHC (22.49±1.1%) and AVA+CHC (14.97±1.9%) treatments with AVA showing highest motility. A similar effect was seen in zone 2 as well with a percentage of human DNA of 1.8±0.4%, 6.0±0.1%, 1.5±0.7% and 0.5±0.4% for respective treatments, while negligible amounts of human DNA where detected in zone 3. These findings demonstrate the overall increase in spread of MDA-MB231 cells with AVA treatment as compared to controls and other treatments. In contrast, reduced spread was observed with CHC treatment and even more with AVA+CHC treatment (figure 17d) demonstrating the suitability of CAM/Tumor explant approach also for studying metastasis behavior of tumor cells. Data are means ±SEM, n=3. Statistical differences among the mean coverage against control were tested with Wilcoxon rank-sum test (Significance was accepted at $p<0.05$=*).

4.12 Metastases detection with MRI

Magnetic resonance imaging in humans is one of the most common medical examinations to detect metastasis. As the CAM vessels convert finally to the embryonic liver we decided to use MRI of the chicken liver obtained from CAM assays with U87 cells explanted and subjected to drug treatment (AVA-only, CHC-only and AVA+CHC applications). Data analysis from diffusion-weighted EPI sequence and Turbo-RARE sequences could not detect metastases in the liver, despite the good image quality (figure 18). To corroborate the observed results, experiments where repeated by i.v. injection of U87 cells in chicken embryo, which as well could not provide the evidence of metastasis (images not shown) probably due to cell behavior. As U87 cell lines rarely metastasize [217], [218], the experiment was repeated in a similar setup (explant + i.v: images not shown) but with the malignant breast cancer (MCF7) cell line. MCF7 is a well described entity with high risk of

spreading to other organs, particularly bone, brain, liver and lung [219]. But again no metastases were detectable (Data from figure 18 not included in the manuscript).

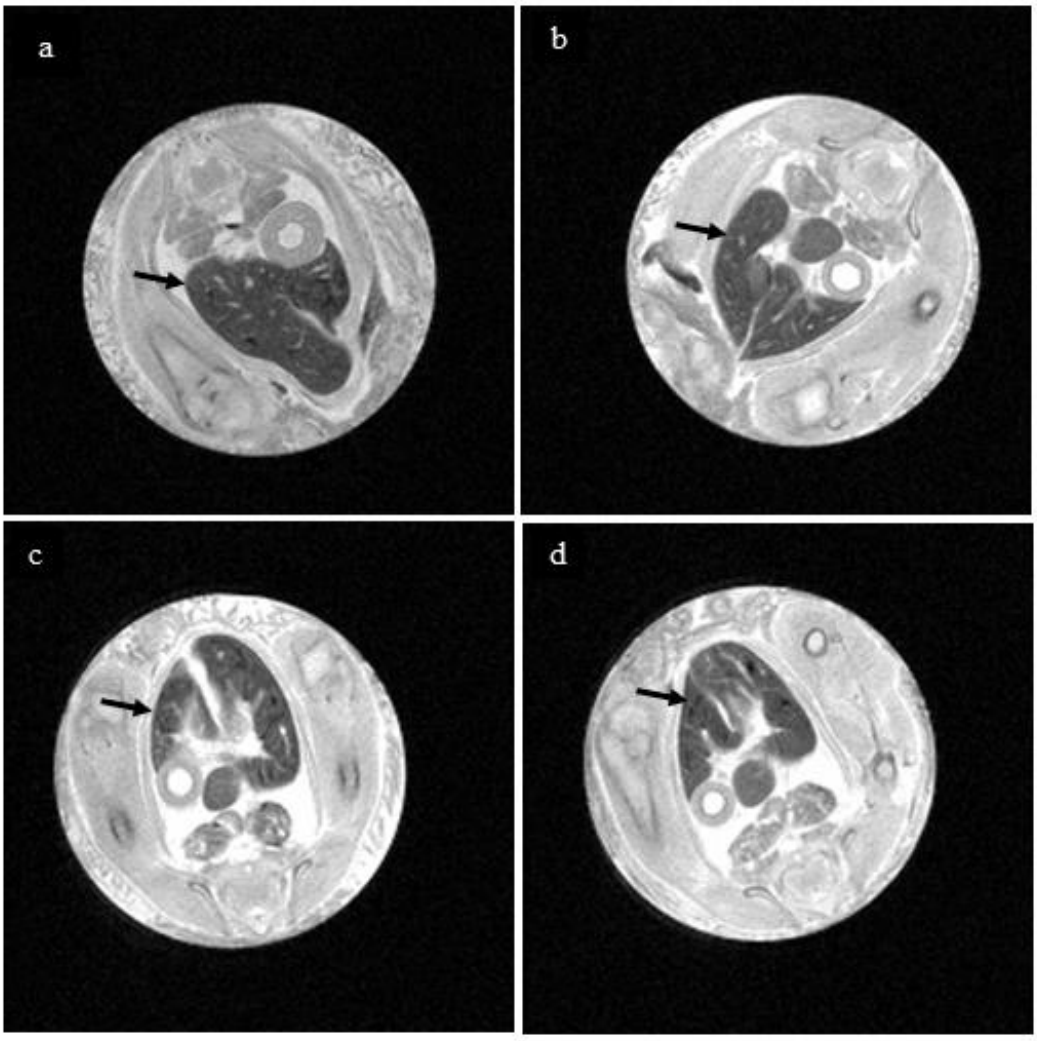

Figure 18 Search for liver metastasis chicken embryos with U87 cell explants on the CAM. Representative Turbo-RARE MRI images showing the organs of 14.5 day old chicken embryos (Liver: arrow) that had been subjected to a) Control (PBS, 10µl topically applied around explant); b) AVA (=; i.v. injected: 10mg/kg); c) CHC, (60mg/kg) topically applied around explant and d) AVA+CHC (10mg/kg+60mg/kg) treatments. No evidence of metastasis was seen in MRI scans in none of the embryos.

5. Discussion

Growth of malignant tumors requires continued supply with oxygen and nutrients, which is achieved through the angiogenesis. Thus, there was great hope that tumor treatment with angiogenesis inhibitors, could be an efficient anti-tumor strategy. However clinical studies showed that AIs often not only induced the expected growth retardation of the primary mass, but also cancer recurrence and metastasis [188], [189]. For this reason, renowned clinical oncologists voiced the growing need for reliable pre-clinical screens to better assess the efficacy and safety of future AI-applications. For example, the previous president of the Swiss Cancer League, Prof. T. Cerny, stressed the urgent need for additional investigation to recognize most effective anti-angiogenic treatment approaches at minimal adverse impact for the patient [193]. Such improved cancer therapies should simultaneously eradicate both aerobic and hypoxic tumor compartments of solid malignancies. Otherwise, surviving hypoxic cells might trigger the emergence of an increasingly virulent and therapy-resistant phenotype. By explanting tumor cell lines on the chorion-allantois-membrane (CAM) of living chicken embryos the objective of the present study was to evaluate both efficacy and safety of AI-applications, given either individually or in combination with antagonists of lactate uptake. That way it was aimed to shed some light on the mechanisms underlying the growth retardation of the primary mass and the heightened risk of tumor spreading in AI-treated cancer models.

The CAM assay characterizes a methodological alternative to the most commonly used tumor model, the mouse xenograft approach. During 2011 alone, around 402,600 mice and nearly 116,000 rats were involved in animal experimentation in Switzerland [220]. Despite the enormous use of rodent models in general, inoculation of tumor cell lines into mice is always an ethical problem due to the potential suffering of animals. In contrast, the CAM contains no nerves thus tumor growth cannot induce pain in the embryo [204]. Consequently, Swiss law does not consider the CAM assay an animal experiment up to embryonic day 14.5 [203], [204]. All experiments of this study have always been performed within this time frame. Additional advantages of the CAM over rodent-xenograft assays include a) ease of accessibility of tumor explants, for example, by optical methods including as Laser Doppler

imaging to allow observation of the tumor growth and functional monitoring of tumor blood flow respectively; b) high throughput screening of tumors treated by different therapeutic protocols; c) natural immunodeficiency of early stage chick embryos (i.e. lack of a mature lymphoid system) which, therefore, cannot reject xenogenic tumor cells [221], and d) excellent tool to study kinetics and single step processes of tumor cell metastasis under quasi *in vivo* conditions [221]. Research by other groups assessed glioblastomas [222], melanomas [223], prostatic cancer cells [224] and osteosarcomas [213] as CAM models.

The present study tested eight different cancer cell lines as CAM models. Tumor grafts onto the CAM remained dormant at the beginning but after 4 days the development of capillary network was observed around the tumor periphery as a result of angiogenesis. Out of these eight cell lines only human hepatoma (Hep3B), glioblastoma (U87) and breast carcinoma (MCF7) formed vascularized solid tumors with active angiogenesis (figure 8), from which we opted to focus on U87 line for pre-clinical drug screens (Table 3). In contrast, B16F10, 501 melanoma and MDA-MB-468 tumors were smaller, not well vascularized with little or no angiogenic effect to CAM. The remaining cell lines tested here, RCC4+/+ and RCC4-/-, didn't show any growth on the CAM. The underlying reason for all the above observations and uneven growth patterns in different cell types remains speculative, but it may be due to difference in source of origin of graft cells or graft-host membrane interactions or trauma of the procedure. Similar results in line with our observations were shown by Kaufman *et al*. [225] and Hurst *et al*. [226], where some cell lines showed tumor development and others not [227].

H&E staining of U87 tumor sections, showed cancer cells, as recognized by their larger size and hyperchromatic nuclei, intimate contact with the CAM surface (figure 9, left) and while invading the chorioallantoic mesenchyma (figure 9, right). Moreover, increased perfusion around the forming mass and penetration of blood vessels into the tumor (figure 12e) was indicative of ongoing tumor-induced neovascularization, presumably through the secretion of angiogenic growth factors. Similarly, using glioblastoma spheroids, Magalhaes *et al*. [228] demonstrated successfully on ex ovo CAM assays the development of the tumor vasculature and invasion without the use of exogenous growth factors. Also Hagedorn *et al*. [222] showed that the model reliably simulates key features of human glioma growth in a

short time span. In line with our findings the CAM/tumor model appears to be suitable not only for the study of angiogenesis and tumor growth but also to analyze invasion and metastasis [229]. Limitations in CAM-based preclinical screenings do include i) non-specific inflammatory reactions as a result of explant, as some publications suggest which can induce a minor secondary angiogenic response [230], [231]. ii) Short time window of the assay (6 days) making it ideal only for fast growing highly aggressive cancer models. iii) High mortality rate due to bleeding with i.v. infusion of test agents (figure 11a, b). iv) An inefficient model for metastases detection by MRI (according to our data, figure 18) due to short time window for cells to undergo metastasis and/or insufficient cell load. Despite these disadvantages, the CAM assay appears to be one of the preferred methods to study angiogenesis [227], [232], [233].

Using cultured U87 cells, the *in vitro* toxicity of established AIs was initially evaluated, including the a) VEGF antibody AVA (Bevacizumab); b) VEGFR2 antagonist Sunitinib®, and c) the vessel-normalization agent Razoxane®. In addition, the toxic effects of an antagonist of lactate uptake, the MCT-1 inhibitor (CHC) was tested. 24 hour application of up to 5mg/ml AVA revealed hardly any detrimental effect on growing U87 cells (figure 10a). Similarly, concentrations of up to 10μM Sunitinib [234] and 200μM Raxozane® did not confer marked cytotoxicity as compared to controls (Figure 10b, c). In contrast, CHC induced significant cell death in U87 cells, at and above concentrations of 5mM, indicating cytotoxicity with higher concentrations.

Colen *et al*. [235] argued that the cytotoxic effect of high CHC concentrations might be due to the general disruption of both mitochondrial and glycolytic metabolism as a result of long-term inhibition of lactate uptake [235]–[237]. Alternatively, CHC might also trigger a disruption of nicotinamide cofactor redox cycling between NAD^+/NADH or $NADP^+$/NADPH forms [235], [238].

Previous *in vitro* studies showed that higher CHC concentrations (10mM) can adversely impact invasive and proliferative character of U87 cells [238]. In line with these findings in the present study a slight anti-proliferative effects of CHC at 0.31mM concentration was seen. Subsequently combination treatment of cultured U87 cells showed similar effect as of

CHC indicating that there is no additive or synergetic effect on cell proliferation under *in-vitro* conditions and, thus, supporting the idea of tumor microenvironments as an ideal target for treatment.

Glioblastomas are a highly vascularized malignant entity and therefore an attractive target for anti-angiogenic therapies. In our case AVA alone was found to considerably slow down the growth of the primary mass (figure 13), and attenuate blood flow (nutrient supply) to the tumor periphery by ~16% (figure 14), which appears to agree with the clinical situation where application of the antibody has been shown to delay disease progression [239], [240]. Despite this moderate starvation and retardation, however, AVA as a monotherapy yielded no improvement of overall survival in patients with glioblastoma [241]–[243]. Similar CAM experiments with bevacizumab supported our findings of strong antiangiogenic effect on the CAM [244], [245]. The lack of complete inhibition of tumor growth and perfusion by AVA can be explained by remaining VEGF-independent angiogenesis signaling and recent publications highlighting increased tissue hypoxia in glioblastomas post-AVA treatment [246], [247]. Accordingly we found that, relative to control grafts, AVA monotherapy augmented both intensity and extent of pimonidazole-positive hypoxia in U87 explants (figure 15 f, g). Thus, AVA-treated malignancies might indeed develop heightened therapy-resistance and tumor spread as they become more hypoxic.

In cancer cells, VEGF is constitutively overexpressed, independent of oxygen tension, but its steady state level can further be increased by hypoxia in HIF-dependent and –independent manner [67], [248], [249]. Once AI treatment targets a specific cascade (e.g. AVA targeting VEGF-A signaling), cancer cells are prone to evade the pharmacological stress by activating alternative factors or signaling events that will continue to promote tumor angiogenesis. These AI-triggered responses may include a) Recruitment of pro-angiogenic cells (vascular progenitor cells, pro-angiogenic monocytes from the bone marrow) to the tumor site [250]–[252], b) up-regulation of substitute pro-angiogenic signaling mechanisms, e.g induction of VEGFC [253], [254] and VEGFD [255], [256] signaling via VEGFR2, and/or stimulation of FGF-mediated neovascularization [257]. Especially glioblastoma cells can respond with a highly versatile defense repertoire during anti-vascular endothelial growth factor therapy. Agda and colleagues [257] recently demonstrated the up-regulation of several angiogenesis-

(interleukins, FGFs, angiogenin) and invasion- (SPARC, TIMPs, MMP-2, MMP-9 and MMP-12) promoting molecules once glioblastomas cells were challenged by AVA *in vitro* [257], [258]. c) Increased and tight pericyte coverage, thus, protecting tumor blood vessels and d) enhanced capabilities for invasion without angiogenesis. Rubenstein *et al*. [259] for the first time demonstrated the invasive nature of orthotopic glioblastomas in mouse models under Anti-VEGF Antibody Treatment.

Yet, despite the various scenarios to stimulate blood supply of nutrients, fast growing glioblastomas are notorious for developing severe local hypoxia and an associated increase in glycolytic flux, which may exceed that of the healthy brain areas by 3-fold or more [260], [261]. Consequently, one finds an increased ratio of lactate to pyruvate in these cancer cells [262]. Thus, upregulation of MCTs is believed to play an important role in intracellular homeostasis of malignant glioma and to support the tumors enormous virulence by enabling the use of lactate as oxidative fuel [191], [263], [264]. A number of reports demonstrated MCT1 to function as effective importer of lactate in tumor cells with active aerobic glycolysis [265]–[269]. Since lactate was shown to promote VEGF production by fibroblasts and macrophages [270]–[272], it might serve as key mediator in the organization, integrity and functionality of the vascular network around neoplastic masses. Accordingly our own data and other related publications [191], [273] suggest that blocking lactate uptake through MCT1 inhibition by CHC could be beneficial in treating tumor hypoxia and angiogenesis. Relative to AVA monotherapy, CHC application alone was far more effective in halting tumor growth (figure 13). It also reduced blood flow and nutrient supply to the tumor periphery by ~37% (figure 14). Most importantly, and in agreement with expectation, application of CHC attenuated intensity and extent of pimonidazole-positive hypoxia in U87 explants, which illustrates the selective cell kill within hypoxic/glycolytic compartments of the tumors (figure 15). These effects of CHC were clearly potentiated by the combinatorial application of AVA+CHC. This dual anti-angiogenic/anti-MCT1 strategy resulted in real shrinkage of tumor growth (figure 13), a nearly 2-fold reduction in overall blood supply to the tumor (see figure 14) and dwindling pimonidazole-positive hypoxia intensities down to 40% of control explants (figure 15f). Hypoxic areas in primary U87 masses were reduced to ~90% of control tumors. This weakened pimonidazole staining in glioblastoma grafts treated

by AVA+CHC combination therapy is indicative for the eradication of hypoxic cells and the effective block of therapeutic resistance. Representative vessel staining with Evans blue as well, showed dwindled vessel at CAM/tumor interphase of combinatorial treatments as compared to monotherapies and controls supporting the hypothesis.

Due to previous failed attempts to detect metastases/mobility in U87 and MCF7 tumors with MRI (figure 18), we switched to completely new cell line and new detection technique (developed in our lab). The major drawback of a CAM/glioblastoma explant setup is the fact that glioblastoma, *in vivo*, hardly ever metastasize [217], [218]. To also be able to assess the efficacy of mono- and combinatorial AVA and CHC treatments on cell metastasis/mobility, we switched our cell system to metastasis-prone MDA-MB 231 breast carcinoma cells [214], [215], [274]. MDA-MB 231 cell migration around the tumor was assessed under AVA-only, CHC-only and AVA+CHC applications (figure 17) with AVA treatments showing increased cell migrations as compared to monotherapies and control treatments supporting our previous findings, but as this assay is not a complete metastasis assay (due to lack of intravasation and extravasation) a thorough investigation is required in this regard before commenting on the metastatic behavior of MDA-MB 231 tumors with AVA-only, CHC-only and AVA+CHC treatments. The reliability of CAM/migration assay for studying the cell behavior (migration), is also reported by a number of other publications [275]–[278] as well.

The major findings of this study are: i) The observed growth of the tumor explant, its active angiogenesis in conjunction with regional pimonidazole-indicated tissue hypoxia and its invasion of host tissue all demonstrate the suitability of the CAM/tumor explant approach as pre-clinical tool for the development and malignant progression of primary tumors (see Table 3 and figure 8). ii) Monotherapy with angiogenic inhibitors (AIs) such as AVA resulted in the increased, not diminished, intensity and extension of pimonidazole-positive tumor hypoxia, a finding in line with the selection towards more hypoxia-tolerant and virulent secondary growth (see figure 15). iii) Anti-angiogenic therapy, when combined with MCT1 inhibitors (i.e. AVA + CHC), did not only inhibit most effectively both growth (see figure 13) and nutrient supply (see figure 14) toward the primary mass by targeting primarily the oxygenated/aerobe compartment of the tumor. This combinatorial treatment also resulted

in a significant diminishment of patches with severe tissue hypoxia within the residual tumor (see figure 15). Particularly the latter observation suggests AI/CHC treatments to be suitable to overcome the compensatory (anti-angiogenic) drug resistance of surviving clones that are adapted to withstand severe deprivation of O_2 and other essential nutrients.

Combinatorial therapeutic practices have become standard procedure for anti-cancer interventions in the clinic [279], [280]. For example, AVA [280] in combination with paclitaxel or temozolomide has been shown to exert potentiated antitumor effects on human breast cancer, glioma xenografts [281]–[284]. Using CHC as a pretreatment modality was found to effectively sensitize U87 tumors to radiotherapy [235].

6. Conclusion

To date, however, pre-clinical data on anti-angiogenic tumor therapy do not translate very productively into the clinic, often associated with tumor aggressiveness and metastatic. But our intervention protocol of combining anti-angiogenic drugs (i.e Avastin) with agents that selectively target hypoxic microenvironments (i.e MCT1 inhibitors) within the tumor, have shown first hand evidence that, it might be able to shrink primary masses and minimize the risk of malignant progression and tumor spread at the same time, thus overcoming the compensatory angiogenic responses responsible for drug resistance and metastasis. Of course, these strategies need further analyses of suitable cell models and drug combinations in CAM and murine models and an appropriate approach for translating the results into the clinic. Also, we demonstrated the animal saving applicability of CAM/explant methodology as a cheap, easy-to-implement pre-clinical drug screen. In conjunction with a reduced number of xenograft analyses in rodents, a two-tiered approach, 1) high-throughput CAM screening of drugs and 2) an alternative to rodent models. That way we hope to address the urgent need for additional pre-clinical tools to identify most effective anti-angiogenic treatment strategies at minimal negative impact for the patient.

7. Future Perspectives

Anti-angiogenic drugs (i.e. AVA) are already approved for clinical use in therapy of solid cancers. CHC (MCT-1 inhibitor) so far to the best of our knowledge is not yet in clinical use however other MCT1 inhibitors like AZD3965 are currently undergoing phase 1 clinical trials [285]. Coupled with anti-angiogenic drugs, the new-found roles of lactate metabolism in solid tumors could be a high- priority target for cancer therapeutics. Our findings with CAM assay has opened a new window in cancer treatment and we hope this findings will first lead to test our concept in animal models and second result in clinical trials. But to optimize the efficacy of this combinatorial protocol a better understanding is needed specifically in understanding the lactate shuttling and VEGF expression in malignancies of different tumor types and development stages along with the identification of biological markers that are associated with response and/or resistance to this combinatorial protocol. Treatments primarily aimed to target one cell compartment also affect several cell types in a tumor, such as tumor cells, endothelial cells and immune cells information on activity or output of precarious signaling pathway that are related to this cell types is also necessary, in order to develop a rational way of targeting. On the long run we expect that our novel therapeutic approach will aid in development of series of clinically potent and selective MCT-1 inhibitors and advancement in best drug combinations with safer and more efficient anti-cancer therapies. Thus, help to save and prolong the life of many patients.

Project B (Side project)

(Role of Interleukin 6 (IL-6) in Ewing's sarcoma spread)

8 Introduction

8.1 Interleukin (IL-6) in Ewing's sarcoma spread

Ewing's sarcoma is a rare disease associated with small round-cell tumor characteristically found in the bones, and sometimes soft tissues[286], [287]. It is most commonly seen in children and adolescents, comprising 16% of the total primary bone sarcomas[288]. Majority of the cases of Ewing sarcoma (85%) are due to Chromosomal translocation (between chromosome 22 and 11), fusing EWS gene from chromosome 22 to FL1 gene from chromosome 11[288]. In children Ewing Sarcomas is often associated with development of fever that is persistent. Cytokines, like IL6, IL8 etc are known fever mediators and at the same time, interleukins like IL-6 are also known to promote cancer progression to a more virulent, invasive stage, working through numerous signaling cascades[289]. It is observed that patients with Ewing's sarcoma, have significant elevated levels of serum IL-6, in correlation with a poor overall survival[290]. And as Ewing sarcomas are characterized with a strong potential to metastasize, the lungs are the most common site (50%), followed by bone (25%) and bone marrow (20%)[291]. In a small study using Cam assay we tried to answer the question. Does the fever mediator IL-6 boost tumor spread in Ewing's sarcoma?

9 Material and methods

9.1 CAM assay to evaluate role of IL-6 in motility Ewing Sarcoma cells

The A4573 Ewing sarcoma cell line, engineered to stably overexpress green fluorescent protein (GFP), was a generous gift from the group of Prof. Kontny (as above). For the *in vivo* motility assay $2.5x10^6$ A4573/GFP cells were initially inoculated on the CAM on d9 of development (as described in section 3.4.1). On the following day, three explants, each

growing on a separate embryo, were treated with a) 10 µl PBS (control), b) 10ul IL-6 (25ng/ul) and c) 10 µl IL-6 (50 ng/µl)). IL-6 was purchased from R&D system (catalog number: 206-IL) and dissolved in PBS. On day 14 CAM images were made with fluorescent microscope to look for cell migration. A4573/GFP cells were detected under the fluorescent microscope (excitation: 488nm; emission: 507nm) and quantified as a function of migration distance from the perimeter of the explant. For that purpose three images per tumor were taken, each superimposed by a 15x12 square grid that allowed to subdivide the entire image into five equal-size zones (each with 3x12 square area) out of five, three zones where analysed: Considering zone 3 (tumor edge), zone 2 (adjacent to zone 3) and zone 1 (adjacent to zone 2) (see figure 19e). Next, cell coverage in each square was estimated with values ranging from 0 (no cells present) to 5 (square 100% filled with cells). Mean coverage values were computed from all three images per zone and tumor modality (control, 250ng IL-6, 500ng IL-6).

10 Results

10.1 Effect of IL6 on cell migration.

Ewing Sarcomas in children are often associated with development of fever. Cytokines, inlcuding IL6, IL8 etc. are known fever mediators. At the same time, interleukins (i.e. IL-6) can promote cancer progression to a more virulent, invasive phenotype. Thus, the question dealt with this experiment was: Does the fever mediator IL-6 boost tumor spread? Ewing Sarcoma-CAM tumor explants, treated with and without IL6, are ex vivo models in this context to look at the role of IL6 for an intensified cell migration on CAM. For this experiment GFP positive Ewing Sarcoma cells (A4573) explants where treated with a) PBS (control), b) 10ul IL-6 (25ng/ul) and c) 10ul IL-6 (50ng/ul)). On day 14 of chick embryo development, images were made around the tumor periphery with fluorescent microscope to look for cell migration (figure 19 a-c). Considering zone 3 (tumor edge), zone 2 (adjacent to zone 3) and zone 1 (adjacent to zone 2) (see figure 19e), data were analyzed as described in materials and methods (section 9.1). 500ng IL6 treatments clearly showed higher migration

rates as compared to controls and 250ng IL6 treatment (figure 19d), thus, confirming the previous findings for role of IL6 in inducing metastasis spread.

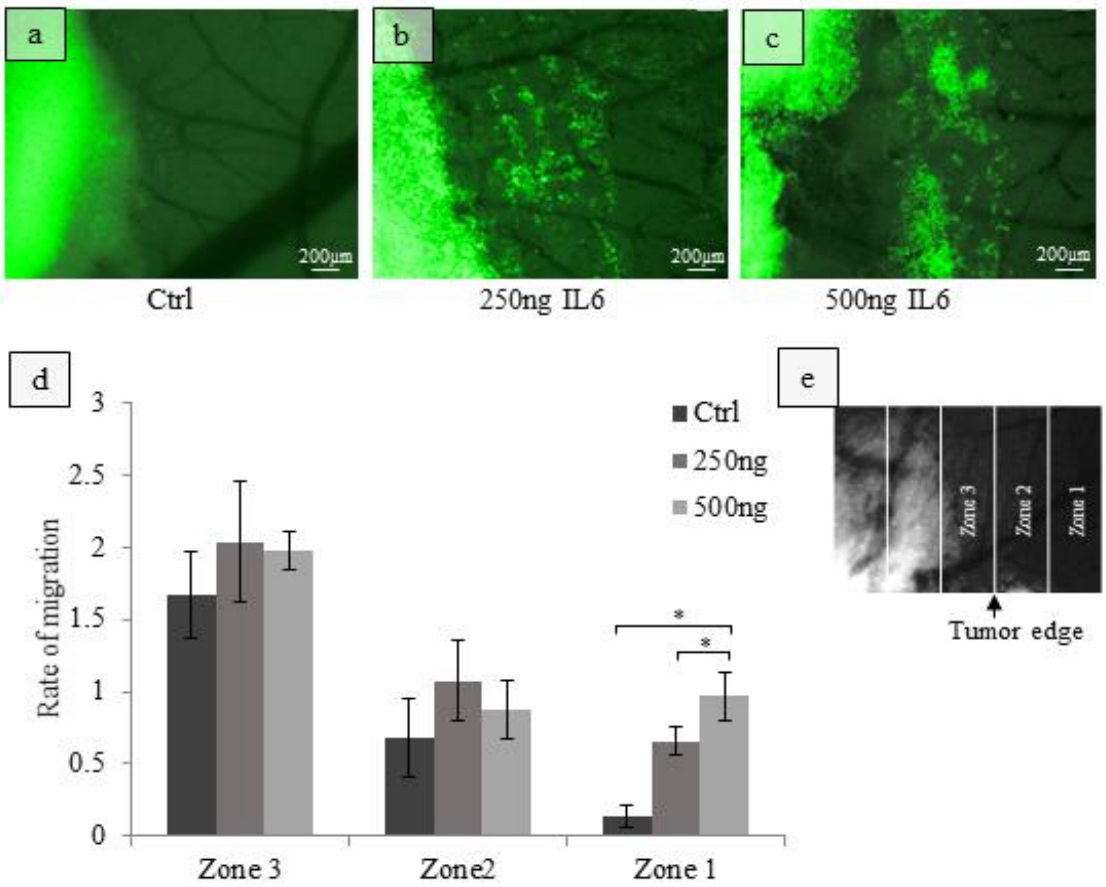

Figure 19: Effect of IL-6 on spreading of GFP positive Ewing Sarcoma cells (A4573) explants. Tumors where treated with a) PBS (control), b) 10ul IL-6 (25ng/ul) and c) 10ul IL-6 (50ng/ul)). Considering zone 3 (tumor edge), zone 2 (adjacent to zone 3) and zone 1 (adjacent to zone 2) (see figure 19e), data was analyzed as described in materials and methods (see section 9.1). 500ng IL6 treatments clearly showed higher migration rates as compared to controls and 250ng IL6 treatment. Data are means ±SEM, n=3. Statistical differences among the mean coverages against control were tested with Kruskal–Wallis one-way analysis of variance, which stated the effect of IL6 was not significant. (Significance was accepted at $p<0.05$, ns = not significant)

11. Comment

Ewing sarcoma is known to show aggressive behavior, disseminating to vital organs (e.g lungs) Our data from Ewing sarcoma tumor showed dose dependent increase in cell migration with IL-6 treatment (figure 19) in line with the previous findings for role of IL6 in inducing metastasis spread [289]. Clinical data suggest patients with Ewing's sarcoma, have significantly high levels of serum IL-6, corelated with poor overall survival [290]. In case of this assay still a thorough investigation is required before commenting on the migration/metastatic behavior of Ewing sarcoma cells on CAM. nonetheless as a first hand evidence, the observed growth of the tumor explant, in conjunction with its cell migration under IL6 treatment all demonstrate the suitability of the CAM/explant approach as pre-clinical tool to portray the development and malignant progression of primary tumors. The reliability of CAM/migration assay for studying the cell behavior (migration), is well reported by a number of other publications [275]–[278] as well.

12. References

[1] F. Baltzer, “Theodor Boveri.,” *Science*, vol. 144, no. 3620, pp. 809–15, May 1964.

[2] B. W. Stewart and C. P. Wild, Eds., *World Cancer Report 2014*. Lyon France: International Agency for Research on Cancer, 2014.

[3] R. A. Kazi and R. E. Peter, “Christian Albert Theodor Billroth: master of surgery.,” *J. Postgrad. Med.*, vol. 50, no. 1, pp. 82–3.

[4] “Emil Grubbe.” [Online]. Available: http://en.wikipedia.org/wiki/Emil_Grubbe. [Accessed: 03-Mar-2014].

[5] *Pioneer in X-Ray Therapy*, Vol. 125,. American Association for the Advancement of Science, 1957, pp. 18–19.

[6] “150 Years of Advances Against Cancer,” *National cancer Institute*. [Online]. Available: http://www.cancer.gov/aboutnci/overview/150-years-advances/page4. [Accessed: 27-Dec-2013].

[7] D. Hanahan and R. A. Weinberg, “The Hallmarks of Cancer,” *Cell*, vol. 100, no. 1, pp. 57–70, 2000.

[8] D. Hanahan and R. A. Weinberg, “Hallmarks of cancer: the next generation.,” *Cell*, vol. 144, no. 5, pp. 646–674, 2011.

[9] C. E. Meacham and S. J. Morrison, “Tumour heterogeneity and cancer cell plasticity.,” *Nature*, vol. 501, no. 7467, pp. 328–37, Sep. 2013.

[10] P. C. Nowell, “The clonal evolution of tumor cell populations.,” *Science*, vol. 194, no. 4260, pp. 23–8, Oct. 1976.

[11] I. J. Fidler and I. R. Hart, “Biological diversity in metastatic neoplasms: origins and implications.,” *Science*, vol. 217, no. 4564, pp. 998–1003, Sep. 1982.

[12] R. Kim, M. Emi, and K. Tanabe, “Cancer immunoediting from immune surveillance to immune escape.,” *Immunology*, vol. 121, no. 1, pp. 1–14, May 2007.

[13] E. J. Villablanca, L. Raccosta, D. Zhou, R. Fontana, D. Maggioni, A. Negro, F. Sanvito, M. Ponzoni, B. Valentinis, M. Bregni, A. Prinetti, K. R. Steffensen, S. Sonnino, J.-A. Gustafsson, C. Doglioni, C. Bordignon, C. Traversari, and V. Russo, “Tumor-mediated liver X receptor-alpha activation inhibits CC chemokine receptor-7 expression on dendritic cells and dampens antitumor responses.,” *Nat. Med.*, vol. 16, no. 1, pp. 98–105, Jan. 2010.

[14] M. R. Junttila and F. J. de Sauvage, “Influence of tumour micro-environment heterogeneity on therapeutic response.,” *Nature*, vol. 501, no. 7467, pp. 346–54, Sep. 2013.

[15] C. Curtis, S. P. Shah, S.-F. Chin, G. Turashvili, O. M. Rueda, M. J. Dunning, D. Speed, A. G. Lynch, S. Samarajiwa, Y. Yuan, S. Gräf, G. Ha, G. Haffari, A. Bashashati, R. Russell, S. McKinney, A. Langerød, A. Green, E. Provenzano, G. Wishart, S. Pinder, P. Watson, F. Markowetz, L. Murphy, I. Ellis, A. Purushotham, A.-L. Børresen-Dale, J. D. Brenton, S. Tavaré, C. Caldas, and S. Aparicio, “The genomic and transcriptomic architecture of 2,000 breast tumours reveals novel subgroups.,” *Nature*, vol. 486, no. 7403, pp. 346–52, Jun. 2012.

[16] D. L. Dexter and J. T. Leith, “Tumor heterogeneity and drug resistance.,” *J. Clin. Oncol.*, vol. 4, no. 2, pp. 244–57, Mar. 1986.

[17] N. Navin, A. Krasnitz, L. Rodgers, K. Cook, J. Meth, J. Kendall, M. Riggs, Y. Eberling, J. Troge, V. Grubor, D. Levy, P. Lundin, S. Månér, A. Zetterberg, J. Hicks, and M. Wigler, “Inferring tumor progression from genomic heterogeneity.,” *Genome Res.*, vol. 20, no. 1, pp. 68–80, Jan. 2010.

[18] L. Khalique, A. Ayhan, M. E. Weale, I. J. Jacobs, S. J. Ramus, and S. A. Gayther, “Genetic intra-tumour heterogeneity in epithelial ovarian cancer and its implications for molecular diagnosis of tumours.,” *J. Pathol.*, vol. 211, no. 3, pp. 286–95, Mar. 2007.

[19] C. L. Sawyers, “Opportunities and challenges in the development of kinase inhibitor therapy for cancer.,” *Genes Dev.*, vol. 17, no. 24, pp. 2998–3010, Dec. 2003.

[20] N. DeWitt, “Angiogenesis,” *Nature*, vol. 438, no. 7070, pp. 931–931, Dec. 2005.

[21] J. M. Kelm, C. Diaz Sanchez-Bustamante, E. Ehler, S. P. Hoerstrup, V. Djonov, L. Ittner, and M. Fussenegger, “VEGF profiling and angiogenesis in human microtissues.,” *J. Biotechnol.*, vol. 118, no. 2, pp. 213–29, Aug. 2005.

[22] M. J. Adair TH, *Overview of Angiogenesis*. Morgan & Claypool Life Sciences, 2010.

[23] H. Kurz, P. H. Burri, and V. G. Djonov, “Angiogenesis and vascular remodeling by intussusception: from form to function.,” *News Physiol. Sci.*, vol. 18, pp. 65–70, Apr. 2003.

[24] V. G. Djonov, H. Kurz, and P. H. Burri, “Optimality in the developing vascular system: branching remodeling by means of intussusception as an efficient adaptation mechanism.,” *Dev. Dyn.*, vol. 224, no. 4, pp. 391–402, Aug. 2002.

[25] V. Djonov, O. Baum, and P. H. Burri, “Vascular remodeling by intussusceptive angiogenesis.,” *Cell Tissue Res.*, vol. 314, no. 1, pp. 107–17, Oct. 2003.

[26] P. H. Burri and M. R. Tarek, “A novel mechanism of capillary growth in the rat pulmonary microcirculation.,” *Anat. Rec.*, vol. 228, no. 1, pp. 35–45, Sep. 1990.

[27] J. H. Caduff, L. C. Fischer, and P. H. Burri, “Scanning electron microscope study of the developing microvasculature in the postnatal rat lung.,” *Anat. Rec.*, vol. 216, no. 2, pp. 154–64, Oct. 1986.

[28] P. H. Burri, R. Hlushchuk, and V. Djonov, “Intussusceptive angiogenesis: its emergence, its characteristics, and its significance.,” *Dev. Dyn.*, vol. 231, no. 3, pp. 474–88, Nov. 2004.

[29] S. Patan, M. J. Alvarez, J. C. Schittny, and P. H. Burri, “Intussusceptive microvascular growth: a common alternative to capillary sprouting.,” *Arch. Histol. Cytol.*, vol. 55 Suppl, pp. 65–75, Jan. 1992.

[30] W. Risau, “Mechanisms of angiogenesis.,” *Nature*, vol. 386, no. 6626, pp. 671–4, Apr. 1997.

[31] R. N. Cleaver O, Krieg PA. Harvey RP, “Molecular mechanisms of vascular development.,” *Heart development. San Diego:Academic Press*, pp. 221–252, 1999.

[32] F. Hillen and A. W. Griffioen, “Tumour vascularization: sprouting angiogenesis and beyond.,” *Cancer Metastasis Rev.*, vol. 26, no. 3–4, pp. 489–502, Dec. 2007.

[33] R. K. Jain, “Molecular regulation of vessel maturation.,” *Nat. Med.*, vol. 9, no. 6, pp. 685–93, Jun. 2003.

[34] P. Carmeliet, “Angiogenesis in health and disease.,” *Nat. Med.*, vol. 9, no. 6, pp. 653–660, Jun. 2003.

[35] G. D. Yancopoulos, S. Davis, N. W. Gale, J. S. Rudge, S. J. Wiegand, and J. Holash, “Vascular-specific growth factors and blood vessel formation.,” *Nature*, vol. 407, no. 6801, pp. 242–8, Sep. 2000.

[36] P. Gerwins, E. Sköldenberg, and L. Claesson-Welsh, “Function of fibroblast growth factors and vascular endothelial growth factors and their receptors in angiogenesis.,” *Crit. Rev. Oncol. Hematol.*, vol. 34, no. 3, pp. 185–94, Jun. 2000.

[37] K. K. Hirschi and P. A. D’Amore, “Pericytes in the microvasculature.,” *Cardiovasc. Res.*, vol. 32, no. 4, pp. 687–98, Oct. 1996.

[38] R. Klein, “Excitatory Eph receptors and adhesive ephrin ligands.,” *Curr. Opin. Cell Biol.*, vol. 13, no. 2, pp. 196–203, Apr. 2001.

[39] S. Ogawa, A. Oku, A. Sawano, S. Yamaguchi, Y. Yazaki, and M. Shibuya, “A Novel Type of Vascular Endothelial Growth Factor, VEGF-E (NZ-7 VEGF), Preferentially Utilizes KDR/Flk-1 Receptor and Carries a Potent Mitotic Activity without Heparin-binding Domain,” *J. Biol. Chem.*, vol. 273, no. 47, pp. 31273–31282, Nov. 1998.

[40] M. Meyer, M. Clauss, A. Lepple-Wienhues, J. Waltenberger, H. G. Augustin, M. Ziche, C. Lanz, M. Büttner, H. J. Rziha, and C. Dehio, “A novel vascular endothelial growth factor encoded by Orf virus, VEGF-E, mediates angiogenesis via signalling through VEGFR-2 (KDR) but not VEGFR-1 (Flt-1) receptor tyrosine kinases.,” *EMBO J.*, vol. 18, no. 2, pp. 363–74, Jan. 1999.

[41] L. Centanin, A. Dekanty, N. Romero, M. Irisarri, T. A. Gorr, and P. Wappner, “Cell Autonomy of HIF Effects in Drosophila: Tracheal Cells Sense Hypoxia and Induce Terminal Branch Sprouting,” *Dev. Cell*, vol. 14, pp. 547–558, 2008.

[42] L. Centanin, T. A. Gorr, and P. Wappner, “Tracheal remodelling in response to hypoxia,” *Journal of Insect Physiology*, vol. 56. pp. 447–454, 2010.

[43] A. P. Berger, K. Kofler, J. Bektic, H. Rogatsch, H. Steiner, G. Bartsch, and H. Klocker, “Increased growth factor production in a human prostatic stromal cell culture model caused by hypoxia.,” *Prostate*, vol. 57, no. 1, pp. 57–65, Sep. 2003.

[44] C. W. Pugh and P. J. Ratcliffe, “Regulation of angiogenesis by hypoxia: role of the HIF system.,” *Nat. Med.*, vol. 9, no. 6, pp. 677–84, Jun. 2003.

[45] Y.-H. Shi, L. Bingle, L.-H. Gong, Y.-X. Wang, K. P. Corke, and W.-G. Fang, “Basic FGF augments hypoxia induced HIF-1-alpha expression and VEGF release in T47D breast cancer cells.,” *Pathology*, vol. 39, no. 4, pp. 396–400, Aug. 2007.

[46] P. C. Maisonpierre, C. Suri, P. F. Jones, S. Bartunkova, S. J. Wiegand, C. Radziejewski, D. Compton, J. McClain, T. H. Aldrich, N. Papadopoulos, T. J. Daly, S. Davis, T. N. Sato, and G. D. Yancopoulos, “Angiopoietin-2, a natural antagonist for Tie2 that disrupts in vivo angiogenesis.,” *Science*, vol. 277, no. 5322, pp. 55–60, Jul. 1997.

[47] S. Davis, T. H. Aldrich, P. F. Jones, A. Acheson, D. L. Compton, V. Jain, T. E. Ryan, J. Bruno, C. Radziejewski, P. C. Maisonpierre, and G. D. Yancopoulos, "Isolation of angiopoietin-1, a ligand for the TIE2 receptor, by secretion-trap expression cloning.," *Cell*, vol. 87, no. 7, pp. 1161–9, Dec. 1996.

[48] D. M. Valenzuela, J. A. Griffiths, J. Rojas, T. H. Aldrich, P. F. Jones, H. Zhou, J. McClain, N. G. Copeland, D. J. Gilbert, N. A. Jenkins, T. Huang, N. Papadopoulos, P. C. Maisonpierre, S. Davis, and G. D. Yancopoulos, "Angiopoietins 3 and 4: diverging gene counterparts in mice and humans.," *Proc. Natl. Acad. Sci. U. S. A.*, vol. 96, no. 5, pp. 1904–9, Mar. 1999.

[49] N. W. Gale and G. D. Yancopoulos, "Growth factors acting via endothelial cell-specific receptor tyrosine kinases: VEGFs, angiopoietins, and ephrins in vascular development.," *Genes Dev.*, vol. 13, no. 9, pp. 1055–66, May 1999.

[50] J. G. Flanagan and P. Vanderhaeghen, "The ephrins and Eph receptors in neural development.," *Annu. Rev. Neurosci.*, vol. 21, pp. 309–45, Jan. 1998.

[51] H. U. Wang, Z. F. Chen, and D. J. Anderson, "Molecular distinction and angiogenic interaction between embryonic arteries and veins revealed by ephrin-B2 and its receptor Eph-B4.," *Cell*, vol. 93, no. 5, pp. 741–53, May 1998.

[52] P. Carmeliet and R. K. Jain, "Angiogenesis in cancer and other diseases.," *Nature*, vol. 407, no. 6801, pp. 249–57, Sep. 2000.

[53] P. Carmeliet, "Angiogenesis in life, disease and medicine.," *Nature*, vol. 438, no. 7070, pp. 932–6, Dec. 2005.

[54] E. Goldmann, "The Growth of Malignant Disease in Man and the Lower Animals, with special reference to the Vascular System.," *Proc. R. Soc. Med.*, vol. 1, no. Surg Sect, pp. 1–13, Jan. 1908.

[55] M. A. Gimbrone, R. H. Aster, R. S. Cotran, J. Corkery, J. H. Jandl, and J. Folkman, "Preservation of vascular integrity in organs perfused in vitro with a platelet-rich medium.," *Nature*, vol. 222, no. 5188, pp. 33–6, Apr. 1969.

[56] B. A. Warren, "The ultrastructure of the microcirculation at the advancing edge of Walker 256 carcinoma.," *Microvasc. Res.*, vol. 2, no. 4, pp. 443–53, Oct. 1970.

[57] T. A. Gorr, D. Wichmann, J. Hu, M. Hermes-Lima, A. F. Welker, N. Terwilliger, J. F. Wren, M. Viney, S. Morris, G. E. Nilsson, A. Deten, J. Soliz, and M. Gassmann, "Hypoxia tolerance in animals: biology and application.," *Physiol. Biochem. Zool.*, vol. 83, no. 5, pp. 733–52.

[58] P. Vaupel, F. Kallinowski, and P. Okunieff, "Blood flow, oxygen and nutrient supply, and metabolic microenvironment of human tumors: a review.," *Cancer Res.*, vol. 49, no. 23, pp. 6449–65, Dec. 1989.

[59] J. M. Brown and W. R. Wilson, "Exploiting tumour hypoxia in cancer treatment.," *Nat. Rev. Cancer*, vol. 4, no. 6, pp. 437–47, Jun. 2004.

[60] P. Vaupel, S. Briest, and M. Höckel, "Hypoxia in breast cancer: pathogenesis, characterization and biological/therapeutic implications.," *Wien. Med. Wochenschr.*, vol. 152, no. 13–14, pp. 334–42, Jan. 2002.

[61] M. Höckel and P. Vaupel, "Tumor hypoxia: definitions and current clinical, biologic, and molecular aspects.," *J. Natl. Cancer Inst.*, vol. 93, no. 4, pp. 266–76, Feb. 2001.

[62] P. Vaupel, O. Thews, and M. Hoeckel, “Treatment resistance of solid tumors: role of hypoxia and anemia.,” *Med. Oncol.*, vol. 18, no. 4, pp. 243–59, Jan. 2001.

[63] D. Hanahan and J. Folkman, “Patterns and Emerging Mechanisms of the Angiogenic Switch during Tumorigenesis,” *Cell*, vol. 86, no. 3, pp. 353–64, Aug. 1996.

[64] C. E. Lewis, R. Leek, A. Harris, and J. O. McGee, “Cytokine regulation of angiogenesis in breast cancer: the role of tumor-associated macrophages.,” *J. Leukoc. Biol.*, vol. 57, no. 5, pp. 747–51, May 1995.

[65] R. M. Strieter, P. J. Polverini, D. A. Arenberg, A. Walz, G. Opdenakker, J. Van Damme, and S. L. Kunkel, “Role of C-X-C chemokines as regulators of angiogenesis in lung cancer.,” *J. Leukoc. Biol.*, vol. 57, no. 5, pp. 752–62, May 1995.

[66] A. P. Levy, N. S. Levy, S. Wegner, and M. A. Goldberg, “Transcriptional regulation of the rat vascular endothelial growth factor gene by hypoxia.,” *J. Biol. Chem.*, vol. 270, no. 22, pp. 13333–40, Jun. 1995.

[67] D. Shweiki, A. Itin, D. Soffer, and E. Keshet, “Vascular endothelial growth factor induced by hypoxia may mediate hypoxia-initiated angiogenesis.,” *Nature*, vol. 359, no. 6398, pp. 843–5, Oct. 1992.

[68] G. Elvert, A. Kappel, R. Heidenreich, U. Englmeier, S. Lanz, T. Acker, M. Rauter, K. Plate, M. Sieweke, G. Breier, and I. Flamme, “Cooperative interaction of hypoxia-inducible factor-2alpha (HIF-2alpha) and Ets-1 in the transcriptional activation of vascular endothelial growth factor receptor-2 (Flk-1).,” *J. Biol. Chem.*, vol. 278, no. 9, pp. 7520–30, Feb. 2003.

[69] H. P. Gerber, F. Condorelli, J. Park, and N. Ferrara, “Differential transcriptional regulation of the two vascular endothelial growth factor receptor genes. Flt-1, but not Flk-1/KDR, is up-regulated by hypoxia.,” *J. Biol. Chem.*, vol. 272, no. 38, pp. 23659–67, Sep. 1997.

[70] R. K. Jain and L. L. Munn, “Leaky vessels? Call Ang1!,” *Nat. Med.*, vol. 6, no. 2, pp. 131–2, Feb. 2000.

[71] G. Neufeld, T. Cohen, S. Gengrinovitch, and Z. Poltorak, “Vascular endothelial growth factor (VEGF) and its receptors.,” *FASEB J.*, vol. 13, no. 1, pp. 9–22, Jan. 1999.

[72] N. Ferrara and T. Davis-Smyth, “The biology of vascular endothelial growth factor.,” *Endocr. Rev.*, vol. 18, no. 1, pp. 4–25, Feb. 1997.

[73] N. Ferrara, “Molecular and biological properties of vascular endothelial growth factor.,” *J. Mol. Med. (Berl).*, vol. 77, no. 7, pp. 527–43, Jul. 1999.

[74] S. M. Weis and D. A. Cheresh, “Pathophysiological consequences of VEGF-induced vascular permeability.,” *Nature*, vol. 437, no. 7058, pp. 497–504, Sep. 2005.

[75] M. E. Hardee, M. W. Dewhirst, N. Agarwal, and B. S. Sorg, “Novel imaging provides new insights into mechanisms of oxygen transport in tumors.,” *Curr. Mol. Med.*, vol. 9, no. 4, pp. 435–41, May 2009.

[76] R. K. Jain, “Normalization of tumor vasculature: an emerging concept in antiangiogenic therapy.,” *Science*, vol. 307, no. 5706, pp. 58–62, Jan. 2005.

[77] M. Mazzone, D. Dettori, R. Leite de Oliveira, S. Loges, T. Schmidt, B. Jonckx, Y.-M. Tian, A. A. Lanahan, P. Pollard, C. Ruiz de Almodovar, F. De Smet, S. Vinckier, J. Aragonés, K. Debackere, A. Luttun, S. Wyns, B. Jordan, A. Pisacane, B. Gallez, M. G. Lampugnani, E. Dejana, M. Simons, P. Ratcliffe, P. Maxwell, and P. Carmeliet, "Heterozygous deficiency of PHD2 restores tumor oxygenation and inhibits metastasis via endothelial normalization.," *Cell*, vol. 136, no. 5, pp. 839–51, Mar. 2009.

[78] S. M. Weis and D. A. Cheresh, "Tumor angiogenesis: molecular pathways and therapeutic targets.," *Nat. Med.*, vol. 17, no. 11, pp. 1359–70, Jan. 2011.

[79] D. SOLT and E. FARBER, "New principle for the analysis of chemical carcinogenesis," *Nature*, vol. 263, no. 5579, pp. 701–703, Oct. 1976.

[80] F. Moinfar, Y. G. Man, L. Arnould, G. L. Bratthauer, M. Ratschek, and F. A. Tavassoli, "Concurrent and independent genetic alterations in the stromal and epithelial cells of mammary carcinoma: implications for tumorigenesis.," *Cancer Res.*, vol. 60, no. 9, pp. 2562–6, May 2000.

[81] Y. Zhu, P. Ghosh, P. Charnay, D. K. Burns, and L. F. Parada, "Neurofibromas in NF1: Schwann cell origin and role of tumor environment.," *Science*, vol. 296, no. 5569, pp. 920–2, May 2002.

[82] R. S. Watnick, "The role of the tumor microenvironment in regulating angiogenesis.," *Cold Spring Harb. Perspect. Med.*, vol. 2, no. 12, p. a006676, Dec. 2012.

[83] O. Picard, Y. Rolland, and M. F. Poupon, "Fibroblast-dependent tumorigenicity of cells in nude mice: implication for implantation of metastases.," *Cancer Res.*, vol. 46, pp. 3290–3294, 1986.

[84] A. M. Grey, A. M. Schor, G. Rushton, I. Ellis, and S. L. Schor, "Purification of the migration stimulating factor produced by fetal and breast cancer patient fibroblasts.," *Proc. Natl. Acad. Sci. U. S. A.*, vol. 86, pp. 2438–2442, 1989.

[85] J. L. Camps, S. M. Chang, T. C. Hsu, M. R. Freeman, S. J. Hong, H. E. Zhau, A. C. von Eschenbach, and L. W. Chung, "Fibroblast-mediated acceleration of human epithelial tumor growth in vivo.," *Proc. Natl. Acad. Sci. U. S. A.*, vol. 87, pp. 75–79, 1990.

[86] G. Parsonage, A. D. Filer, O. Haworth, G. B. Nash, G. E. Rainger, M. Salmon, and C. D. Buckley, "A stromal address code defined by fibroblasts.," *Trends Immunol.*, vol. 26, pp. 150–156, 2005.

[87] J. J. Tomasek, J. McRae, G. K. Owens, and C. J. Haaksma, "Regulation of alpha-smooth muscle actin expression in granulation tissue myofibroblasts is dependent on the intronic CArG element and the transforming growth factor-beta1 control element.," *Am. J. Pathol.*, vol. 166, pp. 1343–1351, 2005.

[88] A. F. Olumi, G. D. Grossfeld, S. W. Hayward, P. R. Carroll, T. D. Tlsty, and G. R. Cunha, "Carcinoma-associated Fibroblasts Direct Tumor Progression of Initiated Human Prostatic Epithelium," *Cancer Res.*, vol. 59, no. 19, pp. 5002–5011, Oct. 1999.

[89] B. Elenbaas and R. A. Weinberg, "Heterotypic Signaling between Epithelial Tumor Cells and Fibroblasts in Carcinoma Formation," *Exp. Cell Res.*, vol. 264, no. 1, pp. 169–184, 2001.

[90] R. Chiquet-Ehrismann, E. J. Mackie, C. A. Pearson, and T. Sakakura, "Tenascin: an extracellular matrix protein involved in tissue interactions during fetal development and oncogenesis," *Cell*, vol. 47, no. 1, pp. 131–139, Oct. 1986.

[91] E. B. Brown, Y. Boucher, S. Nasser, and R. K. Jain, “Measurement of macromolecular diffusion coefficients in human tumors,” *Microvasc. Res.*, vol. 67, no. 3, pp. 231–236, 2004.

[92] P. A. Netti, D. A. Berk, M. A. Swartz, A. J. Grodzinsky, and R. K. Jain, “Role of Extracellular Matrix Assembly in Interstitial Transport in Solid Tumors,” *Cancer Res.*, vol. 60, no. 9, pp. 2497–2503, May 2000.

[93] A. Orimo, P. B. Gupta, D. C. Sgroi, F. Arenzana-Seisdedos, T. Delaunay, R. Naeem, V. J. Carey, A. L. Richardson, and R. A. Weinberg, “Stromal fibroblasts present in invasive human breast carcinomas promote tumor growth and angiogenesis through elevated SDF-1/CXCL12 secretion.,” *Cell*, vol. 121, no. 3, pp. 335–48, May 2005.

[94] M. T. Dimanche-Boitrel, L. Vakaet, P. Pujuguet, B. Chauffert, M. S. Martin, A. Hammann, F. Van Roy, M. Mareel, and F. Martin, “In vivo and in vitro invasiveness of a rat colon-cancer cell line maintaining E-cadherin expression: an enhancing role of tumor-associated myofibroblasts.,” *Int. J. Cancer*, vol. 56, no. 4, pp. 512–21, Feb. 1994.

[95] E. Olaso and F. Vidal-Vanaclocha, “Use of tumor-activated hepatic stellate cell as a target for the preclinical testing of anti-angiogenic drugs against hepatic tumor development.,” *Methods Mol. Med.*, vol. 85, pp. 79–86, Jan. 2003.

[96] E. Olaso, A. Santisteban, J. Bidaurrazaga, A. M. Gressner, J. Rosenbaum, and F. Vidal-Vanaclocha, “Tumor-dependent activation of rodent hepatic stellate cells during experimental melanoma metastasis.,” *Hepatology*, vol. 26, no. 3, pp. 634–42, Sep. 1997.

[97] S. Rogelj, R. A. Weinberg, P. Fanning, and M. Klagsbrun, “Basic fibroblast growth factor fused to a signal peptide transforms cells.,” *Nature*, vol. 331, no. 6152, pp. 173–5, Jan. 1988.

[98] S. Rogelj, R. A. Weinberg, P. Fanning, and M. Klagsbrun, “Characterization of tumors produced by signal peptide-basic fibroblast growth factor-transformed cells.,” *J. Cell. Biochem.*, vol. 39, no. 1, pp. 13–23, Jan. 1989.

[99] M. Gleave, J.-T. Hsieh, C. Gao, A. C. von Eschenbach, and L. W. K. Chung, “Acceleration of Human Prostate Cancer Growth in Vivo by Factors Produced by Prostate and Bone Fibroblasts,” *Cancer Res.*, vol. 51, no. 14, pp. 3753–3761, Jul. 1991.

[100] P. R. Lawler and J. Lawler, “Molecular basis for the regulation of angiogenesis by thrombospondin-1 and -2.,” *Cold Spring Harb. Perspect. Med.*, vol. 2, no. 5, p. a006627, May 2012.

[101] J. C. Rodriguez-Manzaneque, T. F. Lane, M. A. Ortega, R. O. Hynes, J. Lawler, and M. L. Iruela-Arispe, “Thrombospondin-1 suppresses spontaneous tumor growth and inhibits activation of matrix metalloproteinase-9 and mobilization of vascular endothelial growth factor.,” *Proc. Natl. Acad. Sci. U. S. A.*, vol. 98, no. 22, pp. 12485–90, Oct. 2001.

[102] P. Clezardin, L. Frappart, M. Clerget, C. Pechoux, and P. D. Delmas, “Expression of Thrombospondin (TSP1) and Its Receptors (CD36 and CD51) in Normal, Hyperplastic, and Neoplastic Human Breast,” *Cancer Res.*, vol. 53, no. 6, pp. 1421–1430, Mar. 1993.

[103] S. Filleur, O. V Volpert, A. Degeorges, C. Voland, F. Reiher, P. Clézardin, N. Bouck, and F. Cabon, “In vivo mechanisms by which tumors producing thrombospondin 1 bypass its inhibitory effects.,” *Genes Dev.*, vol. 15, no. 11, pp. 1373–82, Jun. 2001.

[104] R. S. Watnick, Y.-N. Cheng, A. Rangarajan, T. A. Ince, and R. A. Weinberg, "RETRACTED: Ras modulates Myc activity to repress thrombospondin-1 expression and increase tumor angiogenesis," *Cancer Cell*, vol. 3, no. 3, pp. 219–231, Mar. 2003.

[105] G. Ferrari, B. D. Cook, V. Terushkin, G. Pintucci, and P. Mignatti, "Transforming growth factor-beta 1 (TGF-beta1) induces angiogenesis through vascular endothelial growth factor (VEGF)-mediated apoptosis.," *J. Cell. Physiol.*, vol. 219, no. 2, pp. 449–58, May 2009.

[106] A. B. Roberts, M. B. Sporn, R. K. Assoian, J. M. Smith, N. S. Roche, L. M. Wakefield, U. I. Heine, L. A. Liotta, V. Falanga, and J. H. Kehrl, "Transforming growth factor type beta: rapid induction of fibrosis and angiogenesis in vivo and stimulation of collagen formation in vitro.," *Proc. Natl. Acad. Sci.*, vol. 83, no. 12, pp. 4167–4171, Jun. 1986.

[107] M. Fràter-Schröder, G. Müller, W. Birchmeier, and P. Böhlen, "Transforming growth factor-beta inhibits endothelial cell proliferation," *Biochem. Biophys. Res. Commun.*, vol. 137, no. 1, pp. 295–302, 1986.

[108] A. Baird and T. Durkin, "Inhibition of endothelial cell proliferation by type β-transforming growth factor: Interactions with acidic and basic fibroblast growth factors," *Biochem. Biophys. Res. Commun.*, vol. 138, no. 1, pp. 476–482, 1986.

[109] S. Schultz-Cherry, "Thrombospondin causes activation of latent transforming growth factor- beta secreted by endothelial cells by a novel mechanism [published erratum appears in J Cell Biol 1993 Sep;122(5):following 1143]," *J. Cell Biol.*, vol. 122, no. 4, pp. 923–932, Aug. 1993.

[110] J. E. Murphy-Ullrich, S. Schultz-Cherry, and M. Hook, "Transforming growth factor-beta complexes with thrombospondin.," *Mol. Biol. Cell*, vol. 3, no. 2, pp. 181–188, Feb. 1992.

[111] E. Brogi, T. Wu, A. Namiki, and J. M. Isner, "Indirect angiogenic cytokines upregulate VEGF and bFGF gene expression in vascular smooth muscle cells, whereas hypoxia upregulates VEGF expression only," *Circulation*, vol. 90, no. 2, pp. 649–652, Aug. 1994.

[112] L. Pertovaara, A. Kaipainen, T. Mustonen, A. Orpana, N. Ferrara, O. Saksela, and K. Alitalo, "Vascular endothelial growth factor is induced in response to transforming growth factor-beta in fibroblastic and epithelial cells," *J. Biol. Chem.*, vol. 269, no. 9, pp. 6271–6274, Mar. 1994.

[113] K. T. Goldsmith, R. B. Gammon, and R. I. Garver, "Modulation of bFGF in lung fibroblasts by TGF-beta and PDGF.," *Am. J. Physiol.*, vol. 261, no. 6 Pt 1, pp. L378–85, Dec. 1991.

[114] J. Dong, J. Grunstein, M. Tejada, F. Peale, G. Frantz, W.-C. Liang, W. Bai, L. Yu, J. Kowalski, X. Liang, G. Fuh, H.-P. Gerber, and N. Ferrara, "VEGF-null cells require PDGFR alpha signaling-mediated stromal fibroblast recruitment for tumorigenesis.," *EMBO J.*, vol. 23, no. 14, pp. 2800–10, Jul. 2004.

[115] R. A. Majack, J. Mildbrandt, and V. M. Dixit, "Induction of thrombospondin messenger RNA levels occurs as an immediate primary response to platelet-derived growth factor.," *J. Biol. Chem.*, vol. 262, no. 18, pp. 8821–8825, Jun. 1987.

[116] K. Sengupta, S. Banerjee, N. K. Saxena, and S. K. Banerjee, "Thombospondin-1 Disrupts Estrogen-Induced Endothelial Cell Proliferation and Migration and Its Expression Is Suppressed by Estradiol," *Mol. Cancer Res.*, vol. 2, no. 3, pp. 150–158, Mar. 2004.

[117] M. Colombel, S. Filleur, P. Fournier, C. Merle, J. Guglielmi, A. Courtin, A. Degeorges, C. M. Serre, R. Bouvier, P. Clezardin, and F. Cabon, "Androgens Repress the Expression of the Angiogenesis Inhibitor Thrombospondin-1 in Normal and Neoplastic Prostate," *Cancer Res.*, vol. 65, no. 1, pp. 300–308, Jan. 2005.

[118] P. B. Gupta, D. Proia, O. Cingoz, J. Weremowicz, S. P. Naber, R. A. Weinberg, and C. Kuperwasser, "Systemic stromal effects of estrogen promote the growth of estrogen receptor-negative cancers.," *Cancer Res.*, vol. 67, no. 5, pp. 2062–71, Mar. 2007.

[119] W. Kalas, J. L. Yu, C. Milsom, J. Rosenfeld, R. Benezra, P. Bornstein, and J. Rak, "Oncogenes and Angiogenesis: down-regulation of thrombospondin-1 in normal fibroblasts exposed to factors from cancer cells harboring mutant ras.," *Cancer Res.*, vol. 65, no. 19, pp. 8878–86, Oct. 2005.

[120] P. Van Lint and C. Libert, "Chemokine and cytokine processing by matrix metalloproteinases and its effect on leukocyte migration and inflammation.," *J. Leukoc. Biol.*, vol. 82, no. 6, pp. 1375–81, Dec. 2007.

[121] A. Noël, A. Hajitou, C. L'Hoir, E. Maquoi, E. Baramova, J. M. Lewalle, A. Remacle, F. Kebers, P. Brown, C. M. Calberg-Bacq, and J. M. Foidart, "Inhibition of stromal matrix metalloproteases: effects on breast-tumor promotion by fibroblasts.," *Int. J. Cancer*, vol. 76, no. 2, pp. 267–73, Apr. 1998.

[122] Q. Yu and I. Stamenkovic, "Cell surface-localized matrix metalloproteinase-9 proteolytically activates TGF-beta and promotes tumor invasion and angiogenesis," *Genes & Dev.*, vol. 14, no. 2, pp. 163–176, Jan. 2000.

[123] D. Lyden, K. Hattori, S. Dias, C. Costa, P. Blaikie, L. Butros, A. Chadburn, B. Heissig, W. Marks, L. Witte, Y. Wu, D. Hicklin, Z. Zhu, N. R. Hackett, R. G. Crystal, M. A. Moore, K. A. Hajjar, K. Manova, R. Benezra, and S. Rafii, "Impaired recruitment of bone-marrow-derived endothelial and hematopoietic precursor cells blocks tumor angiogenesis and growth.," *Nat. Med.*, vol. 7, no. 11, pp. 1194–201, Nov. 2001.

[124] F. Djouad, P. Plence, C. Bony, P. Tropel, F. Apparailly, J. Sany, D. Noël, and C. Jorgensen, "Immunosuppressive effect of mesenchymal stem cells favors tumor growth in allogeneic animals.," *Blood*, vol. 102, no. 10, pp. 3837–44, Nov. 2003.

[125] B. A. Peters, L. A. Diaz, K. Polyak, L. Meszler, K. Romans, E. C. Guinan, J. H. Antin, D. Myerson, S. R. Hamilton, B. Vogelstein, K. W. Kinzler, and C. Lengauer, "Contribution of bone marrow-derived endothelial cells to human tumor vasculature.," *Nat. Med.*, vol. 11, no. 3, pp. 261–2, Mar. 2005.

[126] B. D. Roorda, A. ter Elst, W. A. Kamps, and E. S. J. M. de Bont, "Bone marrow-derived cells and tumor growth: contribution of bone marrow-derived cells to tumor micro-environments with special focus on mesenchymal stem cells.," *Crit. Rev. Oncol. Hematol.*, vol. 69, no. 3, pp. 187–98, Mar. 2009.

[127] K. C. Kemp, J. Hows, and C. Donaldson, "Bone marrow-derived mesenchymal stem cells.," *Leuk. Lymphoma*, vol. 46, no. 11, pp. 1531–44, Nov. 2005.

[128] M. F. Pittenger, "Multilineage Potential of Adult Human Mesenchymal Stem Cells," *Science (80-.).*, vol. 284, no. 5411, pp. 143–147, Apr. 1999.

[129] D. J. Prockop, "Marrow stromal cells as stem cells for nonhematopoietic tissues.," *Science*, vol. 276, no. 5309, pp. 71–4, Apr. 1997.

[130] S. Kidd, E. Spaeth, A. Klopp, M. Andreeff, B. Hall, and F. Marini, "The (in) auspicious role of mesenchymal stromal cells in cancer: be it friend or foe," *Cytotherapy*, vol. 10, no. 7, pp. 657–667, 2008.

[131] E. Spaeth, A. Klopp, J. Dembinski, M. Andreeff, and F. Marini, "Inflammation and tumor microenvironments: defining the migratory itinerary of mesenchymal stem cells.," *Gene Ther.*, vol. 15, no. 10, pp. 730–8, May 2008.

[132] C. Schichor, T. Birnbaum, N. Etminan, O. Schnell, S. Grau, S. Miebach, K. Aboody, C. Padovan, A. Straube, J.-C. Tonn, and R. Goldbrunner, "Vascular endothelial growth factor A contributes to glioma-induced migration of human marrow stromal cells (hMSC)," *Exp. Neurol.*, vol. 199, no. 2, pp. 301–310, 2006.

[133] T. Birnbaum, J. Roider, C. J. Schankin, C. S. Padovan, C. Schichor, R. Goldbrunner, and A. Straube, "Malignant gliomas actively recruit bone marrow stromal cells by secreting angiogenic cytokines.," *J. Neurooncol.*, vol. 83, no. 3, pp. 241–7, Jul. 2007.

[134] R. M. Dwyer, S. M. Potter-Beirne, K. A. Harrington, A. J. Lowery, E. Hennessy, J. M. Murphy, F. P. Barry, T. O'Brien, and M. J. Kerin, "Monocyte chemotactic protein-1 secreted by primary breast tumors stimulates migration of mesenchymal stem cells.," *Clin. Cancer Res.*, vol. 13, no. 17, pp. 5020–7, Sep. 2007.

[135] S. B. Coffelt, F. C. Marini, K. Watson, K. J. Zwezdaryk, J. L. Dembinski, H. L. LaMarca, S. L. Tomchuck, K. Honer zu Bentrup, E. S. Danka, S. L. Henkle, and A. B. Scandurro, "The pro-inflammatory peptide LL-37 promotes ovarian tumor progression through recruitment of multipotent mesenchymal stromal cells.," *Proc. Natl. Acad. Sci. U. S. A.*, vol. 106, no. 10, pp. 3806–11, Mar. 2009.

[136] T. Kinnaird, E. Stabile, M. S. Burnett, C. W. Lee, S. Barr, S. Fuchs, and S. E. Epstein, "Marrow-derived stromal cells express genes encoding a broad spectrum of arteriogenic cytokines and promote in vitro and in vivo arteriogenesis through paracrine mechanisms.," *Circ. Res.*, vol. 94, no. 5, pp. 678–85, Mar. 2004.

[137] M. Crowther, N. J. Brown, E. T. Bishop, and C. E. Lewis, "Microenvironmental influence on macrophage regulation of angiogenesis in wounds and malignant tumors," *J. Leukoc. Biol.*, vol. 70, no. 4, pp. 478–490, Oct. 2001.

[138] L. Soucek, E. R. Lawlor, D. Soto, K. Shchors, L. B. Swigart, and G. I. Evan, "Mast cells are required for angiogenesis and macroscopic expansion of Myc-induced pancreatic islet tumors.," *Nat. Med.*, vol. 13, no. 10, pp. 1211–8, Oct. 2007.

[139] D. J. Manalo, A. Rowan, T. Lavoie, L. Natarajan, B. D. Kelly, S. Q. Ye, J. G. N. Garcia, and G. L. Semenza, "Transcriptional regulation of vascular endothelial cell responses to hypoxia by HIF-1.," *Blood*, vol. 105, no. 2, pp. 659–69, Jan. 2005.

[140] P. H. Maxwell, G. U. Dachs, J. M. Gleadle, L. G. Nicholls, A. L. Harris, I. J. Stratford, O. Hankinson, C. W. Pugh, and P. J. Ratcliffe, "Hypoxia-inducible factor-1 modulates gene expression in solid tumors and influences both angiogenesis and tumor growth.," *Proc. Natl. Acad. Sci. U. S. A.*, vol. 94, no. 15, pp. 8104–9, Jul. 1997.

[141] O. Stoeltzing, M. F. McCarty, J. S. Wey, F. Fan, W. Liu, A. Belcheva, C. D. Bucana, G. L. Semenza, and L. M. Ellis, "Role of hypoxia-inducible factor 1alpha in gastric cancer cell growth, angiogenesis, and vessel maturation.," *J. Natl. Cancer Inst.*, vol. 96, no. 12, pp. 946–56, Jun. 2004.

[142] J. A. Forsythe, B. H. Jiang, N. V Iyer, F. Agani, S. W. Leung, R. D. Koos, and G. L. Semenza, "Activation of vascular endothelial growth factor gene transcription by hypoxia-inducible factor 1.," *Mol. Cell. Biol.*, vol. 16, no. 9, pp. 4604–13, Sep. 1996.

[143] R. L. Jensen, B. T. Ragel, K. Whang, and D. Gillespie, "Inhibition of hypoxia inducible factor-1alpha (HIF-1alpha) decreases vascular endothelial growth factor (VEGF) secretion and tumor growth in malignant gliomas.," *J. Neurooncol.*, vol. 78, no. 3, pp. 233–47, Jul. 2006.

[144] R. Bos, H. Zhong, C. F. Hanrahan, E. C. Mommers, G. L. Semenza, H. M. Pinedo, M. D. Abeloff, J. W. Simons, P. J. van Diest, and E. van der Wall, "Levels of hypoxia-inducible factor-1 alpha during breast carcinogenesis.," *J. Natl. Cancer Inst.*, vol. 93, no. 4, pp. 309–14, Feb. 2001.

[145] P. Carmeliet, Y. Dor, J. M. Herbert, D. Fukumura, K. Brusselmans, M. Dewerchin, M. Neeman, F. Bono, R. Abramovitch, P. Maxwell, C. J. Koch, P. Ratcliffe, L. Moons, R. K. Jain, D. Collen, E. Keshert, and E. Keshet, "Role of HIF-1alpha in hypoxia-mediated apoptosis, cell proliferation and tumour angiogenesis.," *Nature*, vol. 394, no. 6692, pp. 485–90, Jul. 1998.

[146] N. Tang, L. Wang, J. Esko, F. J. Giordano, Y. Huang, H.-P. Gerber, N. Ferrara, and R. S. Johnson, "Loss of HIF-1alpha in endothelial cells disrupts a hypoxia-driven VEGF autocrine loop necessary for tumorigenesis.," *Cancer Cell*, vol. 6, no. 5, pp. 485–95, Nov. 2004.

[147] S. Moncada and A. Higgs, "The L-arginine-nitric oxide pathway.," *N. Engl. J. Med.*, vol. 329, no. 27, pp. 2002–12, Dec. 1993.

[148] D. S. Bredt, P. M. Hwang, C. E. Glatt, C. Lowenstein, R. R. Reed, and S. H. Snyder, "Cloned and expressed nitric oxide synthase structurally resembles cytochrome P-450 reductase.," *Nature*, vol. 351, no. 6329, pp. 714–8, Jun. 1991.

[149] C. J. Lowenstein, C. S. Glatt, D. S. Bredt, and S. H. Snyder, "Cloned and expressed macrophage nitric oxide synthase contrasts with the brain enzyme.," *Proc. Natl. Acad. Sci. U. S. A.*, vol. 89, no. 15, pp. 6711–5, Aug. 1992.

[150] P. A. Marsden, K. T. Schappert, H. S. Chen, M. Flowers, C. L. Sundell, J. N. Wilcox, S. Lamas, and T. Michel, "Molecular cloning and characterization of human endothelial nitric oxide synthase.," *FEBS Lett.*, vol. 307, no. 3, pp. 287–93, Aug. 1992.

[151] T. Michel and O. Feron, "Nitric oxide synthases: which, where, how, and why?," *J. Clin. Invest.*, vol. 100, no. 9, pp. 2146–52, Nov. 1997.

[152] U. Förstermann and W. C. Sessa, "Nitric oxide synthases: regulation and function.," *Eur. Heart J.*, vol. 33, no. 7, pp. 829–37, 837a–837d, Apr. 2012.

[153] M. Ziche, L. Morbidelli, R. Choudhuri, H. T. Zhang, S. Donnini, H. J. Granger, and R. Bicknell, "Nitric oxide synthase lies downstream from vascular endothelial growth factor-induced but not basic fibroblast growth factor-induced angiogenesis.," *J. Clin. Invest.*, vol. 99, no. 11, pp. 2625–34, Jun. 1997.

[154] C. Branco-Price, N. Zhang, M. Schnelle, C. Evans, D. M. M. Katschinski, D. Liao, L. Ellies, and R. S. S. Johnson, "Endothelial Cell HIF-1α and HIF-2α Differentially Regulate Metastatic Success," *Cancer Cell*, vol. 21, no. 1, pp. 52–65, Jan. 2012.

[155] H. Kimura, A. Weisz, Y. Kurashima, K. Hashimoto, T. Ogura, F. D'Acquisto, R. Addeo, M. Makuuchi, and H. Esumi, "Hypoxia response element of the human vascular endothelial growth factor gene mediates transcriptional regulation by nitric oxide: control of hypoxia-inducible factor-1 activity by nitric oxide.," *Blood*, vol. 95, no. 1, pp. 189–97, Jan. 2000.

[156] L. A. Palmer, G. L. Semenza, M. H. Stoler, and R. A. Johns, "Hypoxia induces type II NOS gene expression in pulmonary artery endothelial cells via HIF-1.," *Am. J. Physiol.*, vol. 274, no. 2 Pt 1, pp. L212–9, Feb. 1998.

[157] J. P. Cooke, "NO and angiogenesis.," *Atheroscler. Suppl.*, vol. 4, no. 4, pp. 53–60, Dec. 2003.

[158] L. Morbidelli, S. Donnini, and M. Ziche, "Role of nitric oxide in the modulation of angiogenesis.," *Curr. Pharm. Des.*, vol. 9, no. 7, pp. 521–30, Jan. 2003.

[159] G. Pagès and J. Pouysségur, "Transcriptional regulation of the Vascular Endothelial Growth Factor gene--a concert of activating factors.," *Cardiovasc. Res.*, vol. 65, no. 3, pp. 564–73, Feb. 2005.

[160] D. Schmidt, B. Textor, O. T. Pein, A. H. Licht, S. Andrecht, M. Sator-Schmitt, N. E. Fusenig, P. Angel, and M. Schorpp-Kistner, "Critical role for NF-kappaB-induced JunB in VEGF regulation and tumor angiogenesis.," *EMBO J.*, vol. 26, no. 3, pp. 710–9, Feb. 2007.

[161] E. Racker, "History of the Pasteur effect and its pathobiology.," *Mol. Cell. Biochem.*, vol. 5, no. 1–2, pp. 17–23, Nov. 1974.

[162] G. L. Semenza, D. Artemov, A. Bedi, Z. Bhujwalla, K. Chiles, D. Feldser, E. Laughner, R. Ravi, J. Simons, P. Taghavi, and H. Zhong, "'The metabolism of tumours': 70 years later.," *Novartis Found. Symp.*, vol. 240, pp. 251–60; discussion 260–4, Jan. 2001.

[163] R. A. Gatenby and R. J. Gillies, "Why do cancers have high aerobic glycolysis?," *Nat. Rev. Cancer*, vol. 4, no. 11, pp. 891–9, Nov. 2004.

[164] C. V Dang and G. L. Semenza, "Oncogenic alterations of metabolism," *Trends Biochem. Sci.*, vol. 24, no. 2, pp. 68–72, Mar. 1999.

[165] O. Warburg, "Ist die aerobe Glykolyse spezifisch für die Tumoren?," *Biochem. Z*, vol. 204, pp. 482–483, 1929.

[166] O. Warburg, F. Wind, and E. Negelein, "THE METABOLISM OF TUMORS IN THE BODY.," *J. Gen. Physiol.*, vol. 8, no. 6, pp. 519–30, Mar. 1927.

[167] F. U. Nielsen, P. Daugaard, L. Bentzen, H. Stødkilde-Jørgensen, J. Overgaard, M. R. Horsman, and R. J. Maxwell, "Effect of changing tumor oxygenation on glycolytic metabolism in a murine C3H mammary carcinoma assessed by in vivo nuclear magnetic resonance spectroscopy.," *Cancer Res.*, vol. 61, no. 13, pp. 5318–25, Jul. 2001.

[168] M. Stubbs, C. L. Bashford, and J. R. Griffiths, "Understanding the tumor metabolic phenotype in the genomic era.," *Curr. Mol. Med.*, vol. 3, no. 1, pp. 49–59, Feb. 2003.

[169] J. A. Mares-Perlman and E. Shrago, "Energy substrate utilization in freshly isolated Morris Hepatoma 7777 cells.," *Cancer Res.*, vol. 48, no. 3, pp. 602–8, Feb. 1988.

[170] M. Guppy, P. Leedman, X. Zu, and V. Russell, "Contribution by different fuels and metabolic pathways to the total ATP turnover of proliferating MCF-7 breast cancer cells.," *Biochem. J.*, vol. 364, no. Pt 1, pp. 309–15, May 2002.

[171] X. L. Zu and M. Guppy, "Cancer metabolism: facts, fantasy, and fiction.," *Biochem. Biophys. Res. Commun.*, vol. 313, no. 3, pp. 459–65, Jan. 2004.

[172] M. Guppy, "The hypoxic core: a possible answer to the cancer paradox.," *Biochem. Biophys. Res. Commun.*, vol. 299, no. 4, pp. 676–80, Dec. 2002.

[173] K. A. Brand and U. Hermfisse, "Aerobic glycolysis by proliferating cells: a protective strategy against reactive oxygen species.," *FASEB J.*, vol. 11, no. 5, pp. 388–95, Apr. 1997.

[174] K. Brand, "Aerobic glycolysis by proliferating cells: protection against oxidative stress at the expense of energy yield.," *J. Bioenerg. Biomembr.*, vol. 29, no. 4, pp. 355–64, Aug. 1997.

[175] S. Walenta, A. Salameh, H. Lyng, J. F. Evensen, M. Mitze, E. K. Rofstad, and W. Mueller-Klieser, "Correlation of high lactate levels in head and neck tumors with incidence of metastasis.," *Am. J. Pathol.*, vol. 150, no. 2, pp. 409–15, Feb. 1997.

[176] L. B. Gladden, "Lactate metabolism: a new paradigm for the third millennium.," *J. Physiol.*, vol. 558, no. Pt 1, pp. 5–30, Jul. 2004.

[177] K. S. Dimmer, B. Friedrich, F. Lang, J. W. Deitmer, and S. Bröer, "The low-affinity monocarboxylate transporter MCT4 is adapted to the export of lactate in highly glycolytic cells.," *Biochem. J.*, vol. 350 Pt 1, pp. 219–27, Aug. 2000.

[178] A. P. Halestrap and D. Meredith, "The SLC16 gene family-from monocarboxylate transporters (MCTs) to aromatic amino acid transporters and beyond.," *Pflugers Arch.*, vol. 447, no. 5, pp. 619–28, Feb. 2004.

[179] R. C. Poole, C. E. Sansom, and A. P. Halestrap, "Studies of the membrane topology of the rat erythrocyte H+/lactate cotransporter (MCT1).," *Biochem. J.*, vol. 320 (Pt 3, pp. 817–24, Dec. 1996.

[180] C. K. Garcia, M. S. Brown, R. K. Pathak, and J. L. Goldstein, "cDNA cloning of MCT2, a second monocarboxylate transporter expressed in different cells than MCT1.," *J. Biol. Chem.*, vol. 270, no. 4, pp. 1843–9, Jan. 1995.

[181] V. N. Jackson, N. T. Price, L. Carpenter, and A. P. Halestrap, "Cloning of the monocarboxylate transporter isoform MCT2 from rat testis provides evidence that expression in tissues is species-specific and may involve post-transcriptional regulation.," *Biochem. J.*, vol. 324 (Pt 2, pp. 447–53, Jun. 1997.

[182] N. J. Philp, H. Yoon, and E. F. Grollman, "Monocarboxylate transporter MCT1 is located in the apical membrane and MCT3 in the basal membrane of rat RPE.," *Am. J. Physiol.*, vol. 274, no. 6 Pt 2, pp. R1824–8, Jun. 1998.

[183] L. Bergersen, E. Jóhannsson, M. L. Veruki, E. A. Nagelhus, A. Halestrap, O. M. Sejersted, and O. P. Ottersen, "Cellular and subcellular expression of monocarboxylate transporters in the pigment epithelium and retina of the rat.," *Neuroscience*, vol. 90, no. 1, pp. 319–31, Apr. 1999.

[184] Robert S. Kerbel, "Evaluating Tumor Response and Resistance Mechanisms to Antiangiogenic Drugs using New Preclinical Models of Metastatic Disease," in *Trans-NIH Angiogenesis Workshop*, 2013.

[185] "Angiogenesis Inhibitors," *National cancer Institute*. [Online]. Available: http://www.cancer.gov/cancertopics/factsheet/Therapy/angiogenesis-inhibitors. [Accessed: 03-Mar-2014].

[186] M. R. Mancuso, R. Davis, S. M. Norberg, S. O'Brien, B. Sennino, T. Nakahara, V. J. Yao, T. Inai, P. Brooks, B. Freimark, D. R. Shalinsky, D. D. Hu-Lowe, and D. M. McDonald, "Rapid vascular regrowth in tumors after reversal of VEGF inhibition.," *J. Clin. Invest.*, vol. 116, no. 10, pp. 2610–21, Oct. 2006.

[187] T. Inai, M. Mancuso, H. Hashizume, F. Baffert, A. Haskell, P. Baluk, D. D. Hu-Lowe, D. R. Shalinsky, G. Thurston, G. D. Yancopoulos, and D. M. McDonald, "Inhibition of vascular endothelial growth factor (VEGF) signaling in cancer causes loss of endothelial fenestrations, regression of tumor vessels, and appearance of basement membrane ghosts.," *Am. J. Pathol.*, vol. 165, no. 1, pp. 35–52, Jul. 2004.

[188] M. Pàez-Ribes, E. Allen, J. Hudock, T. Takeda, H. Okuyama, F. Viñals, M. Inoue, G. Bergers, D. Hanahan, and O. Casanovas, "Antiangiogenic therapy elicits malignant progression of tumors to increased local invasion and distant metastasis.," *Cancer Cell*, vol. 15, no. 3, pp. 220–231, Mar. 2009.

[189] J. M. L. Ebos, C. R. Lee, W. Cruz-Munoz, G. A. Bjarnason, J. G. Christensen, and R. S. Kerbel, "Accelerated metastasis after short-term treatment with a potent inhibitor of tumor angiogenesis.," *Cancer Cell*, vol. 15, no. 3, pp. 232–239, Mar. 2009.

[190] H. M. W. Verheul, E. E. Voest, and R. O. Schlingemann, "Are tumours angiogenesis-dependent?," *J. Pathol.*, vol. 202, no. 1, pp. 5–13, Jan. 2004.

[191] P. Sonveaux, F. Végran, T. Schroeder, M. C. Wergin, J. Verrax, Z. N. Rabbani, C. J. De Saedeleer, K. M. Kennedy, C. Diepart, B. F. Jordan, M. J. Kelley, B. Gallez, M. L. Wahl, O. Feron, M. W. Dewhirst, and C. J. De Saedeleer, "Targeting lactate-fueled respiration selectively kills hypoxic tumor cells in mice.," *J. Clin. Invest.*, vol. 118, no. 12, pp. 3930–42, Dec. 2008.

[192] S. Loges, M. Mazzone, P. Hohensinner, and P. Carmeliet, "Silencing or fueling metastasis with VEGF inhibitors: antiangiogenesis revisited.," *Cancer Cell*, vol. 15, no. 3, pp. 167–70, Mar. 2009.

[193] C. Schlatterer, "Krebsbekämpfung mit böser Überraschung-Schlecht durchblutete Tumore werden schneller aggressiv," *Neue Zürcher Zeitung*, Zurich, 11-Mar-2009.

[194] J. B. Murphy, "Transplantability of tissues to the embryo of foreign species: its bearing on questions of tissue specificity and tumor immunity.," *J. Exp. Med.*, vol. 17, no. 4, pp. 482–93, Apr. 1913.

[195] D. H. Ausprunk, D. R. Knighton, and J. Folkman, "Differentiation of vascular endothelium in the chick chorioallantois: a structural and autoradiographic study.," *Dev. Biol.*, vol. 38, no. 2, pp. 237–48, Jun. 1974.

[196] D. O. DeFouw, V. J. Rizzo, R. Steinfeld, and R. N. Feinberg, "Mapping of the microcirculation in the chick chorioallantoic membrane during normal angiogenesis.," *Microvasc. Res.*, vol. 38, no. 2, pp. 136–47, Sep. 1989.

[197] K. V Bilbao, D. V Palanker, P. Huie, M. S. Blumenkranz, T. Leng, and J. M. Miller, "The chick chorioallantoic membrane as a model tissue for surgical retinal research and simulation.," *Retina*, vol. 24, no. 3, pp. 427–34, Jun. 2004.

[198] A. Kuzminienė, S. Šalomskaitė-Davalgienė, I. Balnyte, J. Palubinskienė, A. Valančiūtė, and V. Ulozas, "Evaluation of the chicken embryo chorioallantoic membrane model for laryngeal tumor transplantation," *Pap. Anthropol.*, vol. 20, p. 229, Dec. 2012.

[199] A. Fuchs and E. S. S. Lindenbaum, "The two- and three-dimensional structure of the microcirculation of the chick chorioallantoic membrane.," *Acta Anat. (Basel).*, vol. 131, no. 4, pp. 271–5, Jan. 1988.

[200] E. I. Deryugina and J. P. Quigley, "Chick embryo chorioallantoic membrane model systems to study and visualize human tumor cell metastasis.," *Histochem. Cell Biol.*, vol. 130, no. 6, pp. 1119–30, Dec. 2008.

[201] A. L. Romanoff, *From the Egg to the Chick*, 33rd ed. Cornell Rural School Leaflet, 1939, pp. 57–63.

[202] R. Bellairs and M. Osmond, *Atlas of Chick Development*. Academic Press, San Diego, 2005.

[203] A. Vargas, M. Zeisser-Labouèbe, N. Lange, R. Gurny, and F. Delie, "The chick embryo and its chorioallantoic membrane (CAM) for the in vivo evaluation of drug delivery systems.," *Adv. Drug Deliv. Rev.*, vol. 59, no. 11, pp. 1162–1176, Sep. 2007.

[204] "Alternative CAM: chicken eggs to precede mouse experiments," *BIOPRO Baden-Württemberg GmbH*, 2010. [Online]. Available: http://www.bio-pro.org/magazin/thema/05144/index.html?lang=en&artikelid=/artikel/05166/index.html. [Accessed: 03-Mar-2014].

[205] "Moor Instruments Inc," 2012. [Online]. Available: http://gb.moor.co.uk/product/moorflpi-moorflpi/4. [Accessed: 01-Nov-2013].

[206] J. Hu, D. P. Stiehl, C. Setzer, D. Wichmann, D. A. Shinde, H. Rehrauer, P. Hradecky, M. Gassmann, and T. A. Gorr, "Interaction of HIF and USF signaling pathways in human genes flanked by hypoxia-response elements and E-box palindromes.," *Mol. Cancer Res.*, vol. 9, no. 11, pp. 1520–36, Nov. 2011.

[207] G. Kristiansen, J. Hu, D. Wichmann, D. P. Stiehl, M. Rose, J. Gerhardt, A. Bohnert, A. ten Haaf, H. Moch, J. Raleigh, M. A. Varia, P. Subarsky, F. M. Scandurra, E. Gnaiger, E. Gleixner, A. Bicker, M. Gassmann, T. Hankeln, E. Dahl, and T. A. Gorr, "Endogenous myoglobin in breast cancer is hypoxia-inducible by alternative transcription and functions to impair mitochondrial activity: a role in tumor suppression?," *J. Biol. Chem.*, vol. 286, no. 50, pp. 43417–28, Dec. 2011.

[208] D. S. Dohle, S. D. Pasa, S. Gustmann, M. Laub, J. H. Wissler, H. P. Jennissen, and N. Dünker, "Chick ex ovo culture and ex ovo CAM assay: how it really works.," *J. Vis. Exp. JoVE*, no. 33, pp. 2–7, Jan. 2009.

[209] "From Egg To Chick: Development and Preservation of Embryos." [Online]. Available: http://chickscope.beckman.uiuc.edu/resources/egg_to_chick/development.html. [Accessed: 01-Sep-2012].

[210] I. Genentech, "Avastin prescribing information," 2004. [Online]. Available: http://www.gene.com/download/pdf/avastin_prescribing.pdf. [Accessed: 20-Dec-2013].

[211] Pfizer Inc, “Sutent prescribing information,” 2006. [Online]. Available: http://labeling.pfizer.com/ShowLabeling.aspx?id=607. [Accessed: 04-Jan-2014].

[212] E. Del Prete, T. A. Lutz, and E. Scharrer, “Inhibition of glucose oxidation by α-cyano-4-hydroxycinnamic acid stimulates feeding in rats,” *Physiol. Behav.*, vol. 80, no. 4, pp. 489–498, 2004.

[213] M. Balke, A. Neumann, C. Kersting, K. Agelopoulos, C. Gebert, G. Gosheger, H. Buerger, and M. Hagedorn, “Morphologic characterization of osteosarcoma growth on the chick chorioallantoic membrane,” *BMC Res. Notes*, vol. 3, p. 58, 2010.

[214] A. D. Gruber and B. U. Pauli, “Tumorigenicity of human breast cancer is associated with loss of the Ca2+-activated chloride channel CLCA2.,” *Cancer Res.*, vol. 59, no. 21, pp. 5488–91, Nov. 1999.

[215] I. Zajc, N. Sever, A. Bervar, and T. T. Lah, “Expression of cysteine peptidase cathepsin L and its inhibitors stefins A and B in relation to tumorigenicity of breast cancer cell lines.,” *Cancer Lett.*, vol. 187, no. 1–2, pp. 185–90, Dec. 2002.

[216] B. J. Hindson, K. D. Ness, D. A. Masquelier, P. Belgrader, N. J. Heredia, A. J. Makarewicz, I. J. Bright, M. Y. Lucero, A. L. Hiddessen, T. C. Legler, T. K. Kitano, M. R. Hodel, J. F. Petersen, P. W. Wyatt, E. R. Steenblock, P. H. Shah, L. J. Bousse, C. B. Troup, J. C. Mellen, D. K. Wittmann, N. G. Erndt, T. H. Cauley, R. T. Koehler, A. P. So, S. Dube, K. A. Rose, L. Montesclaros, S. Wang, D. P. Stumbo, S. P. Hodges, S. Romine, F. P. Milanovich, H. E. White, J. F. Regan, G. A. Karlin-Neumann, C. M. Hindson, S. Saxonov, and B. W. Colston, “High-throughput droplet digital PCR system for absolute quantitation of DNA copy number.,” *Anal. Chem.*, vol. 83, no. 22, pp. 8604–10, Nov. 2011.

[217] E. Fonkem, M. Lun, and E. T. Wong, “Rare phenomenon of extracranial metastasis of glioblastoma.,” *J. Clin. Oncol.*, vol. 29, no. 34, pp. 4594–5, Dec. 2011.

[218] B. Pasquier, D. Pasquier, A. N’Golet, M. H. Panh, and P. Couderc, “Extraneural metastases of astrocytomas and glioblastomas: clinicopathological study of two cases and review of literature.,” *Cancer*, vol. 45, no. 1, pp. 112–25, Jan. 1980.

[219] National Cancer Insitute, “Metastatic Cancer.” [Online]. Available: http://www.cancer.gov/cancertopics/factsheet/Sites-Types/metastatic. [Accessed: 19-Oct-2013].

[220] “Schweiz. Nationalfonds SNF.” [Online]. Available: http://www.snf.ch/D/Aktuell/Horizonte/Seiten/201306.aspx. [Accessed: 30-Sep-2013].

[221] M. Hagedorn and W. Jörg, “Chick Chorioallantoic Membrane Assay: Growth Factor and Tumor-induced Angiogenesis and Lymphangiogenesis,” *Methods Endothel. Cell Biol. Springer Lab Manuals*, pp. 247–261, 2004.

[222] M. Hagedorn, S. Javerzat, D. Gilges, A. Meyre, B. de Lafarge, A. Eichmann, and A. Bikfalvi, “Accessing key steps of human tumor progression in vivo by using an avian embryo model.,” *Proc. Natl. Acad. Sci. U. S. A.*, vol. 102, no. 5, pp. 1643–8, Feb. 2005.

[223] I. C. C. MacDonald, E. E. E. Schmidt, V. L. L. Morris, A. F. F. Chambers, and A. C. C. Groom, “Intravital videomicroscopy of the chorioallantoic microcirculation: a model system for studying metastasis.,” *Microvasc. Res.*, vol. 44, no. 2, pp. 185–199, Sep. 1992.

[224] K. Kunzi-Rapp, F. Genze, R. Küfer, E. Reich, R. E. Hautmann, and J. E. Gschwend, "Chorioallantoic membrane assay: vascularized 3-dimensional cell culture system for human prostate cancer cells as an animal substitute model.," *J. Urol.*, vol. 166, no. 4, pp. 1502–7, Oct. 2001.

[225] N. KAUFMAN, T. D. KINNEY, E. J. MASON, and L. C. PRIETO, "Maintenance of human neoplasm on the chick chorioallantoic membrane.," *Am. J. Pathol.*, vol. 32, no. 2, pp. 271–85, 1956.

[226] E. W. Hurst, B. Cooke, and G. C. McLennan, "A note on the survival and growth of human and rabbit tissue (normal and neoplastic) on the chorio-allantois of the chick and duck embryo.," *Aust. J. Exp. Biol. Med. Sci.*, vol. 17, no. 2, pp. 215–224, 1939.

[227] D. Ribatti, B. Nico, A. Vacca, L. Roncali, P. H. Burri, and V. Djonov, "Chorioallantoic membrane capillary bed: a useful target for studying angiogenesis and anti-angiogenesis in vivo.," *Anat. Rec.*, vol. 264, no. 4, pp. 317–24, Dec. 2001.

[228] N. De Magalhães, L.-H. L. Liaw, and M. Berns, "An instruction on the in vivo shell-less chorioallantoic membrane 3-dimensional tumor spheroid model.," *Cytotechnology*, vol. 62, no. 3, pp. 279–83, Jul. 2010.

[229] N. A. Lokman, A. S. F. Elder, C. Ricciardelli, and M. K. Oehler, "Chick Chorioallantoic Membrane (CAM) Assay as an In Vivo Model to Study the Effect of Newly Identified Molecules on Ovarian Cancer Invasion and Metastasis.," *Int. J. Mol. Sci.*, vol. 13, no. 8, pp. 9959–70, Jan. 2012.

[230] J. Splawinski, M. Michna, R. Palczak, S. Konturek, and B. Splawinska, "Angiogenesis: quantitative assessment by the chick chorioallantoic membrane assay.," *Methods Find. Exp. Clin. Pharmacol.*, vol. 10, no. 4, pp. 221–6, Apr. 1988.

[231] N. Katrancioglu, O. Karahan, A. T. Kilic, A. Altun, O. Katrancioglu, and Z. A. Polat, "The antiangiogenic effects of levosimendan in a CAM assay.," *Microvasc. Res.*, vol. 83, no. 3, pp. 263–6, May 2012.

[232] A. Hoeben, B. Landuyt, M. S. Highley, H. Wildiers, A. T. Van Oosterom, and E. A. De Bruijn, "Vascular endothelial growth factor and angiogenesis.," *Pharmacol. Rev.*, vol. 56, no. 4, pp. 549–80, Dec. 2004.

[233] D. Ribatti and A. Vacca, "Models for studying angiogenesis in vivo.," *Int. J. Biol. Markers*, vol. 14, no. 4, pp. 207–13, 1999.

[234] S. de Boüard, P. Herlin, J. G. Christensen, E. Lemoisson, P. Gauduchon, E. Raymond, and J.-S. Guillamo, "Antiangiogenic and anti-invasive effects of sunitinib on experimental human glioblastoma.," *Neuro. Oncol.*, vol. 9, no. 4, pp. 412–23, Oct. 2007.

[235] C. B. Colen, N. Seraji-Bozorgzad, B. Marples, M. P. Galloway, A. E. Sloan, and S. P. Mathupala, "Metabolic remodeling of malignant gliomas for enhanced sensitization during radiotherapy: an in vitro study.," *Neurosurgery*, vol. 59, no. 6, pp. 1313–23; discussion 1323–4, Dec. 2006.

[236] C. Volk, B. Kempski, and O. S. Kempski, "Inhibition of lactate export by quercetin acidifies rat glial cells in vitro.," *Neurosci. Lett.*, vol. 223, no. 2, pp. 121–4, Feb. 1997.

[237] T. L. Spencer and A. L. Lehninger, "L-lactate transport in Ehrlich ascites-tumour cells.," *Biochem. J.*, vol. 154, no. 2, pp. 405–14, Feb. 1976.

[238] C. B. Colen, Y. Shen, F. Ghoddoussi, P. Yu, T. B. Francis, B. J. Koch, M. D. Monterey, M. P. Galloway, A. E. Sloan, and S. P. Mathupala, "Metabolic Targeting of Lactate Efflux by Malignant Glioma Inhibits Invasiveness and Induces Necrosis : An In Vivo Study 1," vol. 13, no. 7, pp. 620–632, 2011.

[239] S. J. Peak and V. A. Levin, "Role of bevacizumab therapy in the management of glioblastoma.," *Cancer Manag. Res.*, vol. 2, pp. 97–104, Jan. 2010.

[240] R. Lakomý, P. Burkon, D. Burkonová, and R. Jancálek, "[New therapeutic options in therapy of glioblastoma multiforme].," *Klin. Onkol.*, vol. 23, no. 6, pp. 381–7, Jan. 2010.

[241] H. S. Friedman, M. D. Prados, P. Y. Wen, T. Mikkelsen, D. Schiff, L. E. Abrey, W. K. A. Yung, N. Paleologos, M. K. Nicholas, R. Jensen, J. Vredenburgh, J. Huang, M. Zheng, and T. Cloughesy, "Bevacizumab alone and in combination with irinotecan in recurrent glioblastoma.," *J. Clin. Oncol.*, vol. 27, no. 28, pp. 4733–40, Oct. 2009.

[242] T. N. Kreisl, L. Kim, K. Moore, P. Duic, C. Royce, I. Stroud, N. Garren, M. Mackey, J. A. Butman, K. Camphausen, J. Park, P. S. Albert, and H. A. Fine, "Phase II trial of single-agent bevacizumab followed by bevacizumab plus irinotecan at tumor progression in recurrent glioblastoma.," *J. Clin. Oncol.*, vol. 27, no. 5, pp. 740–5, Feb. 2009.

[243] K. V Ballman, J. C. Buckner, P. D. Brown, C. Giannini, P. J. Flynn, B. R. LaPlant, and K. A. Jaeckle, "The relationship between six-month progression-free survival and 12-month overall survival end points for phase II trials in patients with glioblastoma multiforme.," *Neuro. Oncol.*, vol. 9, no. 1, pp. 29–38, Jan. 2007.

[244] P. Nowak-Sliwinska, J. R. van Beijnum, M. van Berkel, H. van den Bergh, and A. W. Griffioen, "Vascular regrowth following photodynamic therapy in the chicken embryo chorioallantoic membrane.," *Angiogenesis*, vol. 13, no. 4, pp. 281–92, Dec. 2010.

[245] C. Yildiz, A. Cetin, F. Demirci, Z. A. Polat, T. Kiyan, A. Altun, and M. Cetin, "Anti-Angiogenic Effects of Diltiazem, Imatinib, and Bevacizumab in the CAM Assay," vol. 3, no. 8, pp. 1–8, 2013.

[246] O. Keunen, M. Johansson, A. Oudin, M. Sanzey, S. A. A. Rahim, F. Fack, F. Thorsen, T. Taxt, M. Bartos, R. Jirik, H. Miletic, J. Wang, D. Stieber, L. Stuhr, I. Moen, C. B. Rygh, R. Bjerkvig, and S. P. Niclou, "Anti-VEGF treatment reduces blood supply and increases tumor cell invasion in glioblastoma.," *Proc. Natl. Acad. Sci. U. S. A.*, vol. 108, no. 9, pp. 3749–54, Mar. 2011.

[247] J. F. de Groot, G. Fuller, A. J. Kumar, Y. Piao, K. Eterovic, Y. Ji, and C. A. Conrad, "Tumor invasion after treatment of glioblastoma with bevacizumab: radiographic and pathologic correlation in humans and mice.," *Neuro. Oncol.*, vol. 12, no. 3, pp. 233–42, Mar. 2010.

[248] P. Birner, M. Schindl, A. Obermair, C. Plank, G. Breitenecker, and G. Oberhuber, "Overexpression of hypoxia-inducible factor 1alpha is a marker for an unfavorable prognosis in early-stage invasive cervical cancer.," *Cancer Res.*, vol. 60, no. 17, pp. 4693–6, Sep. 2000.

[249] X. Lu and Y. Kang, "Hypoxia and hypoxia-inducible factors: master regulators of metastasis.," *Clin. Cancer Res.*, vol. 16, no. 24, pp. 5928–35, Dec. 2010.

[250] G. Bergers and D. Hanahan, "Modes of resistance to anti-angiogenic therapy.," *Nat. Rev. Cancer*, vol. 8, no. 8, pp. 592–603, Aug. 2008.

[251] Y. Shaked, A. Ciarrocchi, M. Franco, C. R. Lee, S. Man, A. M. Cheung, D. J. Hicklin, D. Chaplin, F. S. Foster, R. Benezra, and R. S. Kerbel, "Therapy-induced acute recruitment of circulating endothelial progenitor cells to tumors.," *Science*, vol. 313, no. 5794, pp. 1785–7, Sep. 2006.

[252] T. T. Batchelor, A. G. Sorensen, E. di Tomaso, W.-T. Zhang, D. G. Duda, K. S. Cohen, K. R. Kozak, D. P. Cahill, P.-J. Chen, M. Zhu, M. Ancukiewicz, M. M. Mrugala, S. Plotkin, J. Drappatz, D. N. Louis, P. Ivy, D. T. Scadden, T. Benner, J. S. Loeffler, P. Y. Wen, and R. K. Jain, "AZD2171, a pan-VEGF receptor tyrosine kinase inhibitor, normalizes tumor vasculature and alleviates edema in glioblastoma patients.," *Cancer Cell*, vol. 11, no. 1, pp. 83–95, Jan. 2007.

[253] M. Skobe, T. Hawighorst, D. G. Jackson, R. Prevo, L. Janes, P. Velasco, L. Riccardi, K. Alitalo, K. Claffey, and M. Detmar, "Induction of tumor lymphangiogenesis by VEGF-C promotes breast cancer metastasis.," *Nat. Med.*, vol. 7, no. 2, pp. 192–8, Feb. 2001.

[254] V. Joukov, K. Pajusola, A. Kaipainen, D. Chilov, I. Lahtinen, E. Kukk, O. Saksela, N. Kalkkinen, and K. Alitalo, "A novel vascular endothelial growth factor, VEGF-C, is a ligand for the Flt4 (VEGFR-3) and KDR (VEGFR-2) receptor tyrosine kinases.," *EMBO J.*, vol. 15, no. 2, pp. 290–98, Jan. 1996.

[255] M. G. Achen and S. A. Stacker, "Vascular endothelial growth factor-D: signaling mechanisms, biology, and clinical relevance.," *Growth Factors*, vol. 30, no. 5, pp. 283–96, Oct. 2012.

[256] M. G. Achen, M. Jeltsch, E. Kukk, T. Mäkinen, A. Vitali, A. F. Wilks, K. Alitalo, and S. A. Stacker, "Vascular endothelial growth factor D (VEGF-D) is a ligand for the tyrosine kinases VEGF receptor 2 (Flk1) and VEGF receptor 3 (Flt4).," *Proc. Natl. Acad. Sci. U. S. A.*, vol. 95, no. 2, pp. 548–53, Jan. 1998.

[257] A. K. Lucio-Eterovic, Y. Piao, and J. F. de Groot, "Mediators of Glioblastoma Resistance and Invasion during Antivascular Endothelial Growth Factor Therapy," *Clin. Cancer Res.* , vol. 15 , no. 14 , pp. 4589–4599, Jul. 2009.

[258] Y. Wang, D. Fei, M. Vanderlaan, and A. Song, "Biological activity of bevacizumab, a humanized anti-VEGF antibody in vitro," *Angiogenesis*, vol. 7, no. 4, pp. 335–345, Jan. 2004.

[259] J. L. Rubenstein, J. Kim, T. Ozawa, M. Zhang, M. Westphal, D. F. Deen, and M. A. Shuman, "Anti-VEGF antibody treatment of glioblastoma prolongs survival but results in increased vascular cooption.," *Neoplasia*, vol. 2, no. 4, pp. 306–14.

[260] S. Oudard, F. Arvelo, L. Miccoli, F. Apiou, A. M. Dutrillaux, M. Poisson, B. Dutrillaux, and M. F. Poupon, "High glycolysis in gliomas despite low hexokinase transcription and activity correlated to chromosome 10 loss.," *Br. J. Cancer*, vol. 74, no. 6, pp. 839–45, Sep. 1996.

[261] K. S. Lim, K. J. Lim, A. C. Price, B. A. Orr, C. G. Eberhart, and E. E. Bar, "Inhibition of monocarboxylate transporter-4 depletes stem-like glioblastoma cells and inhibits HIF transcriptional response in a lactate-independent manner.," *Oncogene*, Sep. 2013.

[262] P. Tabatabaei, P. Bergström, R. Henriksson, and A. T. Bergenheim, "Glucose metabolites, glutamate and glycerol in malignant glioma tumours during radiotherapy.," *J. Neurooncol.*, vol. 90, no. 1, pp. 35–9, Oct. 2008.

[263] V. Miranda-Gonçalves, M. Honavar, C. C. C. C. C. C. Pinheiro, O. Martinho, M. M. Pires, M. Cordeiro, G. Bebiano, P. Costa, I. Palmeirim, R. M. Reis, and F. Baltazar, "Monocarboxylate

transporters (MCTs) in gliomas: expression and exploitation as therapeutic targets.," *Neuro. Oncol.*, vol. 15, no. 2, pp. 172–88, Feb. 2013.

[264] M. K. Froberg, D. Z. Gerhart, B. E. Enerson, C. Manivel, M. Guzman-Paz, N. Seacotte, and L. R. Drewes, "Expression of monocarboxylate transporter MCT1 in normal and neoplastic human CNS tissues.," *Neuroreport*, vol. 12, no. 4, pp. 761–5, Mar. 2001.

[265] M. L. Wahl, J. A. Owen, R. Burd, R. A. Herlands, S. S. Nogami, U. Rodeck, D. Berd, D. B. Leeper, and C. S. Owen, "Regulation of intracellular pH in human melanoma: potential therapeutic implications.," *Mol. Cancer Ther.*, vol. 1, no. 8, pp. 617–28, Jun. 2002.

[266] J. A. Belt, J. A. Thomas, R. N. Buchsbaum, and E. Racker, "Inhibition of lactate transport and glycolysis in Ehrlich ascites tumor cells by bioflavonoids.," *Biochemistry*, vol. 18, no. 16, pp. 3506–11, Aug. 1979.

[267] R. A. Coss, C. W. Storck, C. Daskalakis, D. Berd, and M. L. Wahl, "Intracellular acidification abrogates the heat shock response and compromises survival of human melanoma cells.," *Mol. Cancer Ther.*, vol. 2, no. 4, pp. 383–8, Apr. 2003.

[268] J. Fang, Q. J. Quinones, T. L. Holman, M. J. Morowitz, Q. Wang, H. Zhao, F. Sivo, J. M. Maris, and M. L. Wahl, "The H+-linked monocarboxylate transporter (MCT1/SLC16A1): a potential therapeutic target for high-risk neuroblastoma.," *Mol. Pharmacol.*, vol. 70, no. 6, pp. 2108–15, Dec. 2006.

[269] S. P. Mathupala, P. Parajuli, and A. E. Sloan, "Silencing of monocarboxylate transporters via small interfering ribonucleic acid inhibits glycolysis and induces cell death in malignant glioma: an in vitro study.," *Neurosurgery*, vol. 55, no. 6, pp. 1410–9; discussion 1419, Dec. 2004.

[270] J. S. Constant, J. J. Feng, D. D. Zabel, H. Yuan, D. Y. Suh, H. Scheuenstuhl, T. K. Hunt, and M. Z. Hussain, "Lactate elicits vascular endothelial growth factor from macrophages: a possible alternative to hypoxia.," *Wound Repair Regen.*, vol. 8, no. 5, pp. 353–60.

[271] M. Xiong, G. Elson, D. Legarda, and S. J. Leibovich, "Production of vascular endothelial growth factor by murine macrophages: regulation by hypoxia, lactate, and the inducible nitric oxide synthase pathway.," *Am. J. Pathol.*, vol. 153, no. 2, pp. 587–98, Aug. 1998.

[272] H. Lu, C. L. Dalgard, A. Mohyeldin, T. McFate, A. S. Tait, and A. Verma, "Reversible inactivation of HIF-1 prolyl hydroxylases allows cell metabolism to control basal HIF-1.," *J. Biol. Chem.*, vol. 280, no. 51, pp. 41928–39, Dec. 2005.

[273] P. Sonveaux, T. Copetti, C. J. De Saedeleer, F. Végran, J. Verrax, K. M. Kennedy, E. J. Moon, S. Dhup, P. Danhier, F. Frérart, B. Gallez, A. Ribeiro, C. Michiels, M. W. Dewhirst, and O. Feron, "Targeting the Lactate Transporter MCT1 in Endothelial Cells Inhibits Lactate-Induced HIF-1 Activation and Tumor Angiogenesis," *PLoS One*, vol. 7, no. 3, p. e33418, Jan. 2012.

[274] H. Harrison, L. Rogerson, H. J. Gregson, K. R. Brennan, R. B. Clarke, and G. Landberg, "Contrasting hypoxic effects on breast cancer stem cell hierarchy is dependent on ER-α status.," *Cancer Res.*, vol. 73, no. 4, pp. 1420–33, Feb. 2013.

[275] C. Lugassy, S. E. Vernon, K. Busam, J. A. Engbring, D. R. Welch, E. G. Poulos, H. K. Kleinman, and R. L. Barnhill, "Angiotropism of human melanoma: studies involving in transit and other cutaneous metastases and the chicken chorioallantoic membrane: implications for extravascular melanoma invasion and metastasis.," *Am. J. Dermatopathol.*, vol. 28, no. 3, pp. 187–93, Jun. 2006.

[276] T. D. Palmer, J. Lewis, and A. Zijlstra, "Quantitative analysis of cancer metastasis using an avian embryo model.," *J. Vis. Exp.*, no. 51, Jan. 2011.

[277] A. Zijlstra, J. Lewis, B. Degryse, H. Stuhlmann, and J. P. Quigley, "The inhibition of tumor cell intravasation and subsequent metastasis via regulation of in vivo tumor cell motility by the tetraspanin CD151.," *Cancer Cell*, vol. 13, no. 3, pp. 221–34, Mar. 2008.

[278] A. Zijlstra, R. Mellor, G. Panzarella, R. T. Aimes, J. D. Hooper, N. D. Marchenko, and J. P. Quigley, "A Quantitative Analysis of Rate-limiting Steps in the Metastatic Cascade Using Human-specific Real-Time Polymerase Chain Reaction," *Cancer Res.*, vol. 62, no. 23, pp. 7083–7092, Dec. 2002.

[279] J. J. Vredenburgh, A. Desjardins, J. E. Herndon, J. Marcello, D. A. Reardon, J. A. Quinn, J. N. Rich, S. Sathornsumetee, S. Gururangan, J. Sampson, M. Wagner, L. Bailey, D. D. Bigner, A. H. Friedman, and H. S. Friedman, "Bevacizumab plus irinotecan in recurrent glioblastoma multiforme.," *J. Clin. Oncol.*, vol. 25, no. 30, pp. 4722–9, Oct. 2007.

[280] G. Gasparini, R. Longo, M. Fanelli, and B. A. Teicher, "Combination of antiangiogenic therapy with other anticancer therapies: results, challenges, and open questions.," *J. Clin. Oncol.*, vol. 23, no. 6, pp. 1295–311, Feb. 2005.

[281] L. D. Volk, M. J. Flister, C. M. Bivens, A. Stutzman, N. Desai, V. Trieu, and S. Ran, "Nab-paclitaxel efficacy in the orthotopic model of human breast cancer is significantly enhanced by concurrent anti-vascular endothelial growth factor A therapy.," *Neoplasia*, vol. 10, no. 6, pp. 613–23, Jun. 2008.

[282] T. Kanzawa, I. M. Germano, T. Komata, H. Ito, Y. Kondo, and S. Kondo, "Role of autophagy in temozolomide-induced cytotoxicity for malignant glioma cells.," *Cell Death Differ.*, vol. 11, no. 4, pp. 448–57, Apr. 2004.

[283] W. P. Roos, L. F. Z. Batista, S. C. Naumann, W. Wick, M. Weller, C. F. M. Menck, and B. Kaina, "Apoptosis in malignant glioma cells triggered by the temozolomide-induced DNA lesion O6-methylguanine.," *Oncogene*, vol. 26, no. 2, pp. 186–97, Jan. 2007.

[284] V. Mathieu, N. De Nève, M. Le Mercier, J. Dewelle, J.-F. Gaussin, M. Dehoux, R. Kiss, and F. Lefranc, "Combining bevacizumab with temozolomide increases the antitumor efficacy of temozolomide in a human glioblastoma orthotopic xenograft model.," *Neoplasia*, vol. 10, no. 12, pp. 1383–92, Dec. 2008.

[285] "A Cancer Research United Kingdom Phase I Trial of AZD3965, a Monocarboxylate Transporter 1 Inhibitor (MCT1) in Patients With Advanced Cancer." [Online]. Available: http://www.clinicaltrials.gov/ct2/show/NCT01791595. [Accessed: 01-Apr-2014].

[286] Y. Iwamoto, "Diagnosis and treatment of Ewing's sarcoma.," *Jpn. J. Clin. Oncol.*, vol. 37, no. 2, pp. 79–89, Feb. 2007.

[287] M. Burt, M. Karpeh, O. Ukoha, M. S. Bains, N. Martini, P. M. McCormack, V. W. Rusch, and R. J. Ginsberg, "Medical tumors of the chest wall. Solitary plasmacytoma and Ewing's sarcoma.," *J. Thorac. Cardiovasc. Surg.*, vol. 105, no. 1, pp. 89–96, Jan. 1993.

[288] L. Goldman and A. Schafer, *Goldman's Cecil Medicine*, 24th ed. Philadelphia: Elsevier Saunders., 2011, p. 2672.

[289] K. Tawara, J. T. Oxford, and C. L. Jorcyk, “Clinical significance of interleukin (IL)-6 in cancer metastasis to bone: potential of anti-IL-6 therapies.,” *Cancer Manag. Res.*, vol. 3, pp. 177–89, Jan. 2011.

[290] P. Rutkowski, J. Kamińska, M. Kowalska, W. Ruka, and J. Steffen, “Cytokine and cytokine receptor serum levels in adult bone sarcoma patients: correlations with local tumor extent and prognosis.,” *J. Surg. Oncol.*, vol. 84, no. 3, pp. 151–9, Nov. 2003.

[291] H. E. Grier, “The Ewing family of tumors. Ewing’s sarcoma and primitive neuroectodermal tumors.,” *Pediatr. Clin. North Am.*, vol. 44, no. 4, pp. 991–1004, Aug. 1997.

[292] A. Fauci, E. Braunwald, D. Kasper, S. Hauser, D. Longo, J. Jameson, and J. Loscalzo, *Harrison’s Principles of Internal Medicine.*, 17th ed. Mcgraw-hill, 2008, p. 2958.

13. Manuscript in preparation

Non-canonical tuning of hypoxia-induced gene expression by HIF-1α/HIF-2α and HIF-2α/HIF-2α dimer formation

(Only abstract included in this thesis: section 13.1).

Jun Hu, Dheeraj A. Shinde*, Thomas A. Gorr*, Joachim Fandrey
Institut fuer Physiologie, Universitaet Duisburg-Essen, Essen
*Institute of Veterinary Physiology, Vetsuisse Faculty, Zurich

13.1 Abstract

Hypoxia inducible factors 1 and 2 (HIF-1 and HIF-2) control hypoxia induced gene expression by activating, in different subsets of cells, common as well as unique HIF-1 or HIF-2 dependent sets of genes. . In general, it is assumed that the oxygen-labile HIF-1α or HIF-2α subunit dimerizes with ARNT (also known as HIF-1β) to form the transcriptionally active HIF complex, which also recruits gene specific coactivators. We have used fluorescence resonance energy transfer (FRET) to measure differences in the assembly of HIF-1 vs. HIF-2 complexes. The FRET method also allowed us to study any potential homodimerization between HIF-1α and HIF-2α subunits. Whereas HIF-1α did not form homodimers, HIF-2α/HIF-2α and HIF-1/HIF-2α dimers were found and their existence confirmed by co-precipitation. Electromobility shift assays, however, revealed the lack of DNA binding to symmetrical or asymmetrical HIF binding sites by these newly described dimers. In addition, deletion constructs lacking the DNA binding domain still revealed HIF-2α/HIF-2α and HIF-1/HIF-2α dimer formation despite the inability to bind DNA. To define a potential function of HIF-2α/HIF-2α and HIF-1/HIF-2α dimers target gene expression for HIF-1 or HIF-2 dependent genes was studied. We were able to show competition for HIF-1α/ARNT complex formation by HIF-1α/HIF-2α dimers reducing the expression of a HIF-1 target by forced accumulation of HIF-2α. Our data indicate a potential non-canonical tuning of the formation and activity of HIF alpha:beta heterodimers by HIF alpha-subunit homodimers in hypoxia induced gene expression.

Note: Above is an abstract of a poster presented at Keystone conference by Prof. Dr. med. Joachim Fandrey.

14. Submitted Manuscript

(Manuscript is submitted to carcinogenesis journal, which includes data, as marked in results section 4)

Chick embryo chorioallantoic membrane assay for pre-clinical assessment of anti-cancer interventions targeting VEGF-based neovascularization and lactate-fueled respiration in model tumor grafts

Dheeraj A. Shinde[1], Max Gassmann[1,2], Daniela Gerst[1], Johannes Vogel[1 #], Thomas A. Gorr[1,3 # *]

Author Affiliations

[1] Institute of Veterinary Physiology, Vetsuisse Faculty, University of Zurich, Zurich, Switzerland.

[2] Institute of Veterinary Physiology, Vetsuisse Faculty and Zurich Center for Integrative Physiology (ZIHP), University of Zurich, Zurich, Switzerland.

[3] Center for Pediatrics and Adolescent Medicine, University Medical Center Freiburg, Freiburg, Germany.

Co-senior authors.

* Corresponding author:

Thomas A. Gorr, PhD

Institute of Veterinary Physiology, Vetsuisse Faculty, University of Zurich, Winterthurerstrasse 260, CH-8057 Zurich, Switzerland

Tel: +41 44 635 8807, Fax: +41 44 635 8932, Email: tgorr@access.uzh.ch

Running Title: CAM assay evaluation of VEGF and MCT1 targeting

15. Accepted Manuscript

As a coauthor, attached is the copy of accepted paper in American Association for Cancer Research (ACCR) journal.

Title:

Interaction of HIF and USF Signaling Pathways in Human Genes Flanked by Hypoxia-Response Elements and E-box Palindromes

Authors

Junmin Hu[1]1, Daniel P. Stiehl[2], Claudia Setzer[1]1, Daniela Wichmann[1]1, Dheeraj A. Shinde[1], Hubert Rehrauer[3], Pavel Hradecky[5], Max Gassmann[1, 4], and Thomas A. Gorr[1, 6]

Authors' Affiliations:

[1] Institute of Veterinary Physiology; University of Zurich, Switzerland;

[2] Institute of Physiology; University of Zurich, Switzerland;

[3] Functional Genomics Center Zurich;

[4] Zurich Center for Integrative Human Physiology, University of Zurich, Switzerland;

[5] Altra-Bio, Lyon, France; and

[6] Center for Pediatrics and Adolescent Medicine,University Medical Center Freiburg, Freiburg, Germany

Corresponding Author:

Thomas A. Gorr, Institute of Veterinary Physiology,
Vetsuisse Faculty, University of Zurich, Winterthurerstrasse 260, 8057
Zurich, Switzerland. Phone 41-44-635-8807; Fax: 41-44-635-8932;
E-mail: tgorr@access.uzh.ch

Published OnlineFirst October 7, 2011; DOI: 10.1158/1541-7786.MCR-11-0090

Signaling and Regulation

Molecular Cancer Research

Interaction of HIF and USF Signaling Pathways in Human Genes Flanked by Hypoxia-Response Elements and E-box Palindromes

Junmin Hu[1], Daniel P. Stiehl[2], Claudia Setzer[1], Daniela Wichmann[1], Dheeraj A. Shinde[1], Hubert Rehrauer[3], Pavel Hradecky[5], Max Gassmann[1,4], and Thomas A. Gorr[1,6]

Abstract

Rampant activity of the hypoxia-inducible factor (HIF)-1 in cancer is frequently associated with the malignant progression into a harder-to-treat, increasingly aggressive phenotype. Clearly, anti-HIF strategies in cancer cells are of considerable clinical interest. One way to fine-tune, or inhibit, HIF's transcriptional outflow independently of hydroxylase activities could be through competing transcription factors. A CACGTG-binding activity in human hepatoma cells was previously found to restrict HIF's access to hypoxia response *cis*-elements (HRE) in a *Daphnia* globin gene promoter construct (phb2). The CACGTG factor, and its impact on hypoxia-responsive human genes, was analyzed in this study by genome-wide computational scans as well as gene-specific quantitative PCR, reporter and DNA-binding assays in hepatoma (Hep3B), cervical carcinoma (HeLa), and breast carcinoma (MCF7) cells. Among six basic helix-loop-helix transcription factors known to target CACGTG palindromes, we identified upstream stimulatory factor (USF)-1/2 as predominant phb2 CACGTG constituents in Hep3B, HeLa, and MCF7 cells. Human genes with adjacent or overlapping HRE and CACGTG motifs included with *lactate dehydrogenase A (LDHA)* and *Bcl-2/E1B 19 kDa interacting protein 3 (BNIP3)* hypoxia-induced HIF-1 targets. Parallel recruitment of HIF-1α and USF1/2a to the respective promoter chromatin was verified for all cell lines investigated. Mutual complementing (*LDHA*) or moderating (*BNIP3*) cross-talk was seen upon overexpression or silencing of HIF-1α and USF1/2a. Distinct (*LDHA*) or overlapping (*BNIP3*) promoter-binding sites for HIF-1 and USFs were subsequently characterized. We propose that, depending on abundance or activity of its protein constituents, O_2-independent USF signaling can function to fine-tune or interfere with HIF-mediated transcription in cancer cells. *Mol Cancer Res; 9(11); 1520–36. ©2011 AACR.*

Introduction

Relaying minutes-to-hours of inadequate oxygenation (hypoxia) onto the level of DNA via the hypoxia-inducible transcription factors 1 and 2 (HIF-1 and HIF-2) is a highly conserved signaling event across the animal kingdom (1–3). When exposed to low oxygen partial pressures (pO_2), the mammalian HIF-1/-2 complexes function as heterodimer of HIF-1α or HIF-2α and HIF-1β subunits (4). Whereas HIF-1β, also known as aryl hydrocarbon receptor nuclear translocator (ARNT), is constitutively present, the activity and abundance of HIF-α subunits are regulated as a function of pO_2. In the presence of oxygen, homologs of prolyl hydroxylase domain 1-3 (PHD1-3) dioxygenases catalyze the Fe (II)-dependent hydroxylation of 2 proline residues contained within the oxygen-dependent degradation (ODD) domain and the N-terminal transactivation domain (NAD; rear proline only) of HIF-1α and HIF-2α (5–7). Once prolyl hydroxylated, HIF-α subunits are captured by the von Hippel-Lindau tumor suppressor protein and rapidly degraded via the ubiquitin–proteasome pathway (6, 8). A second, O_2-requiring posttranslational modification of HIF-1α/-2α targets a single asparagine residue within the subunits' C-terminal transactivation domain (CAD). It is catalyzed by an asparaginyl hydroxylase called factor inhibiting HIF-1 (FIH-1) to prohibit HIF-α:coactivator interaction and suppress transactivation of genes under high oxygen (9, 10). During hypoxia, both PHD and FIH-1 activities are progressively inhibited, leading to α-subunit accumulation, α:β-subunit dimerization in the nucleus and binding of the heterodimer to hypoxia response elements (HRE) within target genes. Being members of canonical CANNTG E-box

Authors' Affiliations: [1]Institute of Veterinary Physiology; [2]Institute of Physiology; [3]Functional Genomics Center Zurich; [4]Zurich Center for Integrative Human Physiology, University of Zurich, Zurich, Switzerland; [5]Altra-Bio, Lyon, France; and [6]Center for Pediatrics and Adolescent Medicine, University Medical Center Freiburg, Freiburg, Germany

Note: Supplementary data for this article are available at Molecular Cancer Research Online (http://mcr.aacrjournals.org/).

Corresponding Author: Thomas A. Gorr, Institute of Veterinary Physiology, Vetsuisse Faculty, University of Zurich, Winterthurerstrasse 260, 8057 Zurich, Switzerland. Phone 41-44-635-8807; Fax: 41-44-635-8932; E-mail: tgorr@access.uzh.ch

doi: 10.1158/1541-7786.MCR-11-0090

Published OnlineFirst October 7, 2011; DOI: 10.1158/1541-7786.MCR-11-0090

motifs, HREs consist of a consensus 5′-VNVBRCGTG-3′ (V = not T; N = any; B = not A; R = A or G; ref. 11). To date, several hundred potential (12) and more than 70 validated (11) hypoxia-responsive and HRE-flanked gene targets of HIF-1 have been identified. Through this transcriptional outflow, HIF-1 is able to reprogram cellular metabolism, growth, apoptosis, and O_2 supply in response to declining pO_2 (11).

Nonredundant roles of these hydroxylase systems in the regulation of HIF-1α/-2α activities were only recently unraveled when it became clear that the Michaelis constant (K_m) of all 3 PHDs and FIH-1 predicted a distinctly lower oxygen affinity for the former (13). Consequently, PHD1-3 hydroxylases start to experience, relative to FIH-1, inactivation at higher pO_2 during progressing hypoxia (14). Differential hydroxylase activities will eventually translate into a differential regulation of HIF-1 targets. By combining transcriptional profiling data (15) with a numerical model of the regulatory dynamics of the FIH-1 and PHD oxygen sensors along a virtual oxygen gradient (16), Pouysségur and colleagues were able to allocate HIF-1 targets into 2 categories: (i) FIH-1–inhibited genes, that is, those induced by progressive hypoxia once the NAD and, subsequently, CAD of HIF-1α/-2α are both released from inhibition (e.g., *CA9*, *PHD3*, and *LDHA*), and (ii) non–FIH-1–inhibited genes, that is, those requiring solely HIF-α NAD activity upon sufficient PHD inhibition while being refractory to any CAD activation (e.g., *PGK1* and *GAPDH*; refs. 15, 17). This categorization predicts expression of FIH-1–inhibited genes to be altered during severe hypoxia, whereas moderate degrees of O_2 deprivation already affect non–FIH-1–inhibited genes.

Yet, as another and hydroxylase-independent layer of control, HIF's transcriptional outflow is also prone to be influenced by competing transcription factors. When we previously used reporter constructs of the tripartite globin-2 gene (hb2) promoter (phb2) of the planktonic crustacean *Daphnia magna* in heterologous transfections of human cancer cells, we noticed a constitutive CACGTG-binding factor which was able to interfere with the HIF-1–driven induction of the phb2 luciferase reporter (18). Now, we identify this phb2 CACGTG factor across several cancer cell lines as a complex of O_2 independently acting upstream stimulatory factors 1 and 2 (USF1 and USF2). To assess both the extent and mode (positive/negative) of the impact of USF signaling on HIF's transcriptional outflow, we implemented a genome-wide computational scan to identify candidate human genes that contain adjacent or overlapping HRE and CACGTG palindrome motifs in their up- or downstream sequences. Our results suggest the occurrence of both positive (promoter of *lactate dehydrogenase A (LDHA)*: USFs complement HIF control) and variably negative [promoter of *Bcl-2/E1B 19 kDa interacting protein 3 (BNIP3):* USF interactions range from moderating to competing with HIF-1] cross-talk modes when HIF-1/USF constituents were overexpressed or silenced. This work, therefore, provides a proof-of-principle for the oxygen-independent USF pathway to influence, and, upon strong activation or overexpression, even inhibit HIF/HRE-mediated gene expression in human cancer cells.

Materials and Methods

Cells, RNA, and quantitative PCR

Human hepatoma (Hep3B; ATCC HB-8064), cervical carcinoma (HeLa; ATCC CCL-2), and breast carcinoma cells (MCF7; ATCC HTB-22) were purchased as short tandem repeat–authenticated lines from the American Tissue Culture Collection (ATCC) and maintained in high glucose (4.5 g/L) Dulbecco's modified Eagle's medium as described earlier (18). Normoxic (N) cultures: 37°C, room air in water–saturated atmosphere with 5% CO_2 (i.e., a pO_2 = 141.6 mmHg, $[O_2]$ = 18.6% O_2). Hypoxic (H) cultures in HERA Cell240 incubator (Heraeus) or a polymer glove box (Coy)—16-hour exposures: 37°C, in water-saturated 1% or 3% or 10% O_2/5% CO_2/balance N_2 atmosphere. Isolation of total RNA, reverse transcriptions, and SYBR-Green quantitative real-time PCR (qRT-PCR) was carried out as previously reported (19, 20). All primers used for qPCR are listed in Supplementary Table S1.

Antibodies

Mouse monoclonal anti–ATF-1 antibody (25C10G, sc-270) and rabbit polyclonal anti-USF1 (C-20, sc-229) were purchased from Santa Cruz Biotechnology, Inc. Rabbit polyclonal anti-USF1M, anti-USF2F, anti-USF2G, anti-USF2Z, and anti-USF2aO antibodies were kindly provided by Dr. B. Viollet (21). Additional antibody gifts included: (i) rabbit anti-human DEC1 (CW27; ref. 22); (ii) rabbit anti-human MYC (23); (iii) rabbit anti-mouse ARNT (anti-mARNT R-1 IgG; ref. 24); (iv) rabbit anti-human ARNT (anti-hARNT C34; ref. 25); (v) rabbit anti-human USF full-length antibody (USF FL; ref. 26).

Sequence scan for HRE motif and CACGTG palindrome

We used the repeat-masked human genome sequence as provided by the UCSC Genome Bioinformatics Website (Version hg19, GRCh37) at http://hgdownload.cse.ucsc.edu/goldenPath/hg19/bigZips/chromFaMasked.tar.gz. Gene definitions and transcription start sites were from http://hgdownload.cse.ucsc.edu/goldenPath/hg19/database/refGene.txt.gz (downloaded April 09, 2010). The search for motifs, implemented as R-script, was conducted among the 1,000 base flanking region up- and downstream (= ± 1,000 bp) of annotated transcripts. Genes containing both HRE and CACGTG palindrome motifs within the ±1,000 bp flanks were considered as HRE/palindrome gene only if the motif–motif distance was 100 bp or less. On the basis of these criteria, we used the GeneGo MetaCore system to identify pathways where HRE/palindrome genes are overrepresented (see Table 1).

Luciferase reporter

With genomic DNA, we amplified the promoter region around the HRE and E-box palindrome motifs via nested PCR (for primers, see Supplementary Table S1). Of note,

Published OnlineFirst October 7, 2011; DOI: 10.1158/1541-7786.MCR-11-0090

the 3′-end of any given amplicon is always extended into the first coding exon of the respective gene. In detail, we amplified and cloned the following promoter regions (start/end always relative to translation start ATG codon): (i) human *4EBP1* gene, −518/+403; (ii) human *MC1R* gene, −880/+9; (iii) human *LDHA* gene, −2,617/+530; (iv) human *TYR* gene, −400/+108. Following TOPO cloning of the PCR products into the pCRII-TOPO vector (Invitrogen), the liberated insert was ligated into pGL3-basic luciferase vector (Promega AG) to generate the luciferase reporter constructs. We also obtained the *BNIP3*/pGL3-basic (−753/+3; ref. 27) and the *PHD2*/pGL3-basic (−607/+3; ref. 28) luciferase reporter vector as kind gifts. HIF-1α (i.e., pcDNA3.1-hHIF-1-PK tag) as well as USF (pCR3-USF1, pCR3-USF2a, and pCR3-USF2b) expression plasmids were generously supplied by Prof. P. Maxwell (29) and Dr. B. Viollet (30), respectively.

Electrophoretic mobility shift assay and pull-down assay

Isolation of nuclear protein extracts of Hep3B, HeLa and MCF7 cells, and analysis of *in vitro* protein–DNA interaction by electrophoretic mobility shift assay (EMSA; ref. 18) and pull-down assays (31), was done as previously reported. All oligonucleotide sequences used as probes for either assay are shown in Supplementary Table S1. For EMSA gel supershifts (ss), 1.0 to 1.5 μL of rabbit anti-USF1M, rabbit anti-USF2G, or mouse anti-HIF-1α (mgc3) was added into the reaction (30 minutes, room temperature). Negative supershift controls included 1.5 μL preimmune serum from the same rabbit to be immunized against USF1M or USF2G, as well as 1.0 μL rabbit anti-human immunoglobulin (IgG; code: 309-005-003 Jackson Immuno Research). About pull-down assays, wild-type and mutated phb2 −146 palindrome or −107 HRE oligonucleotides, and wild-type and mutated *BNIP3* −251/−246 HRE oligonucleotides, biotinylated at the 5′-end and PAGE purified, were annealed into double-stranded DNA and immobilized on streptavidin-coated magnetic beads (Dynal Biotech) as described (31).

Western blot and coimmunoprecipitation

Proteins were resolved in 10% SDS polyacrylamide gels, transferred onto nitrocellulose membranes (Whatman), and the membranes incubated at 4°C overnight with the following primary antibodies diluted in 5% milk Tris-buffered saline and Tween 20: (i) anti-HIF1α (mgc3; 1:500) or (ii) anti-USF1M or anti-USF2G (1:750). The signal was detected with horseradish peroxidase–conjugated goat anti-mouse or anti-rabbit (1:5,000) and luminol substrate. For coimmunoprecipitation experiments, 150 μg nuclear protein was incubated with 20 μL mouse anti-HIF-1α or 0.75 μg anti-mARNT or 2.5 μL USF antiserum and subsequently rotated at 4°C overnight. The next day, 40 μL of protein G beads were added into the mix and incubated at 4°C for another 2.5 hours. The extract/antibody/bead mix was collected by centrifugation, the pellet boiled at 95°C in 1× SDS sample buffer for 10 minutes, and the supernatant analyzed by Western blot.

Chromatin immunoprecipitation assay

Chromatin immunoprecipitation (ChIP) assays were conducted in human Hep3B, HeLa, and MCF7 cells after a 4-hour exposure to normoxic (air) or hypoxic (1% O_2) atmospheres as described (32). In brief, genomic DNA was cross-linked with bound proteins (10 minutes, room temperature) with 1% formaldehyde in 1× PBS and sonicated in a Bioruptor UCD-200 (Diagenode SA) or a Sonifier cell disruptor B15 (Branson) into 500- to 1,000-bp fragments. For immunoprecipitation of the DNA:protein mix, 4.5 μL rabbit polyclonal anti–HIF-1α IgG (ab2185; Abcam) or 10 μL rabbit polyclonal anti-USF1M or anti-USF2G were added into the chromatin solution. Preimmune rabbit antiserum (10 μL) and 2.5 μL rabbit anti-human IgG were used as negative controls. The purified DNA was amplified by PCR using the ChIP primer pairs shown in Supplementary Table S1.

Transient luciferase reporter transfection

Half-confluent Hep3B, HeLa, and MCF7 cells were transfected overnight by the help of the calcium phosphate method with different luciferase reporter constructs and normalization plasmids expressing β-galactosidase. For cotransfections, 15 to 500 ng HIF-1α plasmid and/or 15 to 100 ng USF1, USF2a, or USF2b plasmid were added. In each transfection, pUC18 plasmid was used as filler DNA for a total of 2 to 3 μg DNA. The following day, each batch of transfected cells was split into 2 for parallel 16 hours normoxia and hypoxia exposure. After 16-hour normoxia/hypoxia exposure, cells were lysed and luciferase activity was measured with a commercially available Luciferase Assay System (Promega AG) and a SIRIUS Luminometer (Berthold Technologies). Luciferase activity was normalized by β-galactosidase activity (β-Galactosidase Enzyme Assay kit; Promega AG) and expressed as "relative luciferase activity" in percent (% RLA) of the total activity of all normoxic and hypoxic reactions of a given assay.

Transient knockdown of HIF-1α, USF1, or USF2a

For transient silencing, the specific siRNA HIF-1α and siRNA USF1 oligonucleotides were selected based on previous publications (33–35). All siRNA sequences (see Supplementary Table S1) were synthesized by Dharmacon Research Inc. Si*CONTROL* nontargeting siRNA pool #2 was used as scrambled (scr) siRNA control (Dharmacon). Half-confluent Hep3B cells were transfected with a total of 200 nmol/L of siRNAs using Oligofectamine reagent (Invitrogen). In the combined USF1 + USF2a siRNA transfection targeting both USFs, 100 nmol/L of each siRNA were added to the cells.

Statistics

With STATA 10.0 software (Stata 10.0; StataCorp), we compared control versus experimental mean transcript expression levels (Fig. 3) and RLAs for each reporter assay (Fig. 6) within the same oxygen category (either normoxic or hypoxic results; Figs. 3 and 6) or for the hypoxic/normoxic fold inductions (Fig. 3, Table 3). In accordance with prior

Table 1. Top 10 pathways enriched with HRE/CACGTG genes

GeneGo pathway name	Pathway description	*P*	Network objects	Enriched network gene symbols
Insulin regulation of translation	Control of cap-dependent mRNA translation—from Insulin receptor (INSR) to PI3K, AKT, mTOR, and eIF4F	3.108e-6	10/42	eEF2K, eIF2B5, **eIF4E,** 4EBP1, **eIF4G1,** eIF4H, **INSR,** MAPK1, **PDPK1,** PRKCZ;
Androgen Receptor (AR) nuclear signaling	Control of cell adhesion, apoptosis, and cholesterol metabolism via AR	6.079e-6	10/45	**EGFR,** IGF1R, KLK3, MAPK1, **RAD9A,** SCAP, SMAD3, **SRD5A1,** STAT3, **WNT10A**;
Role of IL-8 in angiogenesis	Control of angiogenesis + cell migration via interleukin 8 + VEGFA	1.064e-5	11/58	ACTR3B (= ARP3B), CARD11, **EGFR,** FASN, MBTPS1 (= S1P), **NFκBIE** (= **I-κBE**), **PDPK1,** RELB (NF-κB), SCAP, SREBF1, STAT3;
Receptor-mediated HIF regulation	Control of HIF-1α translation in normoxia—from INSR → mTOR	1.288e-5	9/39	**eIF4E,** 4EBP1, HIF1A, IGF1R, **INSR,** IRS4, MAPK1, **PDPK1,** PRKCZ;
Cytoskeleton remodeling	Control of cell adhesion + motility—from extracellular matrix to actin filaments	3.350e-5	14/102	**ACTN2,** ACTR3B (= ARP3B), BCAR1, **CFL2, eIF4E,** 4EBP1, **eIF4G1/3 (eIF4G1, eIF4G3),** eIF4H, **LIMK1,** MAPK1, PLAT (= tPA), **RPS6KA5** (= **S6K 90kDa sub., MSK1**), SMAD3;
Ligand-independent activation of ESR1 and ESR2	Control of cellular proliferation + migration via estrogen receptor β	3.636e-5	9/44	DRD1 (= dopamine receptor D1, GPCR), **EGFR,** ESR2 (= ER beta), GNAS (= Galpha-s), IGF1R, MAPK1 (ERK1, ERK2), **PDPK1,** PRKAR1B;
Role of SCF complex in cell-cycle regulation	Control of cell-cycle progression via protein ubiquitylation	8.933e-5	7/29	ANAPC (subunit 1/**2**/4 + FZR1), **CDK4,** CUL1/RBX1 E3 ligase (CUL1 + RBX1), E2F1, **FBXO5** (= **Emi1**), PLK1, SMAD3;
Insulin regulation of fatty acid metabolism	Control of fatty acid homeostasis via insulin/INSR and glucose	1.301 e-4	12/88	FASN, **INSR,** MAPK1, MBTPS1 (= S1P), **PDE3B, PDPK1,** PRKAR1B, SCAP, **SLC2A4** (= **GLUT4**), SREBF1 (3 SREBP1 transcript variants);
Apoptosis and survival_BAD phosphorylation	Control of apoptosis and autophagy - from EGFR to mitochondria	1.685e-4	8/42	**BAX, EGFR,** GNAS (= Galpha-s), **GNB2** (= **Gbeta2**), IGF1R, MAPK1, **PDPK1,** PPM1A (= PP2C), PRKAR1B;

(Continued on the following page)

Published OnlineFirst October 7, 2011; DOI: 10.1158/1541-7786.MCR-11-0090

Table 1. Top 10 pathways enriched with HRE/CACGTG genes (Cont'd)

GeneGo pathway name	Pathway description	*P*	Network objects	Enriched network gene symbols
CREB pathway	Control of amino acid metabolism + cell cycle—from IGF1R + Ca channels → CREB1 transcription factor	2.366e-4	8/44	CaMK II (sub. delta + **gamma),** DRD1 (= dopamine receptor D1, GPCR), GNAS (= Ga-s), IGF1R, MAPK1, **PDPK1, PDYN,** PRKAR1B, **RPS6KA5 (= S6K 90 kDa sub., MSK1);**

NOTE: Pathways with the most significant overrepresentation of HRE/CACGTG genes are listed with their GeneGo Name, a brief description and a *P* value indicating the significance of the overrepresentation of HRE/CACGTG genes. The Network objects column gives the number of network objects of the pathway encoded by HRE/CACGTG genes over the total number of network objects in the pathway. The last column shows the gene symbols of the HRE/CACGTG genes in the pathways. Bold gene symbols denote multiple HRE-CACGTG signatures flanking the gene, whereas symbols in normal font contain 1 HRE-CACGTG signature in their promoter. A more detailed description of these HRE-CACGTG gene candidates can be found in the gene Excel list available upon request.
Abbreviation: PI3K, phosphoinositide 3-kinase.

testing for normality of data populations and for equal variances between samples, statistical significance (i.e., $P < 0.05$) was calculated by (i) one-way ANOVA/post hoc Sidak modeling (normality/variance equality both maintained) or Welch-approximated t tests in case of unequal sample variances (e.g., Fig. 6B and C; symbols used: ∗; +) and (ii) nonparametric Kruskal–Wallis tests plus Wilcoxon rank-sum tests for pairwise sample comparisons when both assumptions were violated (e.g., Figs. 3, 6A and D; symbols used: #; ¶).

Results

CACGTG palindromic E-boxes often serve as binding sites for several non-HIF basic helix-loop-helix (bHLH) transcription factors, including ARNT (36, 37), MYC (38, 39), USFs (21), STRA13/DEC1 (22), ATF-1, and CREB-1 (40). To identify the factor(s) responsible for the HIF-interfering constitutive activity at the −146 CACGTG element within the promoter of the *hb2* gene (phb2) of *Daphnia magna* (18) and map the factor(s) occurrence across different cancer cells, we conducted an EMSA survey using normoxic nuclear extracts from human hepatoma (Hep3B), cervical carcinoma (HeLa), and breast carcinoma cells (MCF7). Because HeLa and MCF7 EMSA screens yielded compatible results, Fig. 1A presents Hep3B data only (Fig. 1A). The protein components within the constitutive complex (cc) of the −146 phb2 binding activity were identified using specific antibodies directed against USFs, DEC1, MYC, ARNT, and ATF-1. Of these 5 factors screened by supershifts, only USF1 and USF2 were recognized as main *in vitro* binding factors of the −146 phb2 palindrome (Fig. 1A; lanes 3, 5, 7, 9, and 11) while all other factors either failed (MYC and ATF-1) binding this motif or interacted (DEC1) weakly with it (Fig. 1A, lane 15; ∼5%−10% of total pool). The preponderance of USFs as protein components in the HIF-interfering complex of *Daphnia*'s hb2 promoter prompted us to subsequently focus on this transcription factor family. Increasing the volume of anti-USF1M (left) and anti-USF2G (right) antiserum in the binding reaction nuclear extracts from normoxic and hypoxic Hep3B reduced the intensity of the CACGTG complex in a dose-dependent manner (Supplementary Fig. S1A). Binding of USF proteins to the −146 phb2 E-box was clearly oxygen independent (Supplementary Fig. S1A).

We reevaluated our EMSA results through independent pull-down assays of Hep3B, HeLa, and MCF7 nuclear proteins with biotinylated phb2 oligonucleotides bound to streptavidin-coated magnetic beads. In a representative assay with HeLa normoxic and hypoxic nuclear extracts (Fig. 1B and C), wild-type biotinylated oligonucleotides (w-bio), containing the −146 CACGTG phb2 palindrome, were able to pull down 43 kDa USF1 (Fig. 1B), 44 kDa USF2a, and 38 kDa USF2b proteins in an oxygen-independent manner (Fig. 1C). In support of a specific interaction, competition assays (50× comp. lanes) or beads coated with −146 mutant (m-bio) E-box motifs (5′-CAATGT-3′) greatly reduced or abolished the USF pull-down. Similar results

Published OnlineFirst October 7, 2011; DOI: 10.1158/1541-7786.MCR-11-0090

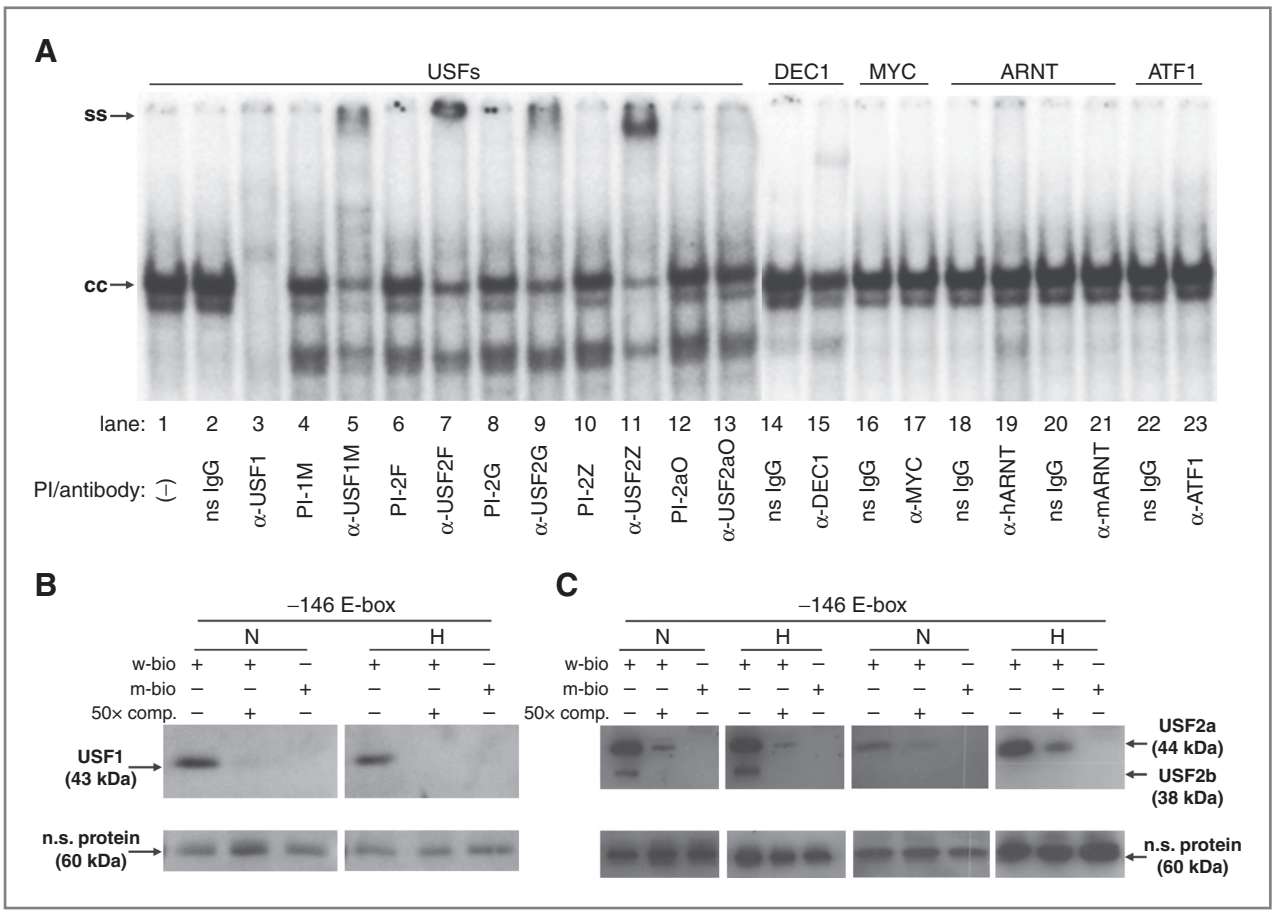

Figure 1. EMSA supershifts and pull-down analysis to identify the phb2-binding CACGTG complex in Hep3B cells. A, to identify factor(s) able to bind to the −146 CACGTG motif in phb2, we used the following antibodies in EMSA supershift reactions with Hep3B normoxic nuclear extracts as indicated in the figure underneath each lane. (–), no antibody; PI, preimmune serum; ns, nonspecific; cc, constitutive CACGTG complex; ss, supershifted CACGTG complex. From lanes 4 to 13, EMSA reactions were supplemented by corresponding PI and immune serum from the same rabbit used to generate anti-USF–directed antibodies (e.g., lanes 4 + 5: PI-1M and anti-USF1M). Results reproduced in $n = 3$ independent assays. B and C, pull-down analysis with beads (w-bio) coated with −146 phb2 E-box–carrying oligonucleotides (5′-CACGTG-3′) and HeLa normoxic (N) and hypoxic (H) nuclear extracts. Binding specificity was assessed either through beads coated with −146 mutant (m-bio) E-box motifs (5′-CAATGT-3′) or with binding reactions containing 50-fold molar excess of free wild-type oligonucleotide as competitor (50× comp.). Immunoblot of bound factors with α-USF1M (B), α-USF2G antibody (C, left), α-USF2aO antibody (C, right). Staining of ns proteins indicated as loading control. Results reproduced in $n = 3$ to 4 independent assays.

were obtained with extracts from Hep3B and MCF7 cells (not shown). Further pull-down and coimmunoprecipitation analyses verified that (i) USF1/2 (CACGTG preference) and HIF-1 complexes (TACGTG preference) display high-affinity binding to distinct elements within phb2 and (ii) the USF–HIF interference within phb2 is DNA context dependent, because we, and others (41), could not detect any direct physical interaction between USFs and HIF subunits (see Supplementary Fig. S1B–E).

To move beyond the *Daphnia* hb2 promoter as a model for occurring cross-talk among E-box complexes, we adopted *Daphnia* phb2 coordinates to conduct a genome-wide screen and enrichment analysis for human genes that harbor, within 1,000 bases from their transcriptional frame (in up- and downstream direction), both a 5′-VNVBRCGTG-3′ HRE consensus motif (11) and a 5′-CACGTG-3′ palindrome with a motif–motif distance of 100 bp or less. According to these criteria, our survey found multiple examples of known HIF targets among the list of HRE/palindrome genes including *VEGF factor C* (*VEGFC*), *LDHA*, *phosphoglucomutase 2, enolase 1, transferrin (TF), eukaryotic translation initiation factor 4E binding protein 1 (4EBP1), Bcl-2/E1B 19 kDa interacting protein 3-like (BNIP3L)*, and *Bcl-2–associated X protein (BAX*; an Excel file with the detected human HRE/palindrome candidate genes is available upon request). When we looked at the top-scoring GeneGo pathways, whose signaling components showed a highly significant enrichment of HRE/palindrome genes (see Table 1), we noticed several signal transductions where USFs seem to impinge on hypoxia signals in a highly localized manner (e.g., insulin-regulated/cap-dependent mRNA translation, HIF-mediated transcription, and cytoskeletal or cell-cycle control functions). Interestingly, particular focal points of HRE/palindrome gene clusters included the eIF4F checkpoint of the cap-dependent translation control, cell surface receptors for insulin and growth factors as well as actin

Published OnlineFirst October 7, 2011; DOI: 10.1158/1541-7786.MCR-11-0090

Table 2. E-box palindromes and HRE sites in promoters of human genes

Gene	Sequence 5′–3′	References
	−183 −178 −91 −86	(67)
TYR	gaaaagtcagt***CATGTG***cttttca–gccaaga***CATGTG***ataat–aggaaga (atg)	
	−413 −408	(28)
PHD2	gccgtggtg**TACGTG**cagagcgcgcagagcgagt–gccgccgccgcc (atg)	
	−179 −174 −120 −115	
4EBP1	ggggatcc***CACGTG***gaagc-caaatcccagg**GGCGTG**gggcgg-gagacc (atg)	
	−2465–2460 −2367–2362 −2353–2348	(62, 68)
LDHA	cagcg*CACGTG*gagcg-actca***CACGTG***ggttcccg**CACGTC**cgccggc-aat (atg)	
	−742 −737 −461 −456	(67)
MC1R	acgttga*CAGCTG*agttgctg-ccccgg***CATGTG***gccgccct-ggacaggact (atg)	
	−251 −246	(61)
BNIP3	cgcgcacgcgccg**CACGTG**ccacacgcacccca–gccctctggcgcc (atg)	

NOTE: HIF-1 and USF coregulated candidate genes: *4EBP1*, *LDHA*, *MC1R*, and *BNIP3*; control genes: *TYR* and *PHD2*. Translation start site ATG as +1 (in brackets). 5′-flanking region upstream of ATG is given for human *TYR*, *PHD2*, *4EBP1*, *LDHA*, *MC1R*, and *BNIP3* genes. HRE and E-box palindromes are capitalized. Human-mouse-rat (hmr) conserved HREs: bold + underlined; variable HREs: bold only; hmr conserved E-boxes: italicized + underlined; variable E-box: italics only. For conservation: see alignments in Supplementary Fig. S2.

remodeling genes (see Table 1; Gene symbols). These pathway aggregations of possibly coregulated genes inspired this study to try and provide solid proof-of-principle for a USF-based modulation of, or interference with, the HIF transcriptional outflow for at least some of the known targets listed above. If successful, future work will need to comprehensively assess USF–HIF cross-talk in cancer cells in a physiologic context (see Discussion).

For initial insights on HIF/USF convergence at DNA level, we (i) established those genes with a strong human–mouse–rat (hmr) conservation of the HRE/palindrome motifs within the aligned promoter regions (Table 2; Supplementary Fig. S2) and (ii) examined the mRNA expression of 5 such hmr-conserved HRE/palindrome candidates by quantitative real-time PCR (qRT-PCR) in conjunction with transient, siRNA-based knockdowns of HIF-1α, USF1, and USF2a in Hep3B (see Fig. 2 for knockdown efficacy assessment by Western blot). Transfection with scrambled RNA did not affect steady-state abundance of HIF-1α, USF1, and USF2a proteins [scrambled: compare with nontransfected (non-TF) cells]. In contrast, exposing Hep3B cells to siRNAs specifically directed against HIF-1α (siHIF-1α), USF1 (siUSF1), USF2a (siUSF2a), or the combination of both USFs (siUSF1/2a) resulted in a drastically diminished expression of the respective factor(s). In cells subjected to a USF1 knockdown (siUSF1), effects on the expression of USF2a ranged from unaltered to a slight elevation. Conversely, silencing of USF2a (siUSF2a) was accompanied by a strong reduction of USF1 protein level (Fig. 2, USF1 signal in siUSF2a). Similar to these findings, both USFs were concomitantly lost in USF2 knockout mouse models, suggesting USF2 to be generally required as USF1 transactivator (42).

Following transient knockdown of HIF-1 and USFs in normoxic and hypoxic Hep3B cells, changes in mRNA levels of the HRE/palindrome candidates *LDHA*, *BNIP3*, *BNIP3L*, *4EBP1*, and *VEGFC* were assessed by qRT-PCR (Fig. 3). Transcripts of *BNIP3*, *BNIP3L*, *LDHA*, and *VEGFC* were all upregulated by 1% O_2/16-hour exposure in Hep3B treated with scrambled RNA. The 4- to 5-fold hypoxic induction of the *BNIP3* and *BNIP3L* mRNA levels was entirely (*BNIP3*) or almost entirely (*BNIP3L*) driven by HIF-1α (see siHIF-1α data). Silencing USF1 and USF2a expression, however, resulted in moderately (siUSF1) or significantly (siUSF2a) increased fold hypoxic inductions of *BNIP3* and *BNIP3L* genes. The stronger effect on the hypoxic induction of *BNIP3* and *BNIP3L* genes by the siUSF2a treatment could result from its effective double knockdown of USF1 and USF2a proteins (Fig. 2). Elevated gene activity of *LDHA* in hypoxic Hep3B was weakly attenuated following siHIF-1α treatment but not impacted by either USF knockdown. Expression of *4EBP1*, mildly suppressed in hypoxic hepatoma cells (scr data), was constitutively reduced upon the knockdown of USF factors. The approximate 2-fold hypoxic induction of *VEGFC* mRNA (scr data) was lost upon USF siRNA treatment due to a strong increase of transcript level in normoxic Hep3B cells.

With regard to the vividly O_2-responsive *BNIP3* and *BNIP3L* genes, we also noted that the potentiation of the induction in USF-silenced cells subjected to 1% O_2 predominantly derived from a reduced normoxic, rather than strengthened hypoxic, gene activation (Fig. 3). This observation highlighted the importance of USF1/2a in maintaining the basal transcription of either gene in oxygenated cells. Because HIF-1 is known to regulate *BNIP3* activity with an unusually broad O_2 response profile (15, 17), the factor could likely encounter USFs at the *BNIP3* promoter even in subnormoxic cells. In additional qRT-PCR analyses, we therefore assessed if, during episodes of moderate (3% O_2) or very mild degrees of O_2 scarcity (10% O_2), HIF-1

Published OnlineFirst October 7, 2011; DOI: 10.1158/1541-7786.MCR-11-0090

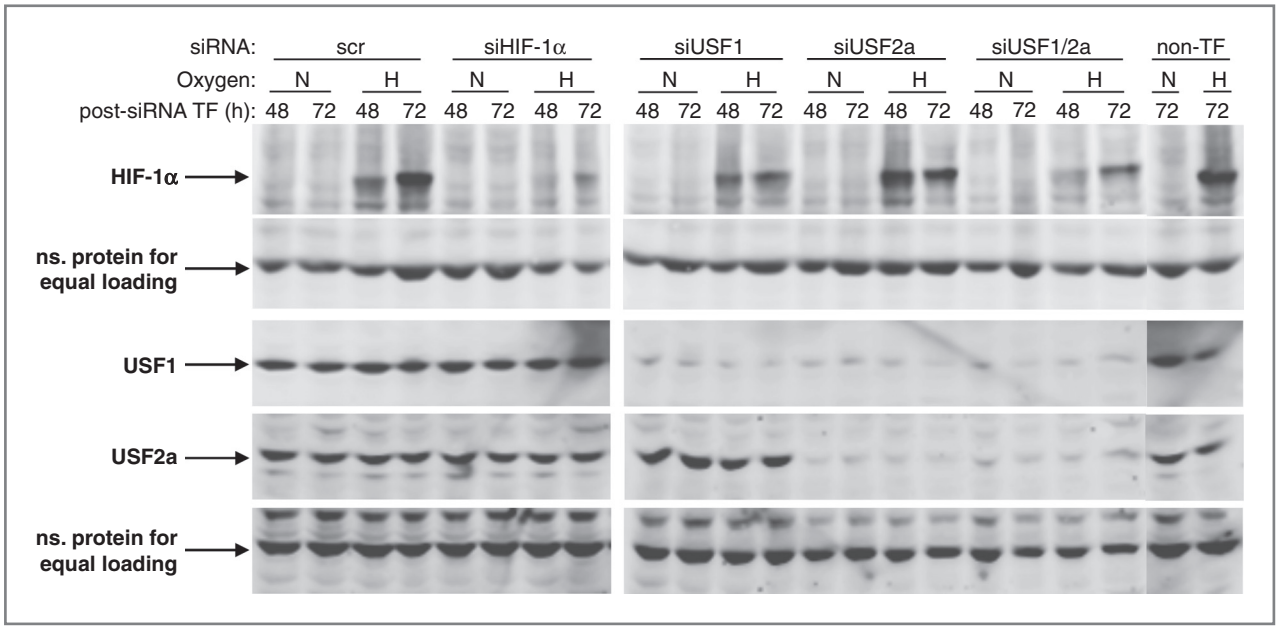

Figure 2. Western blot analysis for assessment of transient siRNA knockdown efficacy of HIF-1α, USF1, and USF2a in Hep3B cells. Transfections with scrambled siRNA (scr) and nontransfected (non-TF) cells were used as negative controls. Cells were harvested at 2 post-siRNA transfection time points: 48 and 72 hours. Hypoxia (H, 1% O_2) exposure started at time point 42 hours post-siRNA transfection for 6 and 30 hours, respectively. Normoxia (N): air exposure. As shown in the figure, protein level expression of HIF-1α and each USF in transiently transfected Hep3B cells was robustly silenced from 48 hours (= 42 + 6 hours hypoxia) up to 72 hours (= 42 + 30 hours hypoxia) post-siRNA transfection. ns, nonspecific.

continues to control *BNIP3*. We also asked if, relative to harsher hypoxia (1% O_2), USFs will compete more potently with HIF-1 for the *BNIP3* regulatory binding sites at 3% and 10% O_2 (see Discussion for further reasoning). Steady-state levels of *BNIP3* mRNA indeed revealed for scr-transfected Hep3B cells robust inductions of 3.3- and 1.6-fold in cells subjected to 16 hours of 3% and 10% O_2, respectively (Table 3). Together with the profiling at 1% O_2 (4.8-fold transcript induction), the exquisite sensitivity of the *BNIP3* gene toward a wide range of changes in oxygen concentrations became fully evident. Moreover, as silencing of HIF-1α expression abrogated the inductions at 1%, 3%, and 10% O_2 all equally efficient down to transcript parity (i.e., H/N ratios = 1.0 for siHIF-1α treatment; see Fig. 3, Table 3), responses of *BNIP3* from 1% to 10% O_2 seem to rest entirely on functional HIF-1. Upon silencing of USF1, but surprisingly not USF2a, we observed the *BNIP3* induction to be potentiated almost significantly at 3% O_2 [3.3-fold (scr) → 4.6-fold (siUSF1); $P = 0.070$] and to a significant extent at 10% O_2 [1.6-fold (scr) → 2.2-fold (siUSF1); $P = 0.019$; Table 3). This USF1 loss-of-function mediated enhancement resulted from the combination of reduced normoxic [1.0 (scr) → 0.7 (siUSF1)] and, toward milder hypoxia, progressively increasing hypoxic levels of *BNIP3* transcripts [with 100% mRNA level (scr) → 84%–95%–105% mRNA level at 1% O_2–3% O_2–10% O_2 (siUSF1)].

Although we were encouraged by these early data suggesting a competitive cross-talk to occur between basally active HIF-1 and USF factors in cells facing a subnormoxic milieu, the remainder of the study focused on providing proof-of-principle evidence for USF-mediated positive or negative functional interactions with HIF-1 at 1% O_2. At this level of deoxygenation, HIF-1 activity peaks in many cell lines, hence, its transcriptional control of the bulk of downstream targets is expected to operate with optimal efficacy. Alignments of the homologous regions of *BNIP3* promoters had revealed a remarkable hmr conservation around the HRE motif (Supplementary Fig. S2). For this reason, we went on to compare the promoter responses of *BNIP3*, where the HRE and CACGTG motifs are contained within a single *cis*-element, with those of *MC1R*, *4EBP1*, and *LDHA* genes, which all possess distinct HRE and palindrome sites of variable hmr conservation (Table 2; Supplementary Fig. S2). Parallel ChIP experiments confirmed the recruitment of HIF-1α- and constitutive USF1- and USF2a-containing complexes to both *LDHA* (Fig. 4A) and *BNIP3* (Fig. 4B) promoter sequences in intact Hep3B (Fig. 4, left), MCF7 (Fig. 4, right), and HeLa cells (not shown). This coordinate binding of HIF-1 and USFs was seen both at low oxygen (at *LDHA* + *BNIP3* promoter) and in oxygenated nuclei as well (see HIF-1α at *BNIP3* promoter; Fig. 4). The latter finding added weight to the notion of HIF-1 controlling BNIP3 transcription even under subnormoxic/normoxic conditions (see previous paragraph).

To further study the convergence of HIF and USF pathways at DNA level, the promoter regions in question were amplified from genomic DNA, cloned, sequence confirmed, and inserted into pGL3 basic luciferase reporter plasmids. The set of luciferase promoter reporters thus obtained included both donated (i.e., *BNIP3* and *PHD2*) and self-generated constructs (*TYR, 4EBP1, LDHA*, and *MC1R*),

Published OnlineFirst October 7, 2011; DOI: 10.1158/1541-7786.MCR-11-0090

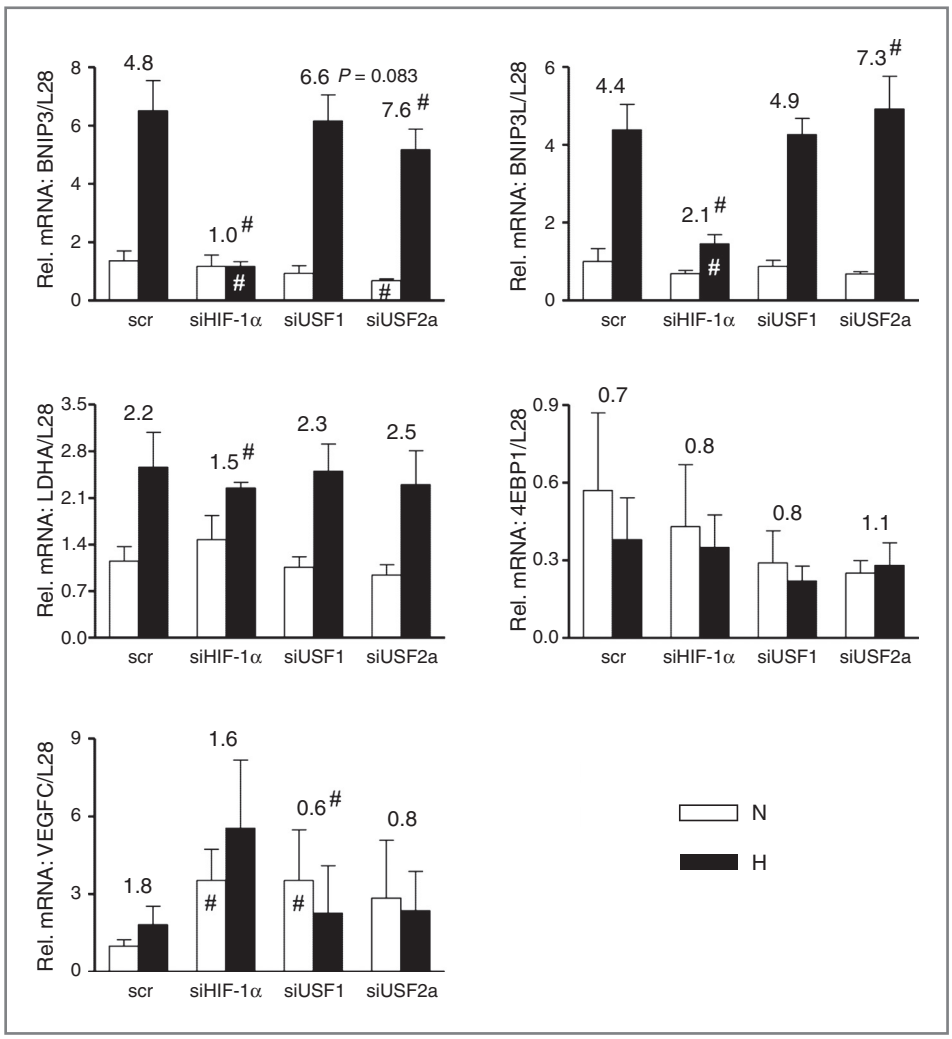

Figure 3. qRT-PCR for (top left to bottom right) *BNIP3*, *BNIP3L*, *LDHA*, *4EBP1*, and *VEGFC* mRNA levels in Hep3B transfected with siRNAs. Hep3B cells were transfected with HIF-1α, USF1, or USF2a siRNA at a final concentration of 200 nmol/L. Scrambled siRNA (scr) was used as negative control. RNA was isolated from Hep3B at 66 hours post-siRNA transfection, that is, at a time point where the silencing effect of HIF-1α and USFs was still in effect (see Fig. 2). Hypoxia exposure started at time point 50 hours post-siRNA transfection for 16 hours. mRNA levels of above named genes were quantified by qRT-PCR and normalized by L28 expression. All data are presented as the means ± SD of 4 independent experiments. Normoxia (N), air; Hypoxia (H), 1% O_2 16 hours. Mean H/N-fold inductions of each transcript are indicated above the respective pair of columns. Mean expression of individual transcripts were compared (i) within same O_2 category (N or H) and (ii) for H/N-fold changes of siRNA-treated experimental groups (siHIF-1α, siUSF1, and siUSF2a) relative to scr controls. For significant scr/si comparisons, the used symbol denotes pairwise nonparametric Wilcoxon rank-sum tests (#). See Materials and Methods for more details.

and covered USF-specific targets (i.e., *TYR*; ref. 43) or HIF-1–specific targets (i.e., *PHD2*; ref. 44) plus 4 HRE/palindrome candidates (*4EBP1*, *LDHA*, *MC1R*, and *BNIP3*; Table 2; Supplementary Fig. S2). We initially examined the hypoxia (1% O_2/16 hours) responsiveness of these candidate promoters. Respective reporter transfections of Hep3B, MCF7, and HeLa cells included negative control reactions (i.e., "bVec" = empty pGL3 basic luciferase vector; Fig. 5) to monitor basal and hypoxia nonresponsive luciferase activity. In contrast, the *PHD2* luciferase construct was induced approximately 3- to 8-fold in hypoxic Hep3B, HeLa, and MCF7 cells (Fig. 5). Luciferase assays with the 4 candidates, *4EBP1, LDHA, MC1R*, and *BNIP3*, revealed only for *LDHA* (~2-fold) and *BNIP3* (4- to 7-fold) a robust upregulation by hypoxic conditions in Hep3B, MCF7, and HeLa cells.

Next, we investigated the possible coregulation of *BNIP3* and *LDHA* reporter by HIF and USF cascades in cotransfections with HIF-1α and USF1, USF2a, or USF2b expression plasmids (Fig. 6). In pilot studies (not shown), we had carefully titrated for each cell line the amount of HIF-1α plasmid (i.e., 15–100 ng) needed for an optimal hypoxic induction of either reporter and of any USF plasmid (i.e., 15 ng) needed for an optimal specific activation of either reporter construct (Fig. 6). The activity of the *TYR* promoter reporter rose constitutively 4- to 7-fold upon USF1-, and up to 20-fold upon USF2a, cotransfection. Overexpression of HIF-1α did not impact the *TYR* reporter (Fig. 6A). On the contrary, *PHD2* reporter activity was significantly increased in normoxic and hypoxic Hep3B upon HIF-1α overexpression. The impact of overexpressed USFs on the *PHD2* reporter was either negligible (USF1) or attributed to nonspecific stimulation by the overexpressed factor (USF2a) exerted on the vector backbone. Therefore, both control reporters responded specifically to the overexpression of their respective transcriptional driver(s) (Fig. 6A).

The *LDHA* promoter was induced by endogenous hypoxia signals almost 2-fold in Hep3B (Fig. 6B), and additionally stimulated upon cotransfection with USF1, and particularly, USF2a and USF2b plasmids. Of note, overexpressed USFs augmented LDHA luciferase activity predominantly under normoxia, thereby reducing the original

Published OnlineFirst October 7, 2011; DOI: 10.1158/1541-7786.MCR-11-0090

Table 3. BNIP3 mRNA fold inductions in mildly deoxygenated Hep3B transfected with siRNAs

O_2	scr	siHIF-1a	siUSF1	siUSF2a
3%	**3.325** ± 0.754	**1.078** ± 0.148	**4.583** ± 0.472	**4.222** ± 0.907
P (siX vs scr)	—	$P = 0.0072$	$P = 0.0704$	ns
10%	**1.622** ± 0.177	**1.055** ± 0.038	**2.145** ± 0.159	**1.560** ± 0.313
P (siX vs scr)	—	$P = 0.0056$	$P = 0.0189$	ns

NOTE: Hep3B transfections with scrambled (scr) control RNA or HIF-1α, USF1 or USF2a siRNA followed the identical protocol used for the quantitative expression analyses in Fig. 3. *Bnip3* mRNA levels were quantified by qRT-PCR and normalized by L28 expression. Fold inductions of *Bnip3* transcript levels in mildly deoxygenated (H: 3% or 10% O_2; 16 hours) versus normoxic (N: air; 16 hours) Hep3B are given as means (± SD) of 3 independent experiments. *P* values for H/N-fold changes between siRNA-treated experimental groups (i.e., siX = siHIF-1α or siUSF1 or siUSF2a) and the scr control group of the same O_2 category (i.e., comparison done only within 3% or 10% O_2 category) are indicated.

hypoxic induction to an almost constitutive expression in Hep3B (Fig. 6B) and MCF7 cells (not shown). The switching from HIF- to USF-driven transactivation modes, and vice versa, was further observed for the endogenous *LDHA* promoter, particularly in Hep3B (Fig. 4A, left) and HeLa cells (not shown). Here, hypoxia clearly promoted HIF-1 binding and, in parallel, attenuated the occupancy of USF1 and USF2a. Thus, HIF-1 and USF complexes recruited to the *LDHA* promoter cap the activity of one another to yield a pO_2-dependent complementation mode of gene control.

On the basis of these data, transactivation of the *LDHA* gene by HIF-1 and USFs proceeds from distinct motifs (below) and peaks at varying pO_2 (USFs → aerobic *LDHA* expression; HIF-1 → hypoxic *LDHA* expression). In contrast, both pathways must converge onto a single stretch of DNA within the *BNIP3* promoter (Supplementary Fig. S2, and below). The relevant reporter was nearly 3-fold hypoxia induced by endogenous HIF-1–mediated (Fig. 3) signaling in Hep3B (Fig. 6C) and HeLa cells (Fig. 6D). Cotransfection with USF1 and USF2a, or with USF2b, enhanced *BNIP3* promoter activity in both cell lines particularly under normoxia and consequently weakened the reporters' hypoxic induction. Overexpression of HIF-1α amplified the hypoxic BNIP3 activity robustly in Hep3B (6.6-fold; Fig. 6C) and moderately in HeLa cells (3.2-fold, Fig. 6D). However, this potentiated hypoxia response of *BNIP3* by ectopic HIF-1α was significantly impaired through the simultaneous cotransfection with USF1 or USF2a, but not USF2b, in Hep3B and HeLa cells (Fig. 6C and D, see ↓ arrows). Increasing the amount of USF1/2a plasmids further (15 → 100 ng) converted the hypoxic transactivation of the reporter into an increasingly constitutive response, especially in Hep3B cells (Fig. 6C). These data suggest that

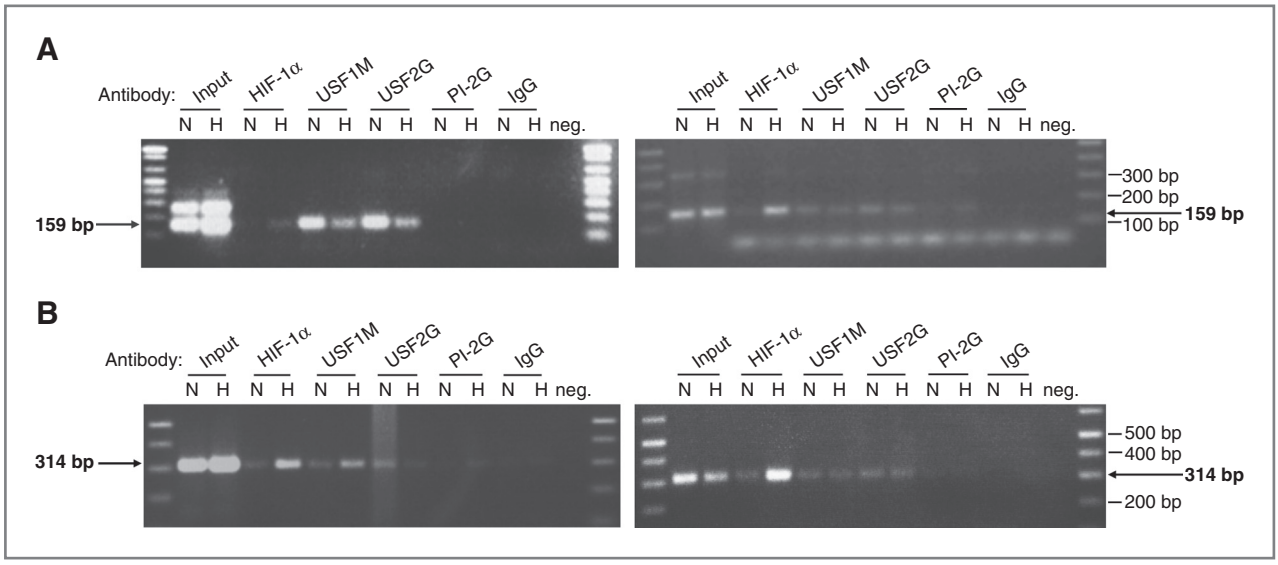

Figure 4. ChIP determination of *in vivo* HIF-1 and USF binding to *LDHA* and *BNIP3* promoters. ChIP assay was carried out in Hep3B (left) and MCF7 (right) cells with indicated antibodies or preimmune serum and nonspecific antibody IgG as negative controls. Purified DNA was subjected to PCR with *LDHA* primer (A, 159-bp amplicon) or *BNIP3* primer (B, 314-bp amplicon). N, air; H, 1% O_2 4 hours. PI-2G preimmune serum for anti-USF2G; neg. PCR with H_2O.

Published OnlineFirst October 7, 2011; DOI: 10.1158/1541-7786.MCR-11-0090

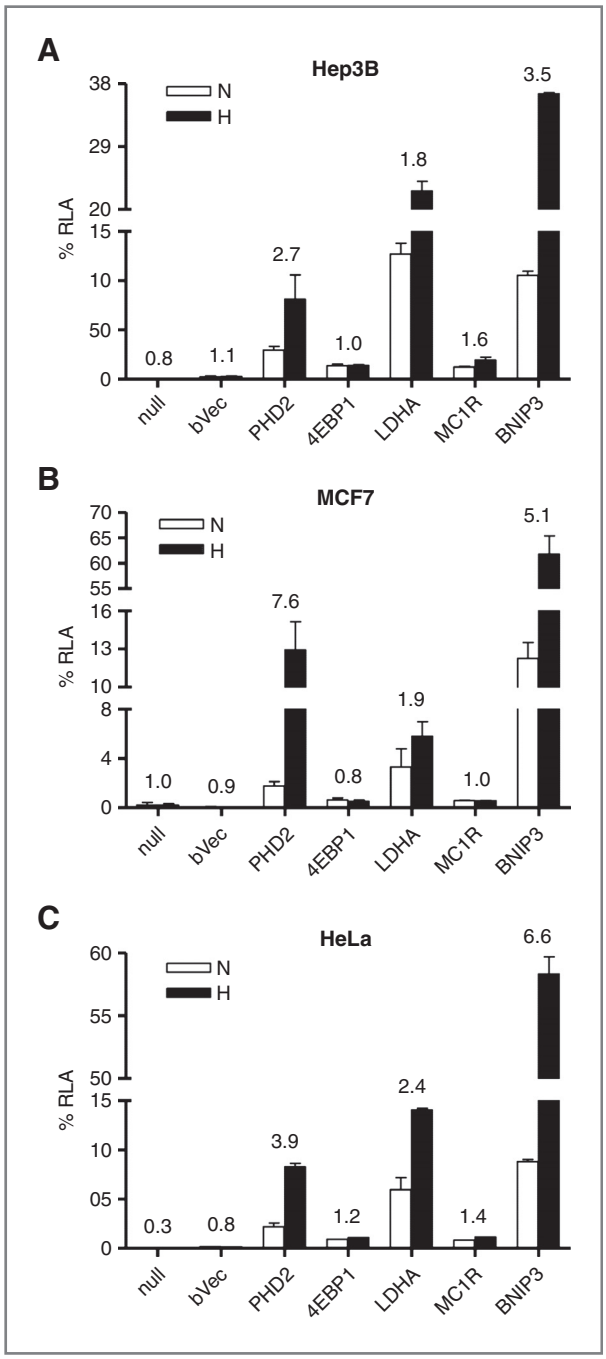

Figure 5. Endogenous response of *PHD2, 4EBP1, LDHA, MC1R*, and *BNIP3* luciferase reporter. Hep3B (A), MCF7 (B), and HeLa (C) cells were transfected with 2.0 μg of *4EBP1, LDHA, and MC1R* or 1.5 μg of *PHD2* or *BNIP3* luciferase reporter plasmid in a total of 3.0 μg plasmid. After 16-hour hypoxic (1% O_2: H, black bars) or normoxic (air; N, white bars) exposure, RLA was determined and normalized with β-galactosidase activity (% RLA, as mean ± SD). Plasmid-free transfections (null) and transfections with the empty pGL3 basic vector (bVec) were used as negative controls. Mean H/N-fold inductions of each reporter are indicated above the respective pair of columns.

HIF-1α and USF1 or USF2a compete dose dependently with each other over the control of the BNIP3 site.

The functionality of the computed HIF-1 and USF1/2 sites in the *LDHA* and *BNIP3* promoter was assessed by EMSA screens with Hep3B, HeLa, and MCF7 normoxic and hypoxic nuclear extracts. Representative results are shown for *LDHA* (MCF7 nuclear extracts, Fig. 7A) and *BNIP3* (Hep3B nuclear extracts, Fig. 7B). The wild-type CACGTG-motif in region I (Supplementary Fig. S2) of the *LDHA* promoter was weakly bound by a hypoxia-regulated complex containing HIF-1α [see supershift (ss)—lane 4; Fig. 7A] and avidly bound by the cc factors USF1 and USF2a (see ss in lanes 6, 7, 9, and 10; Fig. 7A, reg.I wt). Another radiolabeled oligonucleotide, spanning the wild-type region II and III (Supplementary Fig. S2: reg. II/III ww) was tightly bound both by HIF-1α and USF1/2 (Fig. 7A, bottom; detection of HIF-1α ss: lane 4; USF2G ss: 9 + 10). When using a reg. II/III double site oligonucleotide carrying a mutation in region II and an unaltered wild-type sequence in region III (reg. II/III mw), only the hypoxia-inducible complex, supershifted by anti–HIF-1α, was detected in conjunction with a complete loss of the constitutive binding activity by USFs (Fig. 7A: reg. II/III mw). The reverse sequence alteration in region III but not II (reg. II/III wm) left the oligonucleotide attachment by the constitutive USF complex undisturbed, but erased any interaction with HIF-1. Thus, the *LDHA* region II acts as exclusive, high-affinity site for USFs, whereas *LDHA* region III attracts HIF-1 to this promoter in deoxygenated nuclei.

In contrast to this segregated binding of HIF-1 and USFs in the *LDHA* promoter, either complex interacted with the −259/−236 DNA of the *BNIP3* promoter containing the HRE at −251/−246 (Supplementary Fig. S2; Fig. 7B). Specific supershifts were able to positively identify HIF-1α (ss: lane 4) as constituent of a hypoxic binding activity (lane 2), and USF1 (ss: lanes 6 + 7) and USF2 (ss: lanes 9 + 10) as participants of a constitutive complex (lanes 1 + 2; Fig. 7B). We further elaborated whether the HIF–USF interplay at the −251/−246 core element of BNIP3 is governed by differential affinities of the respective factors. To that end, we conducted additional pull-down analyses using magnetic beads coated with w-bio BNIP3 HRE probes (Supplementary Table S1) and assessed binding specificity and avidity in reactions containing 10× or 50× excess of wt competitor (comp.) oligonucleotides or beads coated with mutant (m-bio) probes (Supplementary Fig. S3). Excess probe (10× and 50×) diminished the initial binding activity (set to 100% in each case) to a mean (n = 3–4 independent assays) residual activity of: (i) approximately 8.8% (10×) and approximately 5.4% (50×) for hypoxic HIF-1; (ii) approximately 1.3% and approximately 0.4% for normoxic or hypoxic USF1; and (iii) approximately 2.6% and approximately 1.4% for normoxic or hypoxic USF2a, respectively. The fact that 10×/50× excess probe sufficiently eliminated almost all of the USF–bead interaction showed the, relative to hypoxic HIF-1, much weaker *in vitro* affinity by which USF1 and USF2a constitutively bind to the BNIP3 HRE (Supplementary Fig. S3).

Published OnlineFirst October 7, 2011; DOI: 10.1158/1541-7786.MCR-11-0090

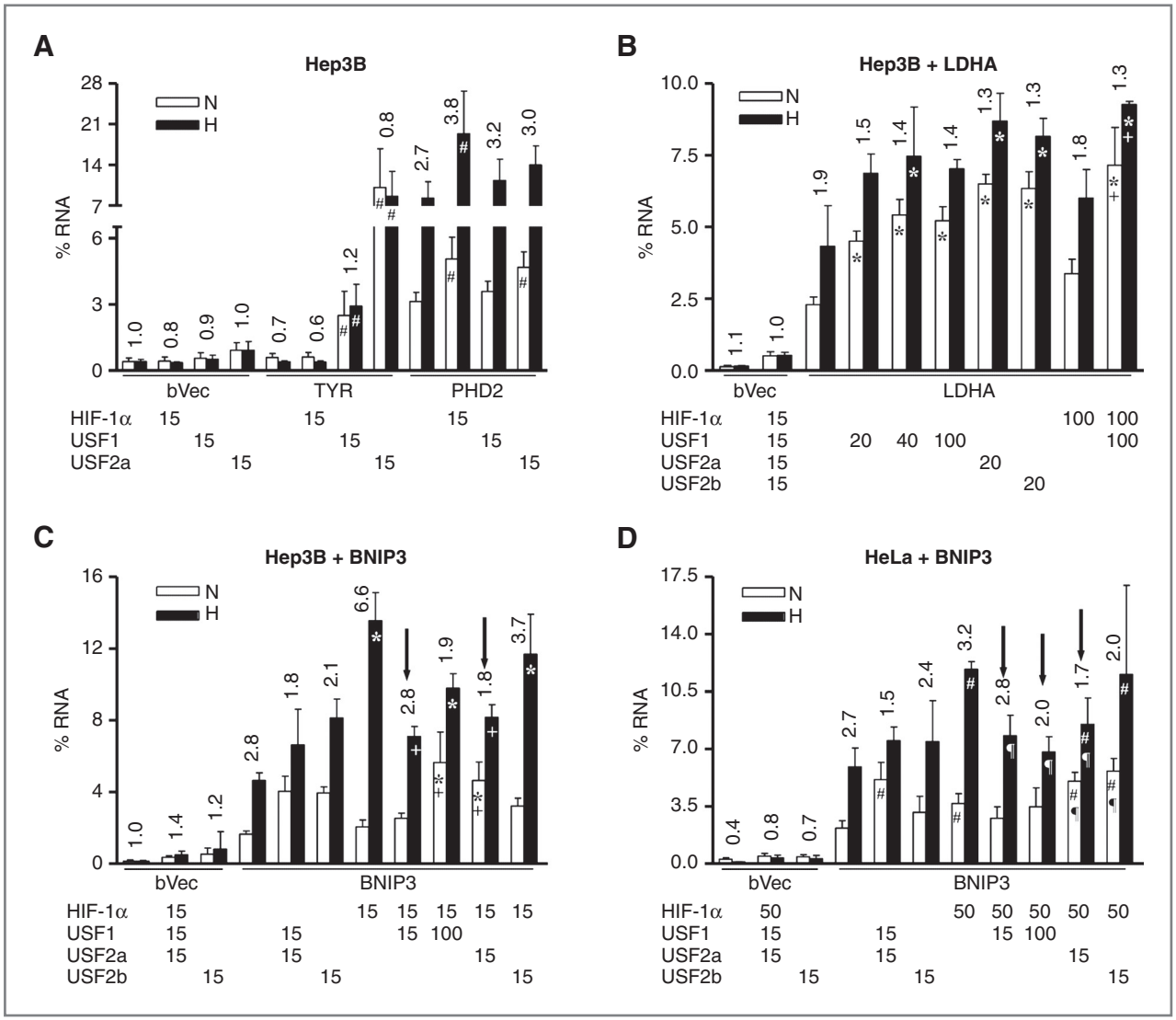

Figure 6. Regulation of *BNIP3* and *LDHA* luciferase activity by overexpressed HIF-1α and USFs. A, Hep3B transfections of USF and HIF-1 control reporter with either 1.5 μg *TYR* plasmid or 0.5 μg *PHD2* plasmid. B, Hep3B transfections with 0.3 μg *LDHA* reporter plasmid. Hep3B (C) or HeLa (D) transfections with 0.3 μg *BNIP3* reporter plasmid. For reporter regulation by overexpressed HIF-1α and USFs, nanogram (ng) amounts of HIF-1α and USF expression plasmids used are indicated underneath the respective cotransfection. RLA is given as in Fig. 5 (mean ± SD% RLA; $n = 3$ independent experiments). N and H conditions and presentation of mean H/N-fold inductions as in Fig. 3. Statistics done in regard to same O_2 category (i.e., N or H): (i) endo/exo test, endogenous controls (reporter alone; no overexpressed HIF/USF) versus HIF/USF cotransfection (reporter with exogenous HIF-1α and/or USF1/2a); (ii) hif/combi test, reporter + exogenous HIF1α versus reporter + exogenous (HIF1α + USF1/2a). Symbols for $P < 0.05$ for (i) nonparametric Wilcoxon rank-sum tests (endo/exo, #; hif/combi, ¶); (ii) ANOVA/Sidak tests (endo/exo, ∗; hif/combi, +). See Materials and Methods for more details.

Discussion

One way to fine-tune, or inhibit, HIF's transcriptional outflow independently of hydroxylase activities could be through competing transcription factors. We reported earlier (18) that binding of a Hep3B factor to CACGTG motifs was able to counteract the HIF-driven induction of the phb2 reporter from HREs at adjacent positions. Evidently, palindrome factors can engage in positive or negative cross-talk with nearby HIF/HRE complexes (45–47). *En route* toward a more physiologic understanding of hypoxic signaling, we thought to analyze gene control mechanisms not just as a function of the stability/activity of HIF-1 *per se*. Rather, the dynamic interplay between transcriptional complexes that governs the hierarchy by which HIF-1 and related factors gain access to DNA and regulate expression was considered. This study, thus, aimed to identify the phb2 CACGTG-binding entity in human cancer cells and investigate the factors interplay with HIF-1 in the control of selected examples of cotargeted genes.

Both, EMSA supershifts and oligonucleotide pull-down assays consistently identified USF1 and USF2a/2b as the main phb2 CACGTG complex in nuclear extracts from Hep3B and HeLa (Fig. 1) or MCF7 cell lines. Our

Published OnlineFirst October 7, 2011; DOI: 10.1158/1541-7786.MCR-11-0090

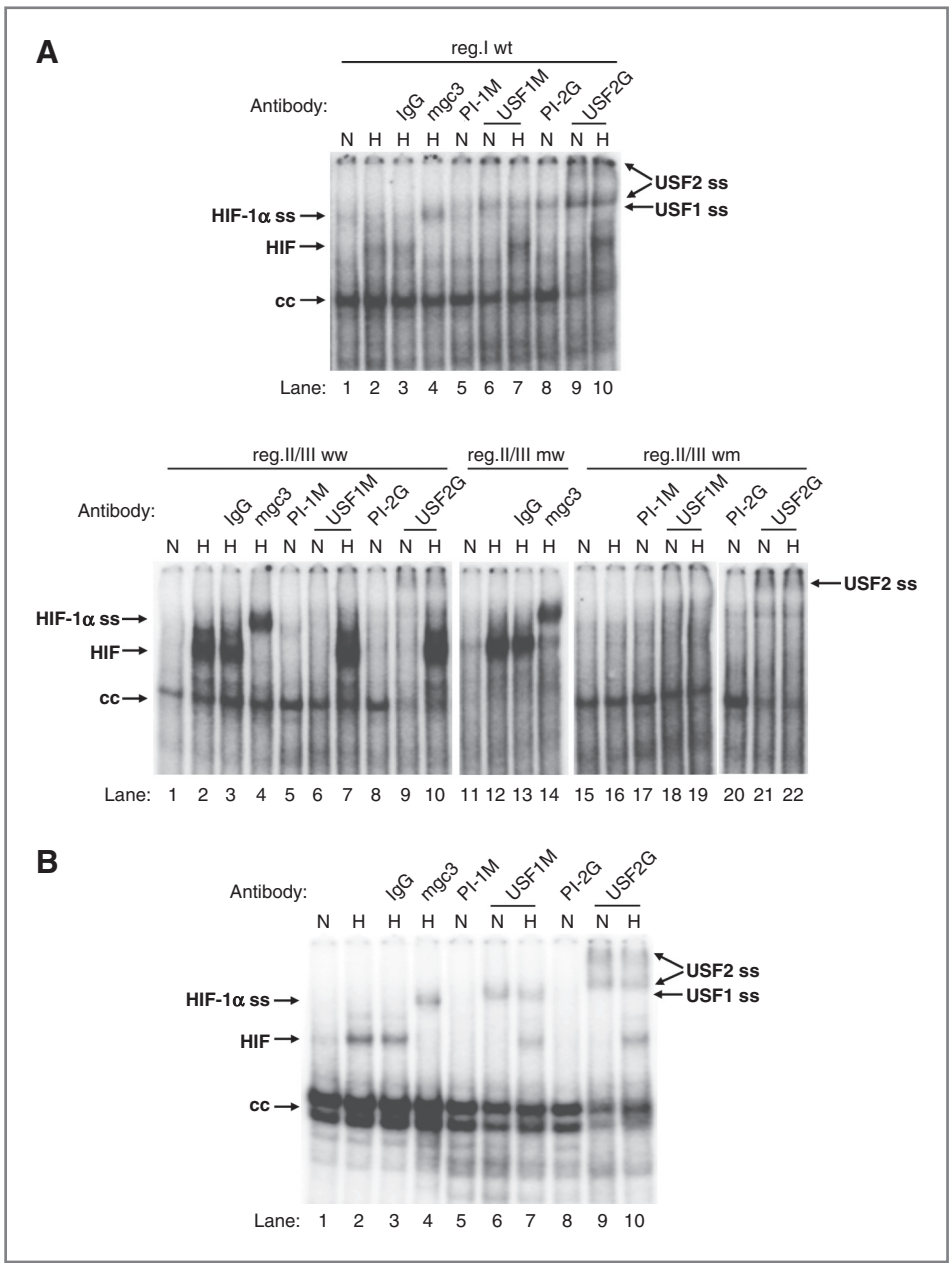

Figure 7. EMSA supershifts with *LDHA* and *BNIP3* E-box oligonucleotides. Gel supershift using *LDHA* HRE and E-box palindrome oligonucleotides together with MCF7 nuclear extracts (A) and *BNIP3* HRE oligonucleotides together with Hep3B nuclear extracts (B). All oligonucleotides used in this EMSA are listed in Supplementary Table S1. For HIF-1α or USFs gel supershifts, 1 μL of the indicated specific antibody was used in comparison with preimmune serum (PI-1M or PI-2G) or nonspecific IgG as negative control. N, normoxia; H, hypoxia; cc, constitutive complex, ss, supershift.

pull-down assays also documented the preferential *in vitro* docking of HIF-1 to the asymmetric −107 phb2 HRE and of USFs to the symmetrical −146 phb2 palindrome motif (Supplementary Fig. S1B and C, 50× comp. lanes). Thus, the single base substitution within the hexameric core of either motif (i.e., −107 HRE: 5′-TACGTG-3′; −146 palindrome: 5′-CACGTG-3′), and presumably additional changes in neighboring nucleotides, are key in conferring the vastly differing affinities of HIF and USF transcription factors to these motifs. This observation fits well with the general perception that CACGTG-palindromes tend to attract non-HIF bHLH factors (25, 36, 37, 47), and, consequentially, are notably underrepresented amongst functional HIF elements (48–50). Our coimmunoprecipitations further demonstrated the interactive precipitation of HIF-1α by ARNT proteins and *vice versa* but failed to reveal any physical contact between USF2a and either subunit of HIF-1 [HIF-1α and ARNT; see Fig. S1D, S1E and ref. 41]. Thus, the constitutive USF1/2a are the main factors that indirectly interfere with the HIF/HRE-driven induction of *hb2* globin gene by binding to the phb2 CACGTG palindrome in human cancer cells (18, 31).

Upstream stimulatory factors belong to the bHLH-leucine zipper family of transcription factors (21, 51, 52). They can mutually influence each other's expression, both in positive [USF2 transactivates *USF1* gene (42); USF2a knockdown yields diminished USF1 levels; Fig. 2)] and negative ways [USF1 represses *USF2* gene; USF1$^{-/-}$ mice

Published OnlineFirst October 7, 2011; DOI: 10.1158/1541-7786.MCR-11-0090

show elevated USF2 levels (42)]. USFs have been implicated in conferring the UV-induced tanning response in melanocytes and in acting as antiproliferative agents in cells transformed by overexpressed MYC or activated RAS signaling (53). Following a marked depletion of intracellular calcium during the differentiation of erythroid progenitor and erythroleukemia cells, endogenous USFs start to accumulate and transactivate several adult marker genes (e.g., *β globin*) that ultimately drive the cells into maturity (54). Beyond MYC, other palindrome complexes can also tailor, or interfere with, HIF's transcriptional read-out. To date, 3 human genes have been examined as HIF/USF coregulated targets, that is, the genes encoding plasminogen activator inhibitor-1 (PAI-1; refs. 55–57), the catalytic subunit telomerase reverse transcriptase (TERT) of the telomerase complex (58–60), and the glycolytic enzyme L-type pyruvate kinase (L-PK; ref. 41).

Guided by phb2 coordinates of *Daphnia*, we conducted a genome-wide computational survey for HIF/USF-coresponsive human genes that were flanked by closely adjacent or overlapping CACGTG palindrome and HRE motifs. Among those, we found *LDHA* and *BNIP3* to be expressed and hypoxia induced at transcript level in human Hep3B cells (Fig. 3). This induction was entirely dependent (*BNIP3*) or aided (*LDHA*), by HIF-1α in Hep3B cells. The O_2-responsive control of *BNIP3* via HIF-1α ranged, in Hep3Bs' at least, from harsh (1% O_2) to moderate (3% O_2) to mild (10% O_2) degrees of deoxygenation. Because the promoter of either gene recruited both HIF-1 and USFs in hypoxic Hep3B and MCF7 cells *in vivo* (Fig. 4), control of *LDHA* and *BNIP3* expression was considered suitable to examine HIF/USF cross-talk at DNA level in greater detail. Previous studies had already validated human *LDHA* and *BNIP3* genes as hypoxia-inducible HIF-1 targets in HeLa and MCF7 cells, respectively (48, 61).

Luciferase reporter of the *LDHA* (~2-fold) and *BNIP3* (3.5- to 7-fold) promoter yielded a robust upregulation by hypoxic (1% O_2/16 hours) conditions across Hep3B, HeLa, and MCF7 cells (Fig. 5). In cotransfection assays in Hep3B cells, overexpressed USFs were found to upregulate the *LDHA* reporter particularly in normoxic conditions (Fig. 6B). The role of USFs in transactivating *LDHA* in oxygenated cells implies the factors as candidate drivers of aerobic glycolysis in cancer cells (Warburg effect). A previous study had already described rat *LDHA* as MYC target and further noticed the weak upregulation of the gene by USFs under normoxia via binding of both E-box sites, regions I and II, within the rat *LDHA* promoter (62). The human *LDHA* promoter was, during low pO_2, predominantly bound by HIF-1, which, in Hep3B and HeLa but not MCF7 cells, evidently served to displace *LDHA*-attached USFs (Fig. 4A). Subsequent EMSA gel supershift assays revealed region I of the 5′ flank of the *LDHA* gene as weak HIF-1 and strong USF1/2a site. The region II palindrome and region III asymmetric E-box of *LDHA*, however, functioned as USF1/2 (reg. II) and HIF-1 (reg. III) binding sites, respectively (Fig. 7A). To rationalize these data, we surmise that, in Hep3B and HeLa cells at least, the sites in regions I to III do not seem to be segregated. Upon changes in pO_2, they rather act as adaptable platform for the dominant transcription factor entity. Thus, in hypoxic Hep3B and HeLa cells, HIF-1 might variably expand its *LDHA* occupancy from its holdout at region III onto regions I and II as well and, by doing so, displaces bound USFs from these regions in intact cells. At the same time, the presence of distinct, nonoverlapping sites in the *LDHA* promoter forms the very foundation for the complementing control of this gene by HIF-1 and USF pathways (Figs. 6and 7A). This complementation allows the HIF-driven expression of *LDHA* during hypoxia to eventually switch to a USF (and MYC)-mediated control under high pO_2 which, in turn, ensures production of this glycolytic enzyme in response to a broader O_2 spectrum and additional microenvironmental stimuli of solid malignancies (i.e., acidic milieu).

Cotransfection of Hep3B and HeLa cells with HIF-1, USF1, and USF2a revealed the dose-dependent interference with the HIF-1–mediated *BNIP3* induction at 1% O_2 by USFs (see arrows, Fig. 6C and D). Conversely, the transient loss of USF1 + USF2a functions (siUSF2a treatment, Fig. 2) or of USF1 activity alone (siUSF1 treatment), resulted in Hep3B cells in a significantly augmented induction of *BNIP3* (and *BNIP3L*) genes at harsh (1% O_2) and mild (10% O_2) degrees of deoxygenation, respectively (Fig. 3, Table 3). These data support the notion of an increasing competition of HIF's *BNIP3* control by endogenous USF1 in mildly O_2-deprived cells (see also below). The HRE at position −251/−246 in the promoter of the human *BNIP3* gene was first identified by Kothari and colleagues to function as a direct functional binding site for HIF-1 under hypoxia (61). Our EMSA screen with a single site oligonucleotide (−259/−236; Supplementary Table S1) characterized this HRE-containing sequence as being cotargeted by HIF-1 and USFs in hypoxic (1% O_2/16 hours) cells (Fig. 7B). Additional pull-down assays revealed hypoxic (1% O_2/16 hours) HIF-1 complexes to dock, *in vitro*, much more tightly to the *BNIP3* HRE than do USF1 and USF2a factors (Supplementary Fig. S3). Because pull-downs use, EMSA-like, nuclear extracts with free, DNA-dissociated α-subunits, they cannot provide insights on the binding of normoxic HIF-1 to the *cis*-element in question. Nonetheless, we extrapolate a markedly inferior affinity of USFs to the *BNIP3* HRE when compared with hypoxic HIF-1 complexes under *in vivo* conditions as well.

Although USF expression manipulations affected *BNIP3* gene/reporter activity particularly in normoxia [i.e., note *BNIP3* inductions at 1% O_2 in (i) Fig. 3, USF1/2a knockdown: 4.8fold (scr) → 6.6- to 7.6-fold knockdown; (ii) Fig. 6C and D; USF1/2a overexpression: 2.8-fold (endogenous) → 1.5- to 1.8-fold (overexpression)], several additional observations implied the USF/HIF convergence onto *BNIP3* to follow far more intricate rules than a *LDHA*-like segregation between normoxic/USF and hypoxic/HIF occupations would suggest. First, ChIP analysis of all 3 cell lines (Hep3B, MCF7, and HeLa) showed measurable amounts of HIF-1 during normoxia, and of USF1/2 complexes during normoxia and hypoxia, attached to the *BNIP3* promoter chromatin (Fig. 4 and data not shown). Second, the USF1/2

Published OnlineFirst October 7, 2011; DOI: 10.1158/1541-7786.MCR-11-0090

dimers, tethered to the same −251/−246 core sequence as the hypoxia-inducible factor during low pO_2 (Fig. 7B), showed virtually no signs of displacement by incoming HIF-1 (Fig. 4). Such a persisting attachment of USF factors during hypoxic periods of HIF-1 occupancy could be achieved by the presence of secondary docking sites within the *BNIP3* promoter. Indeed, we noted hmr conserved CACGCR motifs dubbed E1 and E2, separated by 3-nucleotide spacers on either side of the −251/−246 BNIP3 HRE (i.e., 5′-CACGCGccg**CACGTG**ccaCACGCA-3′; E1/E2 = capital; spacers = small; HRE = capital/bold; see Table 2; Supplementary Fig. S2). Subsequent EMSA experiments with triple site E1-HRE-E2 oligonucleotide probes in www (all 3 sites intact) and mwm (HRE intact, E1 + E2 mutated) configuration revealed for hypoxic extracts (HIF-1 docked to HRE) a 1.3- to 2.3-fold stronger binding of USF complexes to www than mwm sequences (not shown). Thus, intact E1/E2 motifs (and several other CACGCN promoter sites) can temporarily provide alternative USFs sites at the *BNIP3* gene. When HIF-1 approaches the BNIP3 HRE during low pO_2 *in vivo*, USFs may be able to sidestep displacement by sliding onto E1 and E2.

The fact that we detected HIF-1α tethered to the *BNIP3* promoter in normoxia only *in vivo* (ChIP), but not by *in vitro* (EMSA, pull-down) measures, may highlight the protective effect of chromatin and/or the required HIF-1 heterodimer under conditions where free α-subunits are all but depleted due to ongoing hydroxylation and degradation. Because none of the usual proinflammatory agents (e.g., cytokines, growth factors, and reactive oxygen species), known to spark a strong nonhypoxic HIF-1α accumulation and induced expression of HIF-1 targets, were added to our cultures the select interaction of HIF-1 with the *BNIP3* promoter in oxic cells seems to occur independently of changes in cytokine/growth factor/ROS concentrations. About the question whether DNA-bound HIF-1 in oxic cells maintains transcriptional functionality, we found that, in Hep3B cells subjected to 16-hour periods of 3% and 10% O_2, HIF-1α still manages to drive the induction of *BNIP3* (Table 3). Overall, however, our knowledge is meager at best when it comes to events emanating from HIF signaling in mildly deoxygenated or completely aerobic cells. A noted exception is a study by Welford and colleagues which documented HIF-1 to be strictly necessary in delaying the onset of cellular senescence in aerobic murine embryonic fibroblasts, in part via the transcriptional control of the proinflammatory macrophage migration inhibitory factor (63).

Taken together, the distinct sites of the *LDHA* promoter allow switching between USF/normoxic and HIF-1/hypoxic states, in favor of a complementing expression profile with a broadened O_2 sensitivity. In contrast, the single BNIP3 sequence around the −251/−246 CACGTG motif seems to be the platform for a pO_2-dependent, conditional competition between USF1/2a and HIF-1 [i.e., (i) normoxic/subnormoxic state: USF ↔ HIF-1; (ii) hypoxic (1% O_2) state: HIF-1 only; with ↔ = competition]. If so, this conditional competition would argue for different DNA affinities and/or transactivation competences of normoxic and hypoxic HIF-1 complexes, respectively. Inadequate α:β subunit interactions, however, are unlikely be involved in debilitating affinity or transcriptional capacity of normoxic HIFs (relative to species at 1% O_2). Recent fluorescence resonance energy transfer measurements revealed, at least for proteolysis-saturating levels of overexpressed HIF-2α and ARNT, identical α:β distances in normoxic and hypoxic HIF-2 heterodimers (64). Although the assembly of HIF in oxygenated and severely hypoxic nuclei appears to match one another, the α-subunits in such high pO_2, HRE-tethered dimers should show hydroxylation at ODD-prolyl and/or CAD-asparaginyl residues.

The recent categorization of HIF-1 targets into PHD- (driven by HIF-1α NAD activity) and PHD/FIH-dependent cohorts (driven by HIF-1α NAD + CAD activity) has yielded some surprising new insights about the O_2 profiles of *LDHA* and *BNIP3* genes (15–17). Here, *BNIP3* expression was characterized by extremely low FIH-1 sensitivity scores, indicating full responsiveness of the gene by marginal drops of pO_2 and transcriptional gene induction (rather than inhibition) by active FIH-1. In line with this concept, we find *BNIP3* to be induced via HIF-1α in hepatoma cells at 1%, 3%, and 10% O_2 (Fig. 3, Table 3). Although possible functions of BNIP3, in addition to the factors proapoptotic/proautophagic dichotomy (65, 66), need to be clarified for mildly versus profoundly hypoxic cancer cells, the binding of HIF-1 to the *BNIP3* promoter under a wide range of pO_2, and to the LDHA sites selectively during hypoxia, agrees with such nonredundant impacts of PHDs and FIH-1 on the activity of these HIF targets. In USF-1–silenced Hep3B, *BNIP3* mRNA expression levels were, relative to controls transfected with scrambled RNA, reduced in normoxia and steadily increasing in cells experiencing ever milder degrees of hypoxia. This mix of effects yielded, as result of the USF1 knockdown, a progressive potentiation of the *BNIP3* induction from harsh (1% O_2) to moderately (3% O_2) to mildly (10% O_2) deoxygenated Hep3Bs (Fig. 3, Table 3). We therefore surmise that endogenous USFs primarily cap the activity of the HIF-1/HRE complex at *BNIP3* during normoxia-mild hypoxia; that is, interfere with HIF-1 complexes whose α-subunits remain either fully (i.e., at ODD/NAD + CAD) or partially (i.e., at CAD) hydroxylated. The HIF-1/HRE complex under strictly hypoxic (1% O_2) conditions, that is, with complete dehydroxylation of α-subunits at NAD and CAD regions, is, however, due to HIF's superior DNA affinity dominant over endogenous USFs. Now, upstream stimulatory factors will only through overexpression still be able to shift the binding equilibrium to the BNIP3 HRE in their favor and guard the site against HIF-1. Thus, USF1 and USF2a are best viewed as pO_2-dependent conditional, not compulsory, HIF-interfering factors. Their delimiting impact on hypoxic signaling likely occurs most effectively toward HIF's temporal or O_2 limits (i.e., during anoxia or reoxygenation), or in response to a strong physiologic activation of the USF pathway [i.e., (i) UV-induced USF1 phosphorylation in cells of melanocytic origin (53); (ii) Ca^{2+} depletion–based protection from proteolysis in

Published OnlineFirst October 7, 2011; DOI: 10.1158/1541-7786.MCR-11-0090

differentiating erythroid progenitor/erythroleukemia cells (54)]. Future work should tap into genome-wide implications of coactivated cross-talk between endogenous USFs and HIF-1 in appropriate models.

Disclosure of Potential Conflicts of Interest

No potential conflicts of interest were disclosed.

Acknowledgments

The authors thank Dr. Benoit Viollet (Institut Cochin INSERM, Universite Paris, Paris, France) for his generous gifts of USF antibodies and expression plasmids and his unwavering willingness to act as an expert sounding board throughout the project and the following colleagues for their kind contributions of various materials: Prof. Adrian L. Harris (John Radcliffe Hospital, Oxford, United Kingdom); Dr. Makoto Tsuneoka (Kurume University, Fukuoka, Japan); Prof. Richard S. Pollenz (University of South Florida, Tampa); Prof. Kazuhiro Sogawa (Tonoku University, Sendai, Japan); Prof. Robert G. Roeder (Rockefeller University, New York); Prof. P. Maxwell (University College London, London, United Kingdom), and Prof. J. Okami (University of Michigan). The authors also thank Ms. Kristin Wollenick (Institute of Physiology, University of Zurich) for the short version of PHD2 luciferase reporter plasmid and Mr. Kristian Reveles Jensen for his help as a BUSS-2008 summer student at the University of Zurich and lastly two anonymous reviewers whose helpful and constructive comments aided greatly in improving the manuscript's discussion.

Grant Support

This work was supported by grants from the EU's 6th framework programme (Euroxy consortium; partners: to M.Gassmann and T.A. Gorr) and the Swiss National Science Foundation (M. Gassmann).

The costs of publication of this article were defrayed in part by the payment of page charges. This article must therefore be hereby marked *advertisement* in accordance with 18 U.S.C. Section 1734 solely to indicate this fact.

Received February 23, 2011; revised September 2, 2011; accepted September 16, 2011; published OnlineFirst October 7, 2011.

References

1. Centanin L, Gorr TA, Wappner P. Tracheal remodelling in response to hypoxia. J Insect Physiol 2010;56:447–54.
2. Gorr TA, Gassmann M, Wappner P. Sensing and responding to hypoxia via HIF in model invertebrates. J Insect Physiol 2006;52:349–64.
3. Fandrey J, Gorr TA, Gassmann M. Regulating cellular oxygen sensing by hydroxylation. Cardiovasc Res 2006;71:642–51.
4. Wang GL, Jiang BH, Rue EA, Semenza GL. Hypoxia-inducible factor 1 is a basic-helix-loop-helix-PAS heterodimer regulated by cellular O_2 tension. Proc Natl Acad Sci U S A 1995;92:5510–4.
5. Epstein AC, Gleadle JM, McNeill LA, Hewitson KS, O'Rourke J, Mole DR, et al. C. elegans EGL-9 and mammalian homologs define a family of dioxygenases that regulate HIF by prolyl hydroxylation. Cell 2001;107:43–54.
6. Ivan M, Kondo K, Yang H, Kim W, Valiando J, Ohh M, et al. HIFalpha targeted for VHL-mediated destruction by proline hydroxylation: implications for O_2 sensing. Science 2001;292:464–8.
7. Jaakkola P, Mole DR, Tian YM, Wilson MI, Gielbert J, Gaskell SJ, et al. Targeting of HIF-alpha to the von Hippel-Lindau ubiquitylation complex by O_2-regulated prolyl hydroxylation. Science 2001;292:468–72.
8. Krek W. VHL takes HIF's breath away. Nat Cell Biol 2000;2:E121–3.
9. Lando D, Peet DJ, Gorman JJ, Whelan DA, Whitelaw ML, Bruick RK. FIH-1 is an asparaginyl hydroxylase enzyme that regulates the transcriptional activity of hypoxia-inducible factor. Genes Dev 2002;16:1466–71.
10. Lando D, Peet DJ, Whelan DA, Gorman JJ, Whitelaw ML. Asparagine hydroxylation of the HIF transactivation domain a hypoxic switch. Science 2002;295:858–61.
11. Wenger RH, Stiehl DP, Camenisch G. Integration of oxygen signaling at the consensus HRE. Sci STKE 2005;2005:re12.
12. Manalo DJ, Rowan A, Lavoie T, Natarajan L, Kelly BD, Ye SQ, et al. Transcriptional regulation of vascular endothelial cell responses to hypoxia by HIF-1. Blood 2005;105:659–69.
13. Koivunen P, Hirsilä M, Günzler V, Kivirikko KI, Myllyharju J. Catalytic properties of the asparaginyl hydroxylase (FIH) in the oxygen sensing pathway are distinct from those of its prolyl 4-hydroxylases. J Biol Chem 2004;279:9899–904.
14. Stolze IP, Tian YM, Appelhoff RJ, Turley H, Wykoff CC, Gleadle JM, et al. Genetic analysis of the role of the asparaginyl hydroxylase factor inhibiting hypoxia-inducible factor (FIH) in regulating hypoxia-inducible factor (HIF) transcriptional target genes [corrected]. J Biol Chem 2004;279:42719–25.
15. Dayan F, Roux D, Brahimi-Horn MC, Pouysségur J, Mazure NM. The oxygen sensor factor-inhibiting hypoxia-inducible factor-1 controls expression of distinct genes through the bifunctional transcriptional character of hypoxia-inducible factor-1alpha. Cancer Res 2006;66:3688–98.
16. Dayan F, Monticelli M, Pouysségur J, Pecou E. Gene regulation in response to graded hypoxia: the non-redundant roles of the oxygen sensors PHD and FIH in the HIF pathway. J Theor Biol 2009;259:304–16.
17. Pouysségur J, Dayan F, Mazure NM. Hypoxia signalling in cancer and approaches to enforce tumour regression. Nature 2006;441:437–43.
18. Gorr TA, Cahn JD, Yamagata H, Bunn HF. Hypoxia-induced synthesis of hemoglobin in the crustacean Daphnia magna is hypoxia-inducible factor-dependent. J Biol Chem 2004;279:36038–47.
19. Gorr TA, Tomita T, Wappner P, Bunn HF. Regulation of Drosophila hypoxia-inducible factor (HIF) activity in SL2 cells: identification of a hypoxia-induced variant isoform of the HIFalpha homolog gene similar. J Biol Chem 2004;279:36048–58.
20. Gorr TA, Wichmann D, Pilarsky C, Theurillat JP, Fabrizius A, Laufs T, et al. Old proteins - new locations: myoglobin, haemoglobin, neuroglobin and cytoglobin in solid tumours and cancer cells. Acta Physiol (Oxf) 2011;202:563–81.
21. Viollet B, Lefrancois-Martinez AM, Henrion A, Kahn A, Raymondjean M, Martinez A. Immunochemical characterization and transacting properties of upstream stimulatory factor isoforms. J Biol Chem 1996;271:1405–15.
22. Turley H, Wykoff CC, Troup S, Watson PH, Gatter KC, Harris AL. The hypoxia-regulated transcription factor DEC1 (Stra13, SHARP-2) and its expression in human tissues and tumours. J Pathol 2004;203:808–13.
23. Tsuneoka M, Nakano F, Ohgusu H, Mekada E. c-myc activates RCC1 gene expression through E-box elements. Oncogene 1997;14:2301–11.
24. Holmes JL, Pollenz RS. Determination of aryl hydrocarbon receptor nuclear translocator protein concentration and subcellular localization in hepatic and nonhepatic cell culture lines: development of quantitative Western blotting protocols for calculation of aryl hydrocarbon receptor and aryl hydrocarbon receptor nuclear translocator protein in total cell lysates. Mol Pharmacol 1997;52:202–11.
25. Sogawa K, Nakano R, Kobayashi A, Kikuchi Y, Ohe N, Matsushita N, et al. Possible function of Ah receptor nuclear translocator (Arnt) homodimer in transcriptional regulation. Proc Natl Acad Sci U S A 1995;92:1936–40.
26. Kaulen H, Pognonec P, Gregor PD, Roeder RG. The Xenopus B1 factor is closely related to the mammalian activator USF and is implicated in the developmental regulation of TFIIIA gene expression. Mol Cell Biol 1991;11:412–24.
27. Okami J, Simeone DM, Logsdon CD. Silencing of the hypoxia-inducible cell death protein BNIP3 in pancreatic cancer. Cancer Res 2004;64:5338–46.
28. Metzen E, Stiehl DP, Doege K, Marxsen JH, Hellwig-Burgel T, Jelkmann W. Regulation of the prolyl hydroxylase domain protein 2 (phd2/

Published OnlineFirst October 7, 2011; DOI: 10.1158/1541-7786.MCR-11-0090

egln-1) gene: identification of a functional hypoxia-responsive element. Biochem J 2005;387:711–7.
29. Cockman ME, Masson N, Mole DR, Jaakkola P, Chang GW, Clifford SC, et al. Hypoxia inducible factor-alpha binding and ubiquitylation by the von Hippel-Lindau tumor suppressor protein. J Biol Chem 2000;275:25733–41.
30. North S, Espanel X, Bantignies F, Viollet B, Vallet V, Jalinot P, et al. Regulation of cdc2 gene expression by the upstream stimulatory factors (USFs). Oncogene 1999;18:1945–55.
31. Gorr TA, Rider CV, Wang HY, Olmstead AW, LeBlanc GA. A candidate juvenoid hormone receptor cis-element in the Daphnia magna hb2 hemoglobin gene promoter. Mol Cell Endocrinol 2006;247:91–102.
32. Gustafsson MV, Zheng X, Pereira T, Gradin K, Jin S, Lundkvist J, et al. Hypoxia requires notch signaling to maintain the undifferentiated cell state. Dev Cell 2005;9:617–28.
33. Chen L, Shen YH, Wang X, Wang J, Gan Y, Chen N, et al. Human prolyl-4-hydroxylase alpha(I) transcription is mediated by upstream stimulatory factors. J Biol Chem 2006;281:10849–55.
34. Esteban MA, Tran MG, Harten SK, Hill P, Castellanos MC, Chandra A, et al. Regulation of E-cadherin expression by VHL and hypoxia-inducible factor. Cancer Res 2006;66:3567–75.
35. Holmquist-Mengelbier L, Fredlund E, Lofstedt T, Noguera R, Navarro S, Nilsson H, et al. Recruitment of HIF-1alpha and HIF-2alpha to common target genes is differentially regulated in neuroblastoma: HIF-2alpha promotes an aggressive phenotype. Cancer Cell 2006;10:413–23.
36. Swanson HI, Chan WK, Bradfield CA. DNA binding specificities and pairing rules of the Ah receptor, ARNT, and SIM proteins. J Biol Chem 1995;270:26292–302.
37. Swanson HI, Yang JH. Specificity of DNA binding of the c-Myc/Max and ARNT/ARNT dimers at the CACGTG recognition site. Nucleic Acids Res 1999;27:3205–12.
38. Grandori C, Cowley SM, James LP, Eisenman RN. The Myc/Max/Mad network and the transcriptional control of cell behavior. Annu Rev Cell Dev Biol 2000;16:653–99.
39. Grandori C, Mac J, Siebelt F, Ayer DE, Eisenman RN. Myc-Max heterodimers activate a DEAD box gene and interact with multiple E box-related sites *in vivo*. EMBO J 1996;15:4344–57.
40. Kvietikova I, Wenger RH, Marti HH, Gassmann M. The transcription factors ATF-1 and CREB-1 bind constitutively to the hypoxia-inducible factor-1 (HIF-1) DNA recognition site. Nucleic Acids Res 1995;23:4542–50.
41. Krones A, Jungermann K, Kietzmann T. Cross-talk between the signals hypoxia and glucose at the glucose response element of the L-type pyruvate kinase gene. Endocrinology 2001;142:2707–18.
42. Sirito M, Lin Q, Deng JM, Behringer RR, Sawadogo M. Overlapping roles and asymmetrical cross-regulation of the USF proteins in mice. Proc Natl Acad Sci U S A 1998;95:3758–63.
43. Galibert MD, Carreira S, Goding CR. The Usf-1 transcription factor is a novel target for the stress-responsive p38 kinase and mediates UV-induced Tyrosinase expression. Embo J 2001;20:5022–31.
44. Stiehl DP, Wirthner R, Koditz J, Spielmann P, Camenisch G, Wenger RH. Increased prolyl 4-hydroxylase domain proteins compensate for decreased oxygen levels. Evidence for an autoregulatory oxygen-sensing system. J Biol Chem 2006;281:23482–91.
45. Kim JW, Gao P, Liu YC, Semenza GL, Dang CV. Hypoxia-inducible factor 1 and dysregulated c-Myc cooperatively induce vascular endothelial growth factor and metabolic switches hexokinase 2 and pyruvate dehydrogenase kinase 1. Mol Cell Biol 2007;27:7381–93.
46. Lendahl U, Lee KL, Yang H, Poellinger L. Generating specificity and diversity in the transcriptional response to hypoxia. Nat Rev Genet 2009;10:821–32.
47. Mazure NM, Chauvet C, Bois-Joyeux B, Bernard MA, Nacer-Cherif H, Danan JL. Repression of alpha-fetoprotein gene expression under hypoxic conditions in human hepatoma cells: characterization of a negative hypoxia response element that mediates opposite effects of hypoxia inducible factor-1 and c-Myc. Cancer Res 2002;62:1158–65.
48. Firth JD, Ebert BL, Ratcliffe PJ. Hypoxic regulation of lactate dehydrogenase A. Interaction between hypoxia-inducible factor 1 and cAMP response elements. J Biol Chem 1995;270:21021–7.
49. Semenza GL, Roth PH, Fang HM, Wang GL. Transcriptional regulation of genes encoding glycolytic enzymes by hypoxia-inducible factor 1. J Biol Chem 1994;269:23757–63.
50. Wenger RH, Gassmann M. Oxygen(es) and the hypoxia-inducible factor-1. Biol Chem 1997;378:609–16.
51. Sirito M, Lin Q, Maity T, Sawadogo M. Ubiquitous expression of the 43- and 44-kDa forms of transcription factor USF in mammalian cells. Nucleic Acids Res 1994;22:427–33.
52. Sirito M, Walker S, Lin Q, Kozlowski MT, Klein WH, Sawadogo M. Members of the USF family of helix-loop-helix proteins bind DNA as homo- as well as heterodimers. Gene Expr 1992;2:231–40.
53. Corre S, Galibert MD. Upstream stimulating factors: highly versatile stress-responsive transcription factors. Pigment Cell Res 2005;18:337–48.
54. Lin IJ, Zhou Z, Crusselle-Davis VJ, Moghimi B, Gandhi K, Ananthara-man A, et al. Calpeptin increases the activity of upstream stimulatory factor and induces high level globin gene expression in erythroid cells. J Biol Chem 2009;284:20130–5.
55. Dimova EY, Kietzmann T. Cell type-dependent regulation of the hypoxia-responsive plasminogen activator inhibitor-1 gene by upstream stimulatory factor-2. J Biol Chem 2006;281:2999–3005.
56. Fink T, Kazlauskas A, Poellinger L, Ebbesen P, Zachar V. Identification of a tightly regulated hypoxia-response element in the promoter of human plasminogen activator inhibitor-1. Blood 2002;99:2077–83.
57. Samoylenko A, Roth U, Jungermann K, Kietzmann T. The upstream stimulatory factor-2a inhibits plasminogen activator inhibitor-1 gene expression by binding to a promoter element adjacent to the hypoxia-inducible factor-1 binding site. Blood 2001;97:2657–66.
58. Chang JT, Yang HT, Wang TC, Cheng AJ. Upstream stimulatory factor (USF) as a transcriptional suppressor of human telomerase reverse transcriptase (hTERT) in oral cancer cells. Mol Carcinog 2005;44:183–92.
59. Goueli BS, Janknecht R. Regulation of telomerase reverse transcriptase gene activity by upstream stimulatory factor. Oncogene 2003;22:8042–7.
60. Yatabe N, Kyo S, Maida Y, Nishi H, Nakamura M, Kanaya T, et al. HIF-1-mediated activation of telomerase in cervical cancer cells. Oncogene 2004;23:3708–15.
61. Kothari S, Cizeau J, McMillan-Ward E, Israels SJ, Bailes M, Ens K, et al. BNIP3 plays a role in hypoxic cell death in human epithelial cells that is inhibited by growth factors EGF and IGF. Oncogene 2003;22:4734–44.
62. Shim H, Dolde C, Lewis BC, Wu CS, Dang G, Jungmann RA, et al. c-Myc transactivation of LDH-A: implications for tumor metabolism and growth. Proc Natl Acad Sci U S A 1997;94:6658–63.
63. Welford SM, Bedogni B, Gradin K, Poellinger L, Broome Powell M, Giaccia AJ. HIF1alpha delays premature senescence through the activation of MIF. Genes Dev 2006;20:3366–71.
64. Konietzny R, Konig A, Wotzlaw C, Bernadini A, Berchner-Pfannschmidt U, Fandrey J. Molecular imaging: into *in vivo* interaction of HIF-1alpha and HIF-2alpha with ARNT. Ann N Y Acad Sci 2009;1177:74–81.
65. Bellot G, Garcia-Medina R, Gounon P, Chiche J, Roux D, Pouysségur J, et al. Hypoxia-induced autophagy is mediated through hypoxia-inducible factor induction of BNIP3 and BNIP3L via their BH3 domains. Mol Cell Biol 2009;29:2570–81.
66. Mazure NM, Pouysségur J. Atypical BH3-domains of BNIP3 and BNIP3L lead to autophagy in hypoxia. Autophagy 2009;5:868–9.
67. Corre S, Primot A, Sviderskaya E, Bennett DC, Vaulont S, Goding CR, et al. UV-induced expression of key component of the tanning process, the POMC and MC1R genes, is dependent on the p-38-activated upstream stimulating factor-1 (USF-1). J Biol Chem 2004;279:51226–33.
68. Semenza GL, Jiang BH, Leung SW, Passantino R, Concordet JP, Maire P, et al. Hypoxia response elements in the aldolase A, enolase 1, and lactate dehydrogenase A gene promoters contain essential binding sites for hypoxia-inducible factor 1. J Biol Chem 1996;271:32529–37.

16. Acknowledgment

First and foremost, I would like to thank my supervisors Dr. rer. nat. Thomas Gorr and Prof. Dr. med. Johannes Vogel for giving me the opportunity to do my Ph.D. in their lab. I am grateful to them for their valuable guidance, motivation, priceless discussions, suggestions and support throughout the years of my PhD. During these years I have learned a lot, not only about biology, but also personally. I am highly obliged for the time and energy they have dedicated to this project and standing by me in its good and bad times. In all, my PhD proved a challenging, yet rewarding experience that will stay with me forever.

Further I sincerely thank Prof. Dr. med. vet. Max Gassmann for his insightful comments and suggestions and the other members of my Ph.D. committee Prof. Dr. Carsten Lundby and Prof. Dr. Ian Frew for their valuable reviewing of this thesis and suggestions in general.

I gratefully acknowledge Krebsliga Zurich and Forschungskredit (Univ. Zurich) for their financial support, without which this project would not have been possible.

I would also like to thank all my lab members for their help and invaluable assistance and a nice work environment that made life considerably easier. Special thanks to our secretary Gabriela Eger-Brunkow for her support. I would also like to thank all my collaborators for providing us their support and valuable suggestions without which this project would never have come to where it is today.

Finally, I would also like to thank my parents Arun and Sunanda Shinde, my brother Avadhut for their constant encouragement and unwavering support. My friends Abhijeet, Manoj, Rohit, Nikhil and their families for making life fun in Zurich. But above all I would like to thank my lovely wife, Tejashree, for her mental and emotional support during tough time of my PhD. you always stood at my side sharing the good and the bad parts of it.

Curriculum Vitae

Name	:	Dheeraj Arun Shinde
Address	:	Winterthurerstrasse 692, 8051 Zurich.
Phone	:	+41774238440
Email	:	Dheeraj.a.shinde@gmail.com
Nationality	:	Indian
Date of Birth	:	19 March 1986.
Marital Status	:	Married

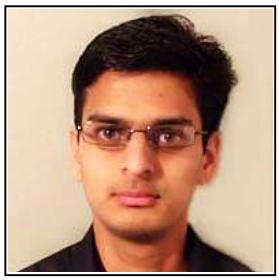

- **Education**

Feb 2010-May 2014	**:**	PhD thesis at Institute of Veterinary Physiology, University of Zurich, Switzerland (Tumoriology). [Titled: *Chicken Embryo Chorioallantoic Membrane Assay for Pre-Clinical Evaluation of Efficacy and Safety of Anti-angiogenic and Hypoxic Cell Starving Tumor Interventions*.]
Mar 2009-Sep 2009	**:**	Master's Thesis work at École polytechnique fédérale de Lausanne (EPFL) Lausanne, Switzerland. [*Titled: Mapping Drosophila melanogaster Transcription factor (TF)-DNA and TF-TF interactions using yeast hybrid methods*].
Jan 2008-Feb 2009	**:**	Master's in Molecular Biology, University of Skövde, Skövde, Sweden.
Jun 2003-Dec 2007	**:**	Bachelor's in Pharmacy from Satara college of Pharmacy, Satara. Shivaji University Kolhapur (MH), India.
Jun 2001-Apr 2003	**:**	Higher Secondary school at A.G High school, Dapoli India.
Jun 1995-Apr 2001	**:**	Secondary School at R.R Vaidya English medium school Dapoli India.
Jun 1991-Apr 1995	**:**	Primary school at Nirmala convent school Satara, India.

- **Working Experience**

Jun 2007-Aug 2007	**:**	Industrial Training at softsole private limited, Mumbai, India**.** Gained experience in manufacturing techniques of soft gelatin capsule with study regarding Quality control Quality Assurance, Storage etc.

- **Current Membership**

2012 - Till Date	**:**	Student membership for Swiss Physiological Society, Switzerland.

- **Awards**

Feb 2012 - Jan 2013	**:**	Scholarship awarded from Forschungskredit der Universität Zürich, Foundation, in the form of 1 Year PhD salary.

- **Talks and Poster Presentation**

Talk at Tagung der Fachgruppe, Physiologie und Biochemie der Deutschen Veterinärmedizinischen Gesellschaft, Zurich Switzerland (15 February 2014). Titled: *Chorioallantoic membrane model for the pre-clinical cancer therapy screening: Disrupting the metabolic symbiosis of solid tumors. (A novel anti-cancer strategy).*

Talk at Zentrums für Kinder- und Jugendmedizin, Universitats Klinikum, Freiburg, Germany (10 June 2013). Titled: *Chorioallantoic membrane model for the pre-clinical and animal-testing free evaluation of novel anti-cancer strategies*.

Poster at Physiological Society meeting, (13 Sep 2012). Fribourg, Switzerland, *Chorio-allantoic membrane assay for pre-clinical cancer therapy screening: simultaneous targeting of oxygenated and hypoxic tumor cells.*

Poster at 11th Day of Clinical Research Zurich, (19 April 2012). *Disrupting the metabolic symbiosis of solid tumors as a novel anti-cancer strategy*.

Poster at Hypoxia sensing, signaling and adaptation`Conference (8-12 Jan 2011). Davos Switzerland. *Chorio-allantoic membrane assay for pre-clinical cancer therapy screening.*

- **Publications**

Shinde D.A., Gassmann M., Vogel J., & Gorr T.A. Chorio-allantoic membrane assay for pre-clinical cancer therapy screening: Disrupting the metabolic symbiosis of solid tumors a novel anti-cancer strategy (Submitted).

Jun Hu, Dheeraj A. Shinde, Thomas A. Gorr, Joachim Fandrey. Non-canonical tuning of hypoxia-induced gene expression by HIF-1α/HIF-2α and HIF-2α/HIF-2α dimer formation (In preparation).

Hu, J., Stiehl, D. P., Setzer, C., Wichmann, D., Shinde, D. A., Rehrauer, H., Gorr, T. A. (2011). Interaction of HIF and USF signaling pathways in human genes flanked by hypoxia-response elements and E-box palindromes. *Molecular Cancer Research : MCR*, *9*(11), 1520–36. doi:10.1158/1541-7786.MCR-11-0090

Ghodake J.D, Vidhate J.S, Shinde D.A, Kadam A.N. Formulation and evaluation of floating microsphere containing anti-diabetic (metformin hydrochloride) drug. International Journal of PharmTech Research Vol.2, No.1, pp 378-384, Jan-Mar 2010.

- **Computer Skills**

Good knowledge of Windows OS, Mac OS, MS Office, Graph Pad: Prism. Familiar with Bioinformatics software's & tools- Rasmol, Swiss-Pdb viewer, Primer3 (Primer Design), BLAST, ClustalW (Sequence alignment Tool), Expasy (analysis of protein sequences and structures), and NTI.

- **Extra-Curricular Activities**

-TOEFL (2006): ETS, USA (score 90/120)
-Participant in work shop on advances in novel drug delivery system (07.10.2006).
-Maharashtra State Certificate In Information Technology (MS-CIT) computer course (Oct 2006).
-German language course A1/2 Intensive, (06.01.2014 to 28.03.2014)

- **Languages:**

English	:	Fluent (Educational Language)
German	:	Elementary
Hindi	:	Fluent
Marathi	:	Fluent (Mother Tongue)

- **Reference**

Dr. Thomas A. Gorr Institute of Veterinary Physiology, University of Zurich Winterthurerstrasse 260 8057 Zurich Tel. +41 44 635 88 78 tgorr@access.uzh.ch	Prof. Dr. Johannes Vogel Institute of Veterinary Physiology, University of Zurich Winterthurerstrasse 260 8057 Zurich Tel. +41 44 635 88 06 jvogel@vetphys.uzh.ch	Prof. Dr. Max Gassmann Institute of Veterinary Physiology, University of Zurich Winterthurerstrasse 260 8057 Zurich Tel. +41 44 635 88 03 maxg@access.uzh.ch